

HUMBOLDT-UNIVERSITÄT ZU BERLIN



Faculty of Life Sciences

Albrecht Daniel Thaer-Institute for Agricultural and Horticultural Sciences

MASTER'S THESIS

to acquire the academic degree Master of Science

**Local Governments in Climate Action: The Role of Temperature Shocks and
Weather-Related Disaster in Driving Global Covenant of Mayors Participation**

Author:

Lauren Henn

573569

laurenhenn@gmail.com

Supervisors:

Prof. Dr. Klaus Eisenack

Prof. Dr. Achim Hagen

*A thesis submitted to the Chair of Resource Economics
in partial fulfillment of the requirements for the degree Master of Science*

March 12, 2025

Declaration of Authorship

I hereby declare that my thesis is the result of my own work and that I have marked all sources, including online sources, which have been cited without changes or in modified form, especially sources of texts, graphics, tables and pictures.

I assure that I have not submitted this thesis for any other examination yet.

I am aware that in case of any breach of these rules procedures concerning fraud or attempted fraud will be taken in accordance with the subject-specific examination regulations and/or the Allgemeine Satzung für Studien- und Prüfungsangelegenheiten (ASSP) or the Allgemeine Satzung zur Regelung von Zulassung, Studium und Prüfung der Humboldt-Universität zu Berlin (ZSP-HU).

Signed:

Date:

HUMBOLDT-UNIVERSITÄT ZU BERLIN

Abstract

Faculty of Life Sciences

Albrecht Daniel Thaer-Institute for Agricultural and Horticultural Sciences

Master of Science

Local Governments in Climate Action: The Role of Temperature Shocks and Weather-Related Disasters in Driving Global Covenant of Mayors Participation

by Lauren Henn

As climate change intensifies, cities face increasing risks from rising temperatures and natural disasters. This may drive them to take action, such as joining trans-municipal climate networks (TMNs) like the Global Covenant of Mayors for Climate and Energy (GCoM). To empirically test this, the following analysis modeled the decision-making process of 11,344 cities globally from 2008 to 2024 to join TMNs, by exploring the impact of seasonal temperature anomalies, shocks, and weather-related disasters on GCoM participation. The focus on the GCoM was justified by its status as the largest network of its kind. The results revealed regional disparities, with European cities showing a higher participation rate than others. Moreover, in Europe, long-term exposure to warmer-than-average conditions and persistent meteorological disasters were associated with increased GCoM participation, while sustained colder-than-average conditions discouraged involvement. In contrast, non-European cities showed less consistent patterns. That said, the findings were accompanied by some degree of uncertainty. Overall, the results contribute to understanding how local exposure to climate events influences cities' engagement in climate networks, adding to the literature on urban climate action.

HUMBOLDT-UNIVERSITÄT ZU BERLIN

Acknowledgements

Faculty of Life Sciences

Albrecht Daniel Thaer-Institute for Agricultural and Horticultural Sciences

Master of Science

**Local Governments in Climate Action: The Role of Temperature Shocks and
Weather-Related Disasters in Driving Global Covenant of Mayors Participation**

by Lauren Henn

I want to thank Konrad Bierl and Prof. Dr. Klaus Eisenack for their support and guidance throughout the writing process. Special thanks also go to Dr. Matthias Eckardt from the Chair of Statistics at Humboldt Universität zu Berlin for sharing his expertise and recommending discrete-time survival methods and inverse probability weighting in the analysis. Additionally, I want to thank the Chair of Economic History of Humboldt Universität zu Berlin for providing the LaTeX template used to compile this thesis. Finally, I want to acknowledge the assistance of OpenAI's ChatGPT and the community of stackoverflow.com in computing various R codes.

Contents

Declaration of Authorship	v
Abstract	vii
List of Figures	xiii
List of Tables	xv
List of Abbreviations	xvi
1 Introduction	1
2 Research Context	7
2.1 Current State of Empirical Research on Urban Vulnerability and Climate Action	7
2.2 The Global Covenant of Mayors for Climate and Energy	10
3 Empirical Strategy	13
3.1 Resulting Hypotheses	13
3.2 Data Selection and Description	14
3.3 Empirical Models	20
4 Results	27
4.1 Descriptive Analysis	27
4.2 Survival Analysis	36
4.2.1 Kaplan-Meier Survival Curves	36
4.2.2 Baseline Estimation	40
4.2.3 Considering Temperature Anomalies and Shocks	43
4.2.4 Considering Weather-Related Natural Disasters	48
4.2.5 Adjusting for Confounding	54
5 Discussion	67
6 Conclusion	73
7 Bibliography	75

Appendix A	84
Appendix B	85
Appendix C	87
Appendix D	90
Appendix E - Data Documentation	95

List of Figures

4.1	Distribution of GHS Urban Centres in Sample	27
4.2	Adherence to the Global Covenant of Mayors in Sample of GHS Urban Centres, by Season (Hot/Cold) & Continent	28
4.3	Global Covenant of Mayors for Climate and Energy Members within Sample of GHS Urban Centres (Data Status: March 2024)	29
4.4	Average GHCN Surface Air Temperature Anomalies within Sample of GHS Urban Centres – 2015-2023 Relative to the 1981-2010 Baseline Period	30
4.5	Average Universal Thermal Comfort Index Anomalies within Sample of GHS Urban Centres – 2015-2023 Relative to 1981-2010 Baseline Period	30
4.6	Temporal Trends of Average GHCN Surface Air Temperature and UTCI Anomalies within Sample of GHS Urban Centres - Hot and Cold Seasons 2000-2024 Relative to the respective 1981 Base Periods	32
4.7	Weather-Related Disaster Events within Sample of GHS Urban Centres, by Type (April 2000 – March 2024)	33
4.8	Weather-Related Disaster Occurrence within Sample of GHS Urban Centres, by Season (Hot/Cold 2000-2024)	35
4.9	Kaplan-Meier Survival Curves for European & Global (excl. Europe) Urban Centres in GHS Sample	37
4.10	Kaplan-Meier Survival Curves for European & Global (excl. Europe) Urban Centres in GHS Sample, by Anomaly Quartiles	38
4.11	Kaplan-Meier Survival Curves for European & Global (excl. Europe) Urban Centres in GHS Sample, by Anomaly Quartiles	40
4.12	Average Dose Response Functions for IPW-Adjusted Estimates of Immediate Temperature Anomalies and Shocks in Global (excl. Europe) Urban Centres	56
4.13	Average Dose Response Functions for IPW-Adjusted Estimates of Temperature Anomalies and Shocks in Global (excl. Europe) Urban Centres (6 & 12 Period Moving Averages)	57
4.14	Average Dose Response Functions for IPW-Adjusted Estimates of Temperature Anomalies and Shocks in European Urban Centres (6 & 12 Period Moving Averages)	60

4.15	Average Dose Response Functions for IPW-Adjusted Estimates of Immediate and Delayed (one-lag) Weather-Related Disasters in European Urban Centres	61
4.16	Average Dose Response Functions for IPW-Adjusted Estimates of Weather-Related Disasters in European Urban Centres (6 & 12 Period Moving Averages) (1)	62
4.17	Average Dose Response Functions for IPW-Adjusted Estimates of Weather-Related Disasters in European Urban Centres (6 & 12 Period Moving Averages) (2)	63
B.1	Summary Statistics of Time-Invariant Variables in Sample of GHS Urban Centres	85
B.2	Summary Statistics of Time-Varying Variables in Sample of GHS Urban Centres	86
C.1	Missingness in Human-Impact Variables in Weather-related Disaster Observations within Sample of GHS Urban Centres (April 2000 - March 2024)	87
C.2	Average Moran's I Across Distance Bands for Exposure Variables in Sample of GHS Urban Centres	88
C.3	Significant Moran's I ($ \hat{I} \geq 0.05, p < 0.1$) in Model Residuals, using various Exposure Variables Across Distance Bands	88
C.4	Variation Inflation Factors for the Estimation of the Effect of Control Variables on the Logit Hazard of City Participation in the GCoM	89
D.1	Love Plots: Covariate Balance Before & After IPW for Global (excl. Europe) Urban Centres Temperature Anomalies & Shock Estimations (1)	90
D.2	Love Plots: Covariate Balance Before & After IPW for Global (excl. Europe) Urban Centres Temperature Anomalies & Shock Estimations (2)	91
D.3	Love Plots: Covariate Balance Before & After IPW for European Urban Centres Temperature Anomalies & Shocks Estimations	92
D.4	Love Plots: Covariate Balance Before & After IPW for European Urban Centres Weather-Related Disasters Estimations (1)	93
D.5	Love Plots: Covariate Balance Before & After IPW for European Urban Centres Weather-Related Disasters Estimations (2)	94

List of Tables

4.1	Estimation of the Effect of Control Variables on the Logit Hazard of City Participation in the GCoM	41
4.2	Estimation of the Immediate Effect of Temperature Anomalies and Shocks on the Logit Hazard of City Participation in the GCoM	44
4.3	Estimation of the Delayed Effect (1 Lag) of Temperature Anomalies and Shocks on the Logit Hazard of City Participation in the GCoM	45
4.4	Estimation of the Effect of Temperature Anomalies and Shocks (6 & 12 Period Moving Averages) on the Logit Hazard of City Participation in the GCoM	47
4.5	Estimation of the Immediate Effect of Weather-Related Disaster Occurrence and Deaths on the Logit Hazard of City Participation in the GCoM	49
4.6	Estimation of the Delayed Effect (1 Lag) of Weather-Related Disaster Occurrence and Deaths on the Logit Hazard of City Participation in the GCoM	51
4.7	Estimation of the Weather-Related Disaster Occurrence and Deaths (6 & 12 Period Moving Averages) on the Logit Hazard of City Participation in the GCoM	53

List of Abbreviations

ADRF Average Dose-Response Function

CCP Cities for Climate Protection

ECMWF European Centre for Medium-Range Weather Forecasts

EM-DAT Emergency Events Database

ERA-5 Fifth-Generation ECMWF Atmospheric Reanalysis

ESS Effective Sample Size

GCoM Global Covenant of Mayors for Climate & Energy

GIS Geographic Information Systems

GDP Gross Domestic Product

GHCN Global Historical Climatology Network

GHS-UCDB Global Human Settlement Urban Centre Database

GISTEMP Goddard Institute for Space Studies Surface Temperature Analysis

GPS Generalized Propensity Score

HDI Human Development Index

ICLEI Local Governments for Sustainability (formerly International Council for Local Environmental Initiatives)

IPCC Intergovernmental Panel on Climate Change

IUCN International Union for Conservation of Nature

IPW Inverse Probability Weighting

LECZ Low-Elevation Coastal Zone

NASA National Aeronautics and Space Administration

NGO Non-governmental organization

PM2.5 Particulate Matter with a Diameter of 2.5 Micrometers or Less

SEDAC Socioeconomic Data and Applications Center

SMD Standardized Mean Difference

UTCI Universal Thermal Climate Index

Chapter 1

Introduction

The year 2023 has been reported as the warmest on record, with global temperatures averaging 1.5°C above pre-industrial levels (Copernicus Climate Change Service, 2024; World Meteorological Organization, 2024). Unlike isolated weather events that can be attributed to natural variability, this rise corresponded with consistent shifts in historical weather patterns that point toward anthropogenic climate change (Pörtner et al., 2022). However, climate change entails more than rising temperatures. It is also reflected in rising sea levels, changing precipitation patterns (leading to both excessive and reduced rainfall) and an increase in climate shocks, i.e. weather events consisting of extreme deviations from normal conditions, such as temperature spikes, or the occurrence of natural disasters like heat waves, droughts, floods and storms (Collins et al., 2019; Pörtner et al., 2022). These events, which have been increasing in intensity and frequency in recent years, already pose complex challenges to both the environment and humans and are only expected to escalate further in the future (Field et al., 2012).

This is especially alarming for cities. For once, the effects of rising temperatures are exacerbated in urban areas because the built environments absorb and re-emit solar heat more than natural landscapes (MIT Climate Portal, 2021). Additionally, the threats associated with sea-level rise primarily affect coastal cities, where 86 percent of the 820 million people at risk from it live (Coalition for Urban Transitions, 2019; Ruiz-Campillo et al., 2022). Moreover, severe weather events such as droughts, floods, storms, and heatwaves place significant strain on residents, water resources, and infrastructures (World Bank, 2010) and, due to high population densities, have an amplified impact on a larger number of people (Dawson, 2017).

At the same time, cities are not only victims but also significant contributors to climate change. This is mainly due to their substantial dependence on fossil fuels, with them being responsible for about 70 percent of global resource consumption and anthropogenic greenhouse gas emissions (UN-Habitat, 2016). Moreover, considering the projected growth in urban population, an increase in the demand for larger or additional cities in the future may worsen climate change impacts as resources will be exhausted further (Rosenzweig et al., 2018).

Despite these considerations, urban areas are also uniquely positioned to lead the way in

combating climate change. Their economic and political importance and, in many cases, status as innovation and technology hubs allow them to implement effective climate change mitigation and adaptation strategies. Furthermore, due to their influential role, the actions taken by cities can spillover and potentially catalyze nationwide environmental initiatives (Castán Broto, 2017; Heidrich et al., 2016; Nguyen Long and Krause, 2021; Reckien et al., 2018).

Local governments have already started to capitalize on this unique position by adopting various strategies. These include improving their infrastructure, transportation, and waste systems, promoting renewable energy use, and participating in trans-municipal climate networks (Castán Broto, 2017; Heidrich et al., 2016; Reckien et al., 2015, 2018). The latter especially plays a role in promoting resource and knowledge sharing among cities while also helping to develop and implement strategies to mitigate and adapt to climate change's impacts (Heidrich et al., 2016; Nguyen Long and Krause, 2021; Reckien et al., 2015, 2018). Currently, the most prominent network, the Global Covenant of Mayors for Climate and Energy (GCoM), unites over 13,000 local governments from 144 countries, collectively representing more than one billion people (Global Covenant of Mayors for Climate & Energy, n.d.b). That said, while participation in trans-municipal climate networks, such as the GCoM, is widespread, certain regions demonstrate more engagement than others (Bansard et al., 2017). These differences may be attributed to a combination of socio-economic and governance factors, along with other city-specific characteristics such as its vulnerability to climate change. Applying the definition given by the Intergovernmental Panel on Climate Change (McCarthy et al., 2001), a city's vulnerability would be shaped by its exposure to extreme weather events, climate shocks, and changing climate patterns; its inherent sensitivities (e.g., age or health-related factors in the population); and its adaptive capacities (i.e., the available resources to respond to climate threats). Depending on the local composition of these three factors, some cities face higher vulnerability to climate change than others. As a result, those may feel more urgency to take climate action, potentially prompting them to engage in climate networks that offer solutions to address their vulnerabilities.

The relationship between subnational vulnerability and climate action has already been central to much empirical research. On one hand, studies within the United States found that highly exposed cities were more engaged in climate action (Gabbe et al., 2024; Hazlett and Mildenerger, 2020; Ji and Darnall, 2022; Zahran et al., 2008a). On the other hand, findings at the European scale have been more nuanced. While research has shown that exposure reinforced green voter behavior at the subnational level (Hoffmann et al., 2022), other studies have indicated that higher vulnerability can hinder the adoption of urban climate mitigation and adaptation strategies (Reckien et al., 2015). At the global level, several studies have highlighted a complex relationship between a local

government's economic condition, its institutional quality, and its responses to climate threats (Nohrstedt et al., 2022), while other findings revealed no consistent link between natural disasters, temperature shocks, sea-level rise, and climate action (Brennan et al., 2022; Rowan, 2022).

Thus, while a substantial body of research has explored why cities engage in climate action, mainly focusing on the role of local-level vulnerability, the mixed findings demonstrate that the relationship is more complex than assumed. Moreover, of the reviewed empirical studies, only two (Zahran et al., 2008a,b) focused on trans-municipal climate networks as a focal point for climate action, emphasizing that they remain an area of investigation. Additionally, as climate shocks intensified in frequency, and as climatic deviations became more significant in scale, local governments may view these as direct consequences of climate change, prompting them to act. These considerations resulted in the central research question of this thesis, which asked: How does exposure to climate shocks, as evidenced by significant temperature deviations, and weather-related disasters, influence a city's decision to join trans-municipal climate networks?

Building upon the existing empirical literature on urban climate action and leveraging on the data at hand, this question was addressed by modelling the decision-making process of 11,344 cities worldwide to participate in the most prominent global climate network, the GCoM, across hot (April to September) and cold (October to March) seasons from 2008 to 2024. The exclusive focus on the GCoM was justified by its status as the largest trans-municipal climate network (United Nations Framework Convention on Climate Change, 2025). Additionally, the capacity to model city adherence on such a large scale was made possible by utilizing the Joint Research Centre's Global Human Settlement – Urban Centre Database (GHS-UCDB) (Florczyk et al., 2019).

The main empirical task involved comparing cities experiencing significant exposure to climate events to those experiencing milder or no considerable exposure to determine if this influenced their decisions to engage in the network. Exposure to climate change was measured by deviations from historical temperature patterns and the occurrence of weather-related natural disasters. Temperature estimates included the total respective seasonal (hot or cold) anomaly based on the 1981-2010 baseline, considering crude, positive, and negative anomalies. These measures were derived using temperature data from the Global Historical Climatology Network (GHCN), provided by the NASA Goddard Institute for Space Studies (GISTEMP Team, 2024), and data on the Universal Thermal Climate Index (UTCI), provided by the Copernicus Climate Change Service (Di Napoli et al., 2021). Additionally, the total number of days within each season classified as a shock was included, defined as the count of daily UTCI values exceeding the 95th percentile or falling below the 5th percentile, based on a 30-day rolling window from 1981 to 2010. The analysis also considered the frequency of heat and cold spells,

identified as periods of at least three consecutive days of positive or negative temperature shocks, respectively. Furthermore, the effect of natural disasters was assessed by including both the occurrence of weather-related disasters and the number of associated deaths for overall and disaggregated disasters (i.e., hydrological, meteorological, and climatological events). This was made possible by leveraging on the Emergency Events Database (EM-DAT) ([Centre for Research on the Epidemiology of Disasters, 2024](#)). Lastly, lagged variables (up to one lag) and lagging means over six and twelve seasons were incorporated for all exposure variables to capture immediate, delayed, and medium- to long-term effects. These exposure measures were then incorporated into discrete-time survival models to evaluate their impact on the hazard of a city joining the GCoM at any given season during the observation period, conditional on it not having joined before. The estimations were conducted separately for European cities, and then for all remaining cities, due to the GCoMs origins in Europe. This framework further included covariates proxying city-level socioeconomic, and other characteristics, which demonstrated strong explanatory power in urban climate action studies. Finally, to strengthen the robustness of the findings, the empirical models were extended to include inverse probability weights, to adjust for potential confounding in the estimated effects of exposure variables.

It should be noted that Geographic Information System (GIS) analytical techniques played a crucial role in this analysis since they enabled the aggregation of exposure measures and other variables within urban spatial boundaries. It should further be noted that the sole focus on the exposure dimension within the vulnerability concept was driven by the ease of computing measurable metrics, such as the frequency and intensity of climate-related events and deviations in delineated geographic areas, compared to other metrics reflecting subnational sensitivity and adaptive capacity.

The primary goal of this research was to investigate the factors that drive city participation in trans-municipal climate networks, focusing on how exposure to climate change influences their decision. A secondary goal was to expand the existing body of research in this field by addressing gaps that often overlook local climate variations over extended periods and across a large number of local governments; to date, no research has focused on such a wide-ranging scope. That said, the findings of the analysis presented regional disparities, with European cities behaving differently than others. Long-term exposure to meteorological events and warmer-than-average conditions encouraged GCoM participation in Europe, while colder-than-average conditions discouraged involvement. Moreover, the findings outside of the European context revealed less consistent patterns, with short-term temperature deviations towards warming having an effect, while no clear trends could be observed from natural disasters. Colder-than-average conditions were also found to have an influence in non-European cities; however, this conclusion was accompanied by a significant degree of uncertainty.

The thesis is organized as follows: **Chapter 2** presents a review of empirical research on the relationship between climate change vulnerability and subnational climate action. It also introduces the Global Covenant of Mayors for Climate and Energy (GCoM), the leading trans-municipal climate network and the focus of the analysis. **Chapter 3** outlines the hypotheses to be tested and describes the data and empirical strategy used for this purpose. **Chapter 4** then provides a descriptive data analysis and presents the results, including findings from the discrete-time survival estimation and the adjusted analysis incorporating inverse probability weights. In **Chapter 5**, these results and implications for future research are discussed, before concluding remarks are made in **Chapter 6**.

Chapter 2

Research Context

2.1 Current State of Empirical Research on Urban Vulnerability and Climate Action

Vulnerability to climate change is most prominently defined by the Intergovernmental Panel on Climate Change (IPCC) (McCarthy et al., 2001) as *“The degree to which a system is susceptible to, or unable to cope with, adverse effects of climate change, including climate variability and extremes. Vulnerability is a function of the character, magnitude, and rate of climate variation to which a system is exposed, its sensitivity, and its adaptive capacity”* (p. 6). Hence, the concept of vulnerability, as described by the IPCC, includes not only the potential for negative impacts from climate change on a system but also its capacity to manage these challenges. Building on this framework, the subsequent analysis primarily focused on city-level exposure to climate shocks instead of other aspects of the vulnerability concept. This decision was mainly driven by the fact that subnational metrics for exposure, such as the frequency and intensity of climate events and variations, were easier to quantify compared to localized indicators for sensitivity and adaptive capacity. For instance, subnational spatial data, with a global coverage, on metrics such as temperature and natural disaster events is more consistently available than data on adaptive capacity (e.g., on infrastructure and institutional quality, education of the population), or sensitivity (e.g., access to healthcare, the age distribution of the population, and the quality of the built environment).

Thus, focusing on exposure, the concept entails understanding the frequency, intensity, and historical persistence of climatic challenges a system faces, encompassing both long-term changes and extreme events. These climatic challenges may include rising temperatures, shifting precipitation patterns, sea-level rise, and extreme weather events (Jurgilevich et al., 2017). Moreover, just as climates vary across different geographical regions, so do exposure levels, with recent studies having further highlighted significant increases affecting some regions more than others (Organisation for Economic Co-operation and Development, 2020; Pörtner et al., 2022; Wei et al., 2024). Hence, areas experiencing higher levels and more frequent exposure are likely to benefit most from climate action. This is particularly relevant at the subnational level, where the impacts

of climate events can be more pronounced compared to national levels (Giordano et al., 2018; Rowan, 2022). These considerations have already been the focus of empirical research, which has, in some cases, demonstrated a connection between urban climate action and local exposure to climate change.

For one, research has indicated a link between exposure to weather-related events and pro-climate political preferences. That said, the persistence of the effects varied based on spatial and temporal proximity, underlying political orientation, and economic conditions. For instance, Hazlett and Mildemberger (2020) found that people living within five kilometers of recent wildfires in California significantly increased their support for climate-related reforms. This effect, however, disappeared almost entirely beyond a 15-kilometer radius and was primarily observed in Democratic-leaning areas. Adding to these findings Baccini and Leemann (2021) observed a 20 percent increase in support for pro-climate policies immediately after flood occurrences in Switzerland, especially in municipalities more conscious of climate change issues. However, they noted that this effect diminished over time, with political behaviors between affected and unaffected areas realigning ten months after the disaster. Moreover, rises in temperature anomalies and the occurrence of heatwaves and droughts were shown to significantly increase subnational Green Party votes in European Parliament elections (Hoffmann et al., 2022). However, these effects varied across climatic regions, with positive temperature anomalies and heat episodes having a more pronounced impact in temperate and colder climates. At the same time, better local economic conditions were also identified to amplify their effect.

Focusing on climate networks, Zahran, Brody, Vedlitz, Grover and Miller (2008a) found that, on the one hand, counties in the United States facing more significant exposure to environmental risks were more likely to commit to the Local Governments for Sustainability's (ICLEI) Cities for Climate Protection (CCP) campaign. Specifically, counties with histories of extreme weather events that led to fatalities, significant projected temperature increases, and at risk of coastal flooding were more inclined to participate. Conversely, those with a higher share of employment in carbon-intensive industries were less likely to join, pointing toward concerns over job losses leading to political resistance against climate policies. Furthermore, nearly all counties engaged in the CCP were shown to rank high in both vulnerability and socioeconomic capacity, indicating that the ability to take climate action depended on available local resources, governance, and the population's education. On the other hand, when the authors conducted a similar study at the more precise Metropolitan Statistical Area level, they no longer identified that the areas most at risk from climate change impacts (assessed through coastal proximity, extreme weather events, ecosystem sensitivity, positive precipitation

anomaly) showed significant motivation to adopt the CCP campaign, while the importance of high socioeconomic capacity remained (Zahran et al., 2008b). Thus, exposure alone may not be enough to drive climate action in some cases, with underlying factors in terms of the socio-economic capacities, and available resources being primary drivers.

Shifting the focus to adopting subnational climate planning, some research focusing on the United States has demonstrated a connection to climate risks. For once, Gabbe, Pierce, Petermann and Marecek (2024) found that Californian cities facing more projected extreme heat days were significantly more likely to adopt urban heat strategies. However, these projections did not influence broader climate adaptation planning, indicating that effective action required a direct link between the type of climate exposure and the specific strategy. Similarly, Ji and Darnall (2022) observed that not all types of climate risks influenced sustainability planning in the same manner in municipalities in the United States. Although overall disaster risk was found to influence the range of environmental issues covered in sustainability strategies, when disaggregating risks, only higher winter storm and geological hazard risks were linked to local governments' strategies. In contrast, no connection was found for water-related hazards. Furthermore, at the global level, local-level affluence was found to influence how cities responded to disasters. For instance, Nohrstedt, Hileman, Mazzoleni et al. (2022) observed that cities reporting to the Carbon Disclosure Project did implement adaptation measures in response to disasters in their regions. However, this only occurred in cities with high political stability. Moreover, economic losses due to disasters influenced actions, but only when underlying economic conditions were favorable. Conversely, the frequency of disaster events, the affected population, and the fatalities generally had no significant impact on adaptation measures.

Thus, these findings suggested that climate risks influence climate planning. However, this was found to be not only shaped by the type of risk but also by a city's underlying economic and political conditions, with wealthier and more politically stable cities being more inclined to translate climate events into action.

In contrast, some research even established a negative correlation between a city's exposure to climate threats and climate action, specifically considering the adoption of climate action plans. For instance, Reckien, Flacke, Olazabal and Heidrich (2015) found that for European cities, warmer summers, coastal proximity, and projected climate impacts acted as hurdles for adaptation and mitigation planning, particularly in Southern Europe. The authors linked this finding to limited governance capacity and economic constraints, as cities at risk often lacked resources to implement effective action. Moreover, the Mediterranean region, which is highly vulnerable and exposed to climate change, has been shown to struggle with implementing effective action (Ruiz-Campillo et al., 2022; Salvia et al., 2021a).

Meanwhile, other research has demonstrated no significant link between exposure to climate change and climate action. Gurney, Meng, Rumschlag and Hamlet (2022) found that economic losses and affected populations from extreme weather events did not drive adaptation action across 88 cities in the United States. Moreover, findings at the global level indicated that neither temperature shocks nor natural disasters (immediate and over time) led to reforms in climate mitigation policies across national and subnational levels. This finding remained robust when accounting for differences between democracies and autocracies or between wealthier and poorer countries (Rowan, 2022). Similarly Brennan et al.'s 2022 study at the global level observed that cities at risk from sea-level rise initially had higher odds of having adaptation and mitigation plans. However, after adjusting for confounders, the effect disappeared, and national income emerged as the key driver.

Thus, the empirical literature presented mixed findings. While some studies indicated that cities exposed to climate threats respond proactively (Baccini and Leemann, 2021; Gabbe et al., 2024; Hazlett and Mildenerger, 2020; Hoffmann et al., 2022; Ji and Darnall, 2022; Zahran et al., 2008a), others showed that this does not always translate into action (Brennan et al., 2022; Gurney et al., 2022; Reckien et al., 2015; Rowan, 2022; Ruiz-Campillo et al., 2022; Salvia et al., 2021a). Moreover, underlying political, socio-economic, and governance structures were found to significantly influence how cities responded to climate threats (Hazlett and Mildenerger, 2020; Hoffmann et al., 2022; Nohrstedt et al., 2022; Zahran et al., 2008a,b). That said, other research pointed to no moderation effects from city-level affluence (Rowan, 2022). Additionally, the impact of climate shocks on climate action were shown to often be temporary and geographically limited, with responses diminishing over time and space (Baccini and Leemann, 2021; Hazlett and Mildenerger, 2020). Whereas climate action was also found to be depended on the type of climate threat, with some threats having a more pronounced effect than others (Gabbe et al., 2024; Ji and Darnall, 2022).

2.2 The Global Covenant of Mayors for Climate and Energy

The previous section provided a summary of the stance of the existing academic literature on how exposure to climate change may facilitate or hinder urban climate action. This subsection now provides a brief overview on one of the forms urban climate actions may take: Trans-municipal climate networks (TMNs), specifically focusing on the Global Covenant of Mayors for Climate and Energy (GCoM).

Transnational Municipal climate networks (TMNs) emerged in the 1990s, with the initiation of the Local Governments for Sustainability (ICLEI) (formerly the International

Council for Local Environmental Initiatives) (Nguyen Long and Krause, 2021). They are characterized as networks of local governments united by a common climate goal and three distinct features: voluntary membership, which allows members to join or leave without repercussions; non-hierarchical organizational structures, which facilitate equitable participation and shared governance among members; and a commitment from members to follow the network's policy decisions (Kern and Bulkeley, 2009; Nguyen Long and Krause, 2021). Moreover, they emphasize on city collaboration across geographic, developmental, and political boundaries with the goal to share knowledge and resources, enabling local climate action, especially when higher authorities or NGOs failed to support (Picavet et al., 2023).

The subsequent analysis focused on the factors that drive cities to join and participate in these networks. However, rather than examining a multitude of climate networks, it centered on the Global Covenant of Mayors for Climate and Energy (GCoM). While several other prominent networks exist, such as the ICLEI, C40 Cities, and the Climate Ambition Alliance, none come close to the global reach and scale of the GCoM (United Nations Framework Convention on Climate Change, 2025), which unites over 13,000 member cities from 144 countries, representing over one billion people (Global Covenant of Mayors for Climate & Energy, n.d.b).

The GCoM was founded in 2016 by the merger of the Covenant of Mayors of the European Union and the UN Compact of Mayors (European Commission, 2016). The Covenant of Mayors was originally initiated by the European Commission in 2008 with the goal of uniting European cities to meet the EU's climate and energy targets. It operated through a bottom-up approach, which enabled local governments to act independently of national governments (Melica et al., 2022; Reckien et al., 2018; Ruiz-Campillo et al., 2022). Member cities were urged to reduce their greenhouse gas emissions by at least 20 percent, increase energy efficiency by 20 percent, achieve a 20 percent share of renewable energy sources by 2020, and implement Sustainable Energy and Climate Action Plans (Pablo Romero et al., 2015; Reckien et al., 2018; Ruiz-Campillo et al., 2022).

In 2014, the UN Compact of Mayors followed, with the objective to unite cities beyond Europe to commit to reducing their greenhouse gas emissions. The Compact focused on accountability and transparency, requiring cities to commit to reducing emissions by tracking and reporting their progress through publicly available platforms (Reckien et al., 2018).

In June 2016, the merger of these two networks led to the creation of the GCoM, with the intention to combine the EU Covenant's bottom-up approach with the UN Compact's emphasis on transparency and accountability (European Commission, 2016). Cities that committed to the GCoM aim to reduce their emissions by 40 percent by 2030, with more significant reductions planned for 2050 (Melica et al., 2022). In terms of aligning with their goals, the reports showed that as of 2021, they have already saved over 2.3 billion

metric tons of CO₂ (Global Covenant of Mayors for Climate & Energy, 2021). Moreover, EU-27 signatories exceeded their 2020 targets by achieving a 25.3 percent reduction from 2005 levels, which surpassed the expected 22.7 percent (Melica et al., 2022). Studies further suggested that GCoM cities were on track to align with the 1.5°C global warming pathway (Hsu et al., 2020; Kona et al., 2021). Moreover, membership has been found to encourage cities to develop climate action plans that address mitigation and adaptation at the European level (Reckien et al., 2015, 2018; Salvia et al., 2021b).

While this sounds promising, some researchers have argued that cities may join the GCoM only to enhance their reputation without being fully committed to the network's goals (Osofsky, 2015). Additionally, concerns emerged that climate networks may not provide inclusive climate agendas since participation tends to be dominated by cities in more economically developed regions (Osofsky, 2015). Finally, ensuring accountability within the network and standardized reporting of progress also remains an issue (Gesing, 2018; Hsu et al., 2020). Nonetheless, in the following analysis, the focus did not linger on the overall effectiveness of the GCoM. Despite these critiques, membership itself can be seen as a proactive step toward climate action, demonstrating at the least a willingness to address climate change issues.

Chapter 3

Empirical Strategy

3.1 Resulting Hypotheses

The research presented in [section 2.1](#) suggested that while not the sole factor and not universal in all cases, a local government's decision to engage in climate action can be influenced by its exposure to climate events. For instance, extreme weather, changing temperatures, and environmental risks have been observed to increase public support for climate policies and Green parties, or make local governments more likely to adopt climate initiatives and implement sustainability strategies ([Baccini and Leemann, 2021](#); [Gabbe et al., 2024](#); [Hazlett and Mildenberger, 2020](#); [Hoffmann et al., 2022](#); [Ji and Darnall, 2022](#)). Additionally, trans-municipal climate networks like the GCoM aim to support cities in coordinating mitigation and adaptation efforts ([Picavet et al., 2023](#); [Reckien et al., 2018](#)), providing another important avenue for climate action. As climate events have grown more frequent and intense in recent years, with cities being affected the most ([Dawson, 2017](#); [Field et al., 2012](#); [Pörtner et al., 2022](#)), temperature shifts and disasters may serve as tangible, omnipresent reminders of their vulnerability to climate change. This raised the question of whether cities might also turn to trans-municipal climate networks to secure resources, share knowledge, and strengthen their climate governance in response to climate threats. Thus, to assess this question, the following analysis examined the relationship between climate exposure and network participation by testing these hypotheses:

H1-A: Cities are more likely to join the GCoM when confronted with a temperature shock.

H1-B: Cities are more likely to join the GCoM when confronted with a weather-related natural disaster.

That said, it should further be considered that while climate shocks may trigger action, cities may also initially dismiss isolated events as natural variability or one-time external shocks. Consequently, repeated exposure to climate events may more effectively reinforce the connection to shifting climate patterns. As a result, cities facing more frequent climate threats may become increasingly motivated to engage in climate action and seek

support through trans-municipal climate networks, such as the GCoM. Based on these considerations, the following hypotheses are proposed:

H2-A: Cities are more likely to join the GCoM when confronted with prolonged changing temperature patterns.

H2-B: Cities are more likely to join the GCoM when confronted with repeated weather-related natural disasters.

The following analysis explored these relationships by examining both immediate shocks and long-term climatic patterns. As underlying conditions have also been shown in the literature to play a role in shaping subnational climate action, these have further been controlled for in the analysis.

3.2 Data Selection and Description

The measures used to quantitatively test the hypotheses discussed are presented following this section. Summary statistics of the incorporated variables are further provided in [Appendix B](#).

First, to establish a consistent city dataset for the analysis, the Global Human Settlement-Urban Centre Database (GHS-UCDB), provided by the European Commission's Joint Research Centre, served as the foundation (Florczyk et al., 2019). This database includes GIS boundaries for 13,135 urban centers as of 2015, each detailed with precise information on location and dimension, alongside a variety of geographical, socio-economic, and environmental variables. Urban centres within this database were defined by the authors as "high-density clusters of contiguous grid cells of 1 km² with a density of at least 1500 inhabitants per km² and a minimum population of 50000" (p. 6) (Poelman and Dijkstra, 2014), i.e. were characterized by high population figures and density, and significant built-up area. For the purposes of this analysis, 11,344 cities were selected from the original database. Cities were excluded if they had missing urban names, had substantial data gaps in explanatory variables, faced uncertainties in matching with the outcome variable, or belonged to countries without any GCoM members. The latter was necessary since the subsequent analysis included country-fixed effects, which would then fully absorb their variation. The selected cities spanned a wide geographical distribution, including 2,273 in Africa, 6,892 in Asia, 1,006 in Europe, 771 in Latin America and the Caribbean, 323 in North America, and 79 in Oceania, which allowed for the examination of the research question from a global perspective.

At the beginning of the analysis, each urban centre within the GHS-UCDB was assigned to having a GCoM membership, if applicable. The matching process involved geocoded

data from the GCoM's website ([Global Covenant of Mayors for Climate & Energy, n.d.a](#)), although this presented challenges due to missing or incorrect spatial information (e.g., Freiburg im Breisgau having coordinates that put it 500 km off). A two-step matching process was therefore applied to address these issues. First, a spatial join was conducted between the GHS-UCDB boundaries and the GCoM shapefile. To ensure consistency, the urban names from the matches within the GCoM dataset were compared to those in the GHS-UCDB. For this purpose, the names were standardized by converting them to lowercase and removing accents and punctuation. Afterward, the results were manually verified before being deemed safe matches. Secondly, a reverse matching process was applied to further address errors in the spatial information within the GCoM dataset. This entailed pairing unmatched GHS-UCDB cities from the first matching process with the GCoM data, based on urban names and country codes, before spatially filtering them. The latter was done by excluding cities matched previously by name if they had a location mismatch exceeding 20 km from the urban centre boundary to the GCoM coordinate. Cities successfully matched by both name and location were then added to the safe matches, while those meeting only one criterion were considered uncertain and removed from the analysis (338 cities). It needs to be noted that some GCoM cities had multiple matches within the GHS-UCDB, as certain members were districts rather than whole cities (e.g., Dhaka North and Dhaka South). In such instances, only the earliest match in terms of timing was retained. This processing resulted in 1,126 GCoM members within the GHS-UCDB sample (approximately 10 percent), which had joined from its initiation as the EU Covenant of Mayors in 2008 to March 2024, corresponding to a 0.53 percentage seasonal probability for all cities to join the GCoM. For the subsequent analysis, the data was structured as a panel data frame, segmented into bi-seasonal periods (hot: from March to September; and cold: from October to April) from 2008 to 2024. The event of joining the GCoM was represented as a binary indicator, coded as "1" if an urban centre joined during the respective season and "0" if it did not.

Moreover, since the analysis focused on exposure to climate change, including among others temperature shocks, data on temperature readings served as a natural proxy. However, to distinguish natural variability from long-term climate trends, the analysis focused on deviations from historical climate patterns using anomaly measures. A positive anomaly would indicate temperatures above the baseline average, reflecting warmer conditions, while a negative anomaly would mean colder temperatures relative to the baseline. To this end, data from the Global Historical Climatology Network Version 4 (GHCNv4), which integrates information from over 25,000 weather stations and provided by the Goddard Institute for Space Studies Surface Temperature Analysis ([GISTEMP Team, 2024](#); [Lenssen et al., 2024](#)) was included. The GHCN temperature anomaly data was calculated as the average deviation (degrees Celsius) from a baseline over a given reference period. The baseline period was set from 1981 to 2010 and was

chosen to align closely with the observation period so that perceived climatic differences are within a timeframe still relevant to current city populations, whereas the reference period spanned the given season in the observation period. Anomalies were computed separately for the hot and cold seasons to account for seasonal differences. The hot season spanned from April to September, while the cold season spanned from October to March of the following year. GHCN temperature anomalies were then joined with the GHS-UCDB by calculating mean temperature anomalies within each city boundary. Furthermore, [Hoffmann, Muttarak, Peisker et al. \(2022\)](#) highlighted the different implications coming from positive and negative temperature anomalies. While climate change is often associated with rising temperatures and prolonged heatwaves, it also intensifies coldwaves, both having distinct environmental, social, and policy implications. Hence, anomalies were also disaggregated into positive and negative values, setting negative anomalies to zero when calculating positive anomalies and vice versa.

Additionally, the analysis incorporated another anomaly measure using the Universal Thermal Climate Index (UTCI), obtained from the ERA5-HEAT database provided by the European Centre for Medium-Range Weather Forecasts (ECMWF) through the Copernicus Climate Change Service ([Di Napoli et al., 2021](#)). UTCI is an index that extends temperature measures to include further humidity, wind, clothing insulation, and solar radiation to capture the climate as perceived by the human body ([Fiala et al., 2012](#)), and was also applied, among others, in [Hoffmann, Muttarak, Peisker et al. \(2022\)](#). However, it should be noted that UTCI has limitations, as it represents reanalysis data derived from an energy-balance model ([Dell et al., 2014](#); [Fiala et al., 2012](#)). In contrast, the GHCN temperature data is based on real weather station observations, though it can be less accurate in areas with sparse station coverage. While reanalysis improves data availability in such regions, it remains a model output and cannot fully match the accuracy of direct observations ([Dell et al., 2014](#)), which is why including both in the subsequent analysis can overcome these gaps. To integrate UTCI into the analysis, data was extracted from the NetCDF files containing daily UTCI values for 24 hours for the period 1981–2024. Before processing, UTCI values were converted from Kelvin to Celsius by subtracting 273.14 before averaging the 24 raster bands to a single daily value band ([Di Napoli et al., 2021](#)). These were then aggregated over the GHS-UCDB polygons to obtain the daily mean UTCI for each urban centre. Anomalies were then computed by establishing a baseline for hot and cold seasons, averaging data from 1981 to 2010 for each urban boundary. For the observation period, the respective hot and cold season means were then calculated, and anomalies were determined as their deviations from the baseline. Finally, as with the GHCN temperature data, crude, positive, and negative anomalies per urban centre were derived.

Moreover, the availability of daily UTCI data enabled the computation of extreme temperature deviations as a measure of temperature shocks and spells. Heat and cold

shocks were identified by first calculating the 95th and 5th percentiles of UTCI from 1981 to 2010 using a rolling 30-day window for each urban boundary. A day within the observation period was then classified as a heat shock if its UTCI exceeded the 95th percentile and a cold shock if it fell below the 5th percentile of its 30-day baseline. Furthermore, spells were defined based on consecutive shocks. A heat spell was identified as three or more consecutive days of heat shocks, while a cold spell was defined as three or more consecutive days of cold shocks. This follows the application in [Hoffmann, Muttarak, Peisker et al. \(2022\)](#). The shocks and spells were then aggregated to capture the total number of heat and cold shocks and spells experienced by each urban centre in each season within the observation period.

Since the analysis also considered exposure to natural disasters, data from the Emergency Events Database (EM-DAT) ([Centre for Research on the Epidemiology of Disasters, 2024](#)), which has been widely used in research, including in the studies by [Rowan \(2022\)](#) and [Nohrstedt, Hileman, Mazzoleni et al. \(2022\)](#), was incorporated. EM-DAT records significant disaster events based on having at least ten fatalities, 100 or more people affected, a declared state of emergency, or an international assistance request ([Centre for Research on the Epidemiology of Disasters, n.d.b](#)). To ensure that only disasters potentially related to climate change were considered, the focus was on the three primary EM-DAT disaster categories: hydrological (floods, including coastal and riverine), meteorological (storms and extreme temperatures), and climatological (wildfires and droughts). EM-DAT has aligned all data from 2000 onwards with the Global Administrative Unit Layers (GAUL) ([Food and Agriculture Organization of the United Nations, 2018](#)) at the Admin-1 (e.g., regions) and Admin-2 (e.g., cities, districts) levels, which was particularly useful for integrating the database with the GHS-UCDB. Thus, to incorporate the EM-DAT into the analysis, the GAUL layer was first spatially joined with the GHS-UCDB, which assigned each urban boundary its corresponding Admin-1 and Admin-2 codes. The two databases were then merged by matching disaster events to Admin-2 codes where available, otherwise to Admin-1 codes, following the recommendations described in the EM-DAT documentation ([Centre for Research on the Epidemiology of Disasters, n.d.c](#)). It should be noted that the administrative boundaries, particularly in cases where second-level ones were missing, often covered larger areas than the actual disaster impact. This led to spatial overcounting, where some disasters recorded within GHS-UCDB boundaries may have occurred near, rather than directly within urban centres. This introduced a measurement error, which is acknowledged as a limitation of this approach. Nonetheless, nearby disasters may remind urban centres of their own vulnerability and including them may still prove valuable. Moreover, substantial missing data was observed in the human impact variables after matching with the GHS-UCDB panel: 87% of records lacked information on homelessness, 86% on insured damages (USD), 77% on injuries, 41% on total damages (USD), 41% on affected

populations, 27% on total affected individuals, and 10% on fatalities (see [Appendix C](#)). Previous research (e.g., [Jones, Kharb and Tubeuf \(2023\)](#)) highlighted the risks of relying on incomplete disaster data, and therefore, the analysis focused on disaster occurrences and fatalities, despite the latter having 10% of missingness. Death figures were averaged over the corresponding seasonal period to address this issue rather than relying on individual event counts, which would have been more intuitive. To further reduce bias, cities with more than five missing records over the observation period were excluded from the estimations involving disaster-related deaths. Finally, the start date of each disaster was used to assign its corresponding season and integrate it into the panel data frame. Moreover, since it was shown in previous research that different type of disasters had different implications for climate action ([Gabbe et al., 2024](#); [Ji and Darnall, 2022](#)), this process was repeated for hydrological, climatological, and meteorological disasters. This resulted in the seasonal weather-related (crude and disaggregated considering hydrological, meteorological, and climatological disaster) disaster occurrences and associated average fatalities experienced by each urban centre. The fatality figures were further adjusted in the analysis by applying a log transformation.

Beyond the presented exposure measures, the analysis incorporated additional controls informed by the literature on urban climate action.

For instance, to account for the potential influence of sea-level rise on network participation, as highlighted by [Reckien, Flacke, Olazabal and Heidrich \(2015\)](#) and [Zahran, Brody, Vedlitz, Grover and Miller \(2008a\)](#), the Low Elevation Coastal Zone (LECZ) layer from the Socioeconomic Data and Applications Center (SEDAC) ([CIESIN, Columbia University, 2013](#)) was included in the analysis. The LECZ dataset identifies coastal areas below 10 and 5 meters in elevation. An overlap analysis was conducted to integrate this measure with the GHS-UCDB, calculating the percentage of each city's boundary that intersected with a low-elevation coastal zone of less than 10 meters above sea level.

Moreover, the analysis included species threatened by climate change as a proxy for eco-sensitivity since cities may be more inclined to engage in climate action, such as joining the GCoM, driven by the need to protect their ecosystems, as was discussed in [Zahran, Grover, Brody and Vedlitz \(2008b\)](#). Hence, spatial data from the International Union for Conservation of Nature Red List ([International Union for Conservation of Nature, 2023](#)), which maps the distribution of species threatened by climate change, was spatially joined with GHS-UCDB boundaries to determine the count of endangered species within each urban area.

Furthermore, as previously determined by [Nohrstedt, Hileman, Mazzoleni et al. \(2022\)](#), [Reckien, Flacke, Olazabal and Heidrich \(2015\)](#), [Zahran, Grover, Brody and Vedlitz \(2008b\)](#), and [Zahran, Brody, Vedlitz, Grover and Miller \(2008a\)](#) city-level affluence may be an important determinant of climate action. To this end, the analysis incorporated the

Human Development Index (HDI), which measures three dimensions: economic conditions (GNI per capita, adjusted for purchasing power parity), education (mean years of schooling), and health (life expectancy) (United Nations Development Programme, n.d.). Given its strong correlation with governance quality and GDP (Stryzhak et al., 2022), and its inclusion of education levels, which was also linked to greater support for climate policies (Zahran et al., 2008a,b), HDI was preferred over GDP as a more comprehensive indicator of city-level affluence. Kummu, Taka and Guillaume (2018) improved HDI estimates by breaking down national data into a detailed grid using population distribution and information on the level of infrastructure, which enhanced typical country-level HDI measures. This gridded HDI data was then spatially merged with the GHS-UCDB boundaries to calculate the average HDI values within each urban centre, with its logarithmic transformation included in the subsequent analysis.

Additionally, since capital cities often act as innovative hubs and frontrunners in climate action, their influence may extend to nearby urban areas (Orttung, 2019). To account for spillover effects from capital cities, the analysis included the logarithm of each urban centre's travel time to the national capital (in minutes, excluding flights), which was already available in the GHS-UCDB (Weiss et al., 2018).

The analysis further included city size as a control variable, acknowledging that larger cities with denser populations face more significant climate threats but often have more resources to implement climate initiatives. The positive relationship between city size and climate action has been further established in the empirical literature by Reckien, Flacke, Olazabal and Heidrich (2015), Salvia et al. (2021a), and was theoretically supported in Eisenack (2024). Thus, city size was controlled by including a logarithmic transformation of the polygon size of each urban centre.

Moreover, Zahran, Brody, Vedlitz, Grover and Miller (2008a) highlighted that cities with high industrial activity may rely more on carbon-intensive industries, creating conflicts of interest that hinder climate action. To account for this, the analysis included non-short-cycle industry CO emissions from the European Commission's Emissions Database for Global Atmospheric Research (EDGAR v4.3.2) (Crippa et al., 2018), which was pre-included in the GHS-UCDB for the year 2012. Non-short-cycle emissions come from fossil fuels that have been stored for millions of years. When burned, they release CO that has been long removed from the atmosphere. In contrast, short-cycle emissions are part of the natural carbon cycle and can be absorbed by vegetation within years or decades (National Aeronautics and Space Administration, NASA). This measure was further standardized per capita to ensure comparability across cities before a logarithmic transformation was applied in the analysis.

Finally, data on fine particulate matter was included to account for the potential role of air pollution on climate action. Since fine particulate matter can penetrate the lungs and bloodstreams and therefore pose serious health risks for urban populations (Xing et al.,

2016), cities with higher pollution levels may face greater pressure to address environmental concerns and take on climate action. Thus, the logarithmic transformation of PM_{2.5} concentration levels for each urban centre in 2014, which were already available in the GHS-UCDB and originally sourced from the Global Burden of Disease ([Global Burden of Disease Collaborative Network, 2017](#)), was included in the analysis.

3.3 Empirical Models

To test the hypotheses presented in [section 3.1](#), the subsequent analysis applied discrete-time survival models which estimated the seasonal likelihood of cities in the GHS-UCDB sample joining the GCoM, provided they had not done so before. Discrete-time survival analysis was suitable for this analysis, as GCoM participation is a one-time event per city, which this method can accommodate. Moreover, it handles time-to-event data in discrete intervals, which aligned with the fixed seasonal observation periods ([Allison, 1982](#); [Tutz and Schmid, 2016](#)). Another advantage of this method is that it didn't require the hazard, i.e., the probability of a city joining the GCoM at a given season, to be proportional (referring to the risk of an event occurring when all covariates are set to zero being constant) across all time points ([Suresh et al., 2022](#)). Instead, it allowed for the probability of participation to vary at different time intervals, which was important in this case, as external factors, such as growing awareness of the GCoM with time, may influence its participation rate. Moreover, discrete-time modeling can handle right censoring, allowing for cities that may join after the observation period but whose exact timing remains unknown, to be included ([Tutz and Schmid, 2016](#)). Additionally, this approach can easily be implemented using logistic regression, where the log-odds of joining the GCoM in each period would be estimated as a function of time and other covariates ([Tutz and Schmid, 2016](#)).

Due to their different eligibility periods, the following estimations were conducted separately for European and non-European cities. European cities became eligible in 2008, resulting in 33 seasons during which they were at risk of joining, while non-European cities could join only from 2014, i.e., their at-risk period covered 19 seasons ([European Commission, 2016](#); [Reckien et al., 2018](#)). While differences in time at risk, which is known as left truncation, are generally not an issue in discrete-time survival analysis ([Tutz and Schmid, 2016](#)), the subsequent analysis modelled each season as a fixed effect. By incorporating time at risk as a fixed effect, the model estimated a logit-hazard rate that varied across periods while also allowing for time-fixed effects, which further permitted to control for differences in exposure between hot and cold seasons, as well as other unobserved time-related factors. For these reasons, European and non-European cities were estimated separately. Moreover, to reduce omitted variable bias, and to control for national differences in climate policies, and approximate the underlying socio-economic

factors, and governance conditions, which have been previously shown to shape climate action, country-fixed effects were included in the analysis. This resulted in the following model specification which presents the estimated discrete-time survival model with a logit link function, time-varying exposure variable, fixed covariates, and country-fixed effects:

$$\text{logit}(h_{it}) = \alpha_t + \gamma_i + \beta X_{it} + \delta Z_i + \epsilon_{it} \quad (3.1)$$

In which the hazard probability h_{it} represents the likelihood that city i joins the GCoM at time t conditional on not having joined before. The model includes time fixed effects α_t to account for the baseline hazard varying across time periods and country fixed effects γ_i to control for unobserved country-level factors. The main explanatory variable X_{it} represents the time-varying exposure measure (e.g., GHCN or UTCI temperature anomalies, UTCI cold or heat shocks and spells, the number of natural disasters crude, or disaggregated, or the logarithm of deaths from disasters), whose effect on participation is reflected in the coefficient β . Additionally, Z_i represents the set of time-invariant city-level covariates, with their respective coefficients denoted by δ , while ϵ_{it} denotes the error terms. It should be noted that the estimation presented in Equation 3.1 was extended to assess the role of exposure over different time horizons, with an additional model incorporating a one-period lag of the exposure variables $X_{i,t-1}$ to account for potential delays in bureaucratic decision-making following a climate shock. Moreover, to test for more persistent effects, further specifications also included six-period ($\frac{1}{6} \sum_{t-5}^t X_{it}$) and twelve-period ($\frac{1}{12} \sum_{t-11}^t X_{it}$) lagged means.

Spatial autocorrelation in the exposure variables was another concern in this analysis. If cities close to one another have similar characteristics, they may also exhibit similar probabilities of joining the GCoM, potentially leading to member cities being clustered in space. This aligned with Tobler's First Law of Geography, which stated that "*Everything is related to everything else, but near things are more related than distant things*" (Miller, 2004, p 284). As Lichstein et al. (2002) has noted, spatial autocorrelation could pose a significant problem in an estimation since its presence violates the assumption of the independence of the observation and thus of the residuals. This would lead to an underestimation of the sum of squared errors and an inflated test statistic, potentially distorting the estimated effects of exposure on GCoM participation. To this end the Moran's I statistics were computed to assess whether GCoM membership and the exposure variables exhibited spatial autocorrelation. Moran I is a correlation coefficient ranging from -1 to +1 and measures whether a variable tends to be spatially clustered or randomly distributed. When the statistic takes a positive value, all similar values appear together, while with a negative value, distinct values appear in close association. Cliff and Ord (1981) defined the statistic as follows:

$$I = \left(\frac{N}{W} \right) \times \frac{\left(\sum_i \sum_j w_{ij} (x_i - \bar{x})(x_j - \bar{x}) \right)}{\sum_i (x_i - \bar{x})^2} \quad (3.2)$$

Where N represents the total number of observations (cities), x_i and x_j are the values of the variable of interest for cities i and j , and \bar{x} is the mean of this variable. The spatial weight matrix w_{ij} defines the relationship between cities i and j , while W is the sum of all spatial weights.

Moran's I was computed separately for each season, across multiple distance bands (0-500 km, 500-1000 km, 1000-1500 km, 1500-2000 km, and 2000-2500 km), for all exposure measures and the outcome variable, GCoM participation. All results revealed to be highly significant, and Moran's I was then averaged across all seasons to provide an overall estimate of the correlation. As shown in [Appendix C](#), substantial spatial autocorrelation in both exposure measures and GCoM participation was observed. Additionally, since neighboring regions often share similar socioeconomic characteristics and climate conditions ([Dell et al., 2014](#); [Rowan, 2022](#)), this type of spatial dependence should also be considered.

Since spatial autocorrelation was present in both the exposure and outcome variables, each model was estimated using Conley robust standard errors. Instead of assuming that residuals are entirely independent, Conley standard errors account for spatial correlation between nearby observations by applying a weighting function that determines how much influence one city's residual has on another based on their distance. This method assumes that the correlation between cities weakens as distance increases, and at a predefined cutoff distance, it is assumed to be zero ([Conley, 1999](#)). Thus, the choice of cutoff distance is crucial. In this analysis, the distance cutoff was informed by Moran's I tests on the residuals, as detailed in [Appendix C](#). Residuals from estimations including various exposure measures were tested for spatial autocorrelation across multiple distance bands (0-500 km, 500-1000 km, 1000-1500 km, 1500-2000 km, and 2000-2500 km). A cutoff was then determined based on statistical significance ($p < 0.1$) and Moran's I values falling below an absolute threshold of 0.05, which was considered negligible autocorrelation. Spatial dependence in the residuals, if present, were all observed within the first distance band (0-500 km), which resulted in the Conley cutoff level of 500 km applied in the estimations.

Furthermore, to compare survival probabilities over the observation period, stepwise Kaplan-Meier survival curves were plotted. To this end, the Kaplan-Meier estimator was computed, which estimates the probability that a city has not yet joined the GCoM (i.e., it "survived") by a given time. The Kaplan-Meier estimator $S(t)$ is defined as ([Tutz and Schmid, 2016](#)):

$$S(t) = \prod_{j:t_j \leq t} \left(1 - \frac{d_j}{n_j}\right) \quad (3.3)$$

Where $S(t)$ represents the probability that a city remains a non-member (i.e., “survived”) at time t , d_j is the number of cities joining (i.e., “failed”) the GCoM at time t_j , and n_j is the number of cities still at risk of joining just before t_j . The estimator calculates survival probability by multiplying conditional probabilities of “surviving” each season, adjusting for the decreasing number of cities still at risk over time (Tutz and Schmid, 2016). Kaplan-Meier survival curves were plotted separately for European and non-European cities to visualize differences in their participation rates. Furthermore, Kaplan-Meier curves were computed for cities within different temperature anomalies quartiles (calculated as deviations from 2015 to 2023, with respect to the 1981-2010 baseline) for both UTCI and GHCN data, separately for European and non-European urban centres. Similarly, survival curves were also estimated for cities across different quartiles of the number of weather-related disasters experienced between 2000 and 2024.

In addition, a log-rank test was conducted to assess whether the observed differences in participation rates among groups in the Kaplan-Meier survival curves were statistically significant. The test statistic is defined as (Kalbfleisch and Prentice, 2002):

$$\chi^2 = \sum_j \left(\frac{(O_{j,1} - E_{j,1})^2}{E_{j,1}} \right) + \left(\frac{(O_{j,2} - E_{j,2})^2}{E_{j,2}} \right) \quad (3.4)$$

Where $O_{(j,k)}$ is the observed number of cities in group k (e.g., European or non-European) that joined the GCoM at time t_j , and $E_{(j,k)}$ is the expected number of cities in group k that would have joined if survival probabilities were the same across groups. The log-rank test compares observed and expected events at each time point, summing the squared differences to determine whether the survival curves diverged significantly. The test follows a chi-square distribution, with a p-value below 0.05 indicating a statistically significant difference between the survival curves (Kalbfleisch and Prentice, 2002).

Finally, one of the main challenges was isolating the effect of the exposure measures, especially when dealing with such a large dataset and geographic scope, which introduced the potential for high sensitivity in the estimates. Moreover, confounding could arise if factors influencing a city’s exposure to climate events also impacted its probability of joining the GCoM. For example, if more affluent cities also experienced higher levels of exposure, they may be more likely to join the GCoM due to their greater capacity to take climate action. In this case, the climate exposure coefficient β could be biased as it may reflect the effect of a city’s affluence rather than the effect of its exposure. Thus, to

enhance the robustness of the survival estimations, Inverse Probability Weighting (IPW) was applied. This method addressed potential confounding by reweighting observations according to their probability of experiencing a given exposure level, as determined by the covariates. Thus, it made cities comparable of their baseline characteristics, which allowed for a more accurate estimation of the relationship between climate exposure and GCoM participation. (Hirano and Imbens, 2004; Naimi et al., 2014).

Inverse probability weights were derived following recommendations for continuous treatments, using first a generalized propensity score (GPS) model to estimate the conditional density of the exposure variable based on the observed covariates (Naimi et al., 2014). These covariates aligned with those used in the discrete-time survival model in Equation 3.1. However, the specification was adjusted to account for geographical differences in exposure without overfitting. Thus, unlike the survival model, which incorporated country-fixed effects, the GPS model included broader regional fixed effects (e.g., Southern Europe, Eastern Asia). Additionally, time-fixed effects were omitted, as the GPS model did not operate within the survival framework. The GPS model followed a Gaussian specification and was estimated as follows:

$$X_{it} = \gamma_r + \beta Z_i + \epsilon_{it}, \quad \epsilon_{it} \sim N(0, \sigma^2) \quad (3.5)$$

Where X_{it} represents the continuous exposure variable (e.g., GHCN anomalies) for city i at time t . The vector Z_i includes covariates related to GCoM participation and potentially influencing exposure. γ_r represents the regional fixed effects, while the error term $\epsilon_{it} \sim N(0, \sigma^2)$ accounts for unobserved variation. From this, the GPS, representing the conditional probability density of exposure, was then derived as (Naimi et al., 2014):

$$e(X_{it}|Z_i) = \frac{1}{\sqrt{2\pi\sigma^2}} \exp\left(-\frac{(X_{it} - \hat{\gamma}_r - \beta Z_i)^2}{2\sigma^2}\right) \quad (3.6)$$

Which corresponded to the predicted probability density function of the exposure variable X_{it} conditional on the covariates Z_i and regional fixed effects γ_r . In another step, the unconditional probability density $f_x(X_{it})$ was estimated. The unconditional probability density represented the general likelihood of an exposure level across all observations in the dataset, independent of the covariates (Naimi et al., 2014). It was obtained using a Gaussian model with only an intercept as:

$$X_{it} = \mu_x + \epsilon_{it}, \quad \epsilon_{it} \sim N(0, \sigma_x^2) \quad (3.7)$$

Where, μ_x represented the unconditional mean of the exposure X_{it} , while σ_x^2 represents its variance. This allowed to derive the unconditional probability density function as

(Naimi et al., 2014):

$$f_X(X_{it}) = \frac{1}{\sqrt{2\pi\sigma_X^2}} \exp\left(-\frac{(X_{it} - \hat{\mu}_X)^2}{2\sigma_X^2}\right) \quad (3.8)$$

And finally, the so-called stabilized inverse probability weights were computed as (Naimi et al., 2014):

$$w_i = \frac{f_X(X_{it})}{e(X_{it} | Z_i)} \quad (3.9)$$

Where $f_X(X_{it})$ represents the unconditional probability density of the exposure variable, i.e., independent of the covariates, which is the overall likelihood of exposure across all cities. While $e(X_{it} | Z_i)$ corresponds to the probability density of the exposure variable, conditioned on the included covariates (Naimi et al., 2014). By dividing these, the weights corrected for confounding, making cities more comparable in terms of the included covariates (Hirano and Imbens, 2004).

To guarantee the stability of the weights, they were further normalized to ensure that the average weight remained centered around 1, and trimmed at the 5th and 95th percentile to cap extreme values (Lee et al., 2011). Moreover, covariate balance was assessed to ensure that the weighting process successfully adjusted for confounding. This involved comparing the correlation of covariates with the exposure measure, both before and after weighting, which is presented via love plots in Appendix D. Additionally, a threshold of 0.1 on standardized mean differences (SMDs) was applied. SMDs measure the difference in the mean values of each covariate between cities with different levels of exposure, relative to the overall variability in that covariate (Greifer, 2025a). For example, if cities experiencing higher temperature anomalies also tended to have a much higher HDI than those with lower anomalies, the standard mean difference would be large, indicating imbalance. Thus, in this analysis, a SMD below 0.1 was deemed good balance, meaning the weighting successfully reduced bias in covariate distributions, while an SMD above 0.1 suggested that the weighting did not fully correct for differences, meaning potential confounding remained (Greifer, 2025a; Zhu et al., 2015). Finally, the weights were included in the initial discrete-time survival model in Equation 3.1 to estimate the effect of climate exposure on GCoM participation while accounting for confounding. All original covariates were retained, even after adjusting for confounding, to ensure double-robust estimation (Greifer, 2025b). That said, as opposed to the previous survival estimations, the coefficients from the weighted estimations were not directly interpreted, but instead, G-computation was applied to estimate treatment effects, as recommended by Greifer (2025b). This approach involved computing predicted probabilities of the outcome at

different levels of the continuous treatment variable while averaging over the covariate distribution (Greifer, 2025b). From these, average dose-response functions (ADRFs) were plotted to provide a visual representation of how predicted probabilities of GCoM participation changed across different levels of the exposure measures. These were necessary steps as misinterpreting the coefficients in the weighted model is not advised and known as the Table 2 fallacy (Greifer, 2025b; Westreich and Greenland, 2013).

Chapter 4

Results

4.1 Descriptive Analysis

The following section provides a descriptive overview of the variables used to analyze the effect of exposure to climate change on local governments' propensity to join the GCoM.

The final analyzed dataset contained 11,344 cities and their geographical distribution across the globe is displayed in [Figure 4.1](#). The countries with the most representation were India (3,247), China (1,849), Ethiopia (557), Nigeria (483), and Indonesia (391). Due to the GHS-UCDB inclusion criteria requiring urban areas to have a minimum population of 50,000, there was a disproportionate representation from countries with larger urban populations. However, no adjustments were made, as the sample was considered representative of the global distribution of cities. Furthermore, the included country-fixed effects in the subsequent analysis were deemed to account for this.

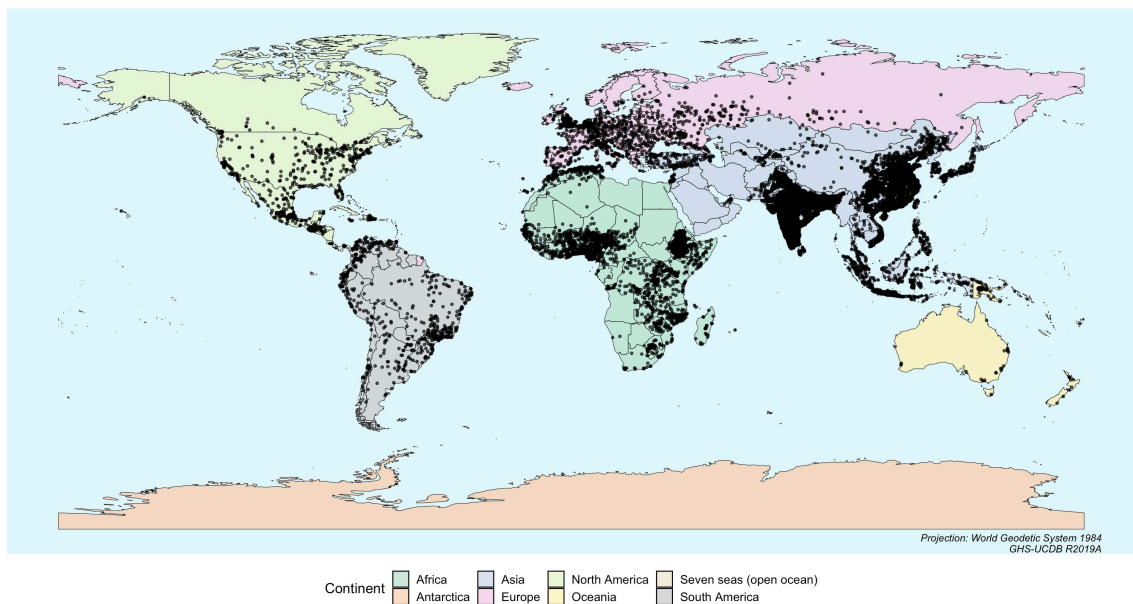


FIGURE 4.1: Distribution of GHS Urban Centres in Sample

Regarding the distribution of GCoM member cities by country, Italy had the highest membership in the sample, with 83 cities, followed by the United States with 78. Spain and Ukraine each had 60 member cities, Brazil had 59, and Mexico and France had 44 and 40, respectively. Argentina (34), the United Kingdom (31), and Germany (29) completed the top ten. Several countries exhibited a high overall presence of GCoM member cities, with almost all cities included in the sample from Italy, France, Ukraine, and Spain being members.

Of the 11,344 urban centres considered, 1,126 had joined the GCoM by March 2024, accounting for approximately 10 percent of the sample. Figure 4.2 illustrates the adherence of these cities by hot and cold seasons, categorized by continent. The EU Covenant of Mayors, launched in January 2008, initially targeted European cities (European Commission, 2016), as visible in the left portion of the graph. Membership surged from October 2008 to March 2009, followed by a gradual but slower increase among European cities until the launch of the UN Compact of Mayors in September 2014 (Reckien et al., 2018). Following this, some Latin American cities joined immediately, while cities in North America, Asia, Africa, and Oceania began participating in the following season. From 2015/2016 onward, membership growth in North America, Europe, and Oceania slowed, while cities in Asia, Africa, and Latin America & the Caribbean continued to join. By the end of the observation period, European urban centres remained dominant, accounting for nearly half (501) of all GCoM members, most of whom had joined before the launch of the GCoM in 2016. Nonetheless, participation was geographically diverse and included 137 African cities, 174 Asian cities, 202 in Latin America and the Caribbean, 96 in North America, and 16 in Oceania.

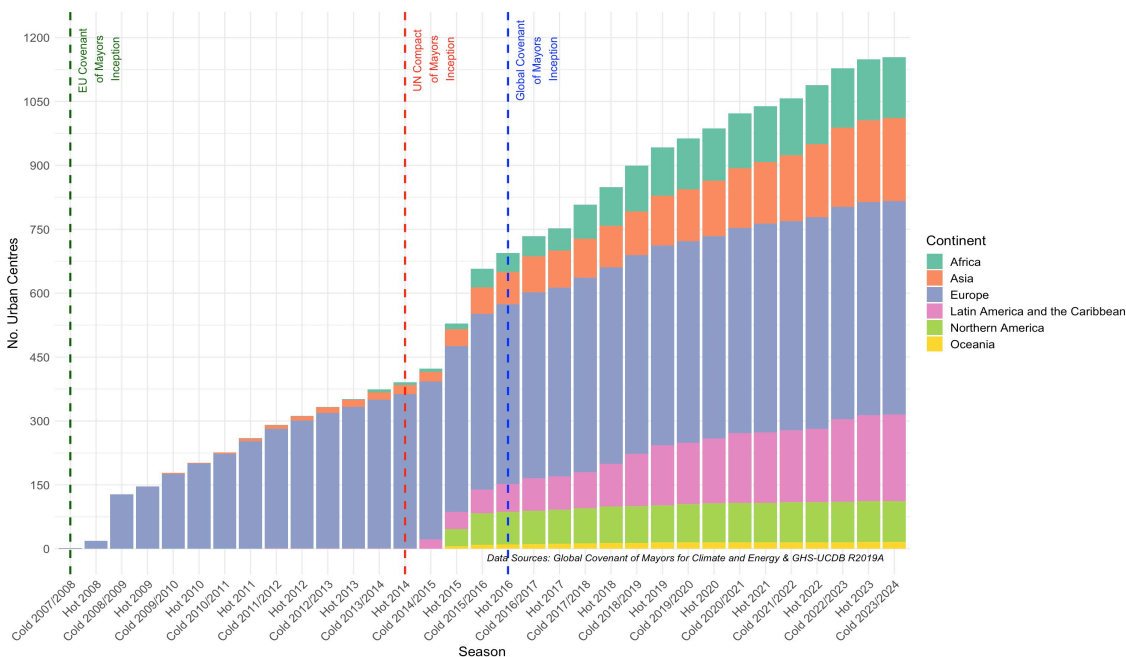


FIGURE 4.2: Adherence to the Global Covenant of Mayors in Sample of GHS Urban Centres, by Season (Hot/Cold) & Continent

To further highlight the geographical reach of the GCoM, the map in [Figure 4.3](#) displays the distribution of GCoM member cities within the GHS-UCDB sample in red dots. A high concentration of members is notable in Europe, across all countries except for Russia. Furthermore, GCoM membership expanded beyond Europe: In North America, participation is widespread, particularly in the United States and Mexico, while in Latin America, it is broadly distributed across the region. Moreover, although fewer cities from Oceania were included in the sample, the map indicates that many of those were members. In contrast, while urban centres across East and Southeast Asia were densely represented in the sample, this density is not mirrored in the map, though some participation is still evident, most of which is in Japan. This was also the case for Indian, as well as for East, West, and Northern African cities, where, despite some being members, participation remained low relative to the number of cities included in the analysis.

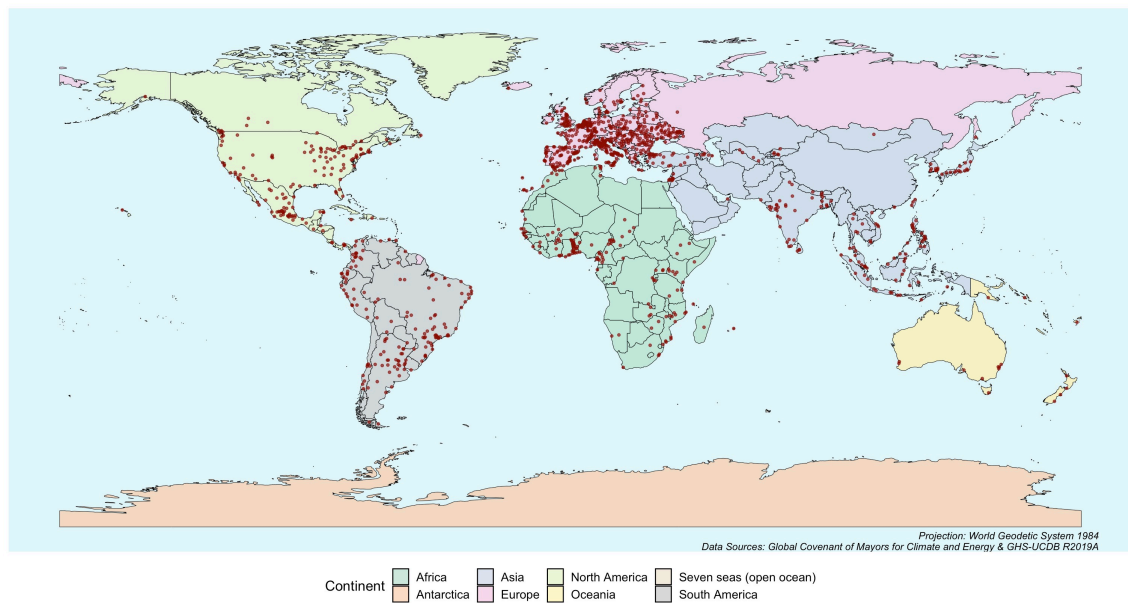


FIGURE 4.3: Global Covenant of Mayors for Climate and Energy Members within Sample of GHS Urban Centres (Data Status: March 2024)

To test the hypotheses presented in [Chapter 3.1.](#), the subsequent analysis examined whether member cities also corresponded to those with high exposure. Therefore, the focus now shifts to the exposure measures incorporated in the analysis.

The maps in [Figures 4.4](#) and [4.5](#) illustrate average surface air temperature anomalies (derived from GHCN data) and Universal Thermal Climate Index (UTCI) anomalies for the urban centres in the GHS sample, using the 1981-2010 baseline and the 2015-2023 reference period. Both maps employed the same color gradient, which ranges from -0.5 to +2 degrees Celsius, to ensure comparability. Warmer-than-baseline temperatures are represented in shades of orange and red, with darker colors indicating stronger positive anomalies. It should be noted that in the map in [Figure 4.4](#), one surface air temperature anomaly slightly exceeded the 2-degree mark in the legend, being Norilsk, Russia,

at 2.16°C. Additionally, only a few urban centres had negative anomalies: four in the GHCN data (three in Chile and one in Argentina) and six when considering UTCI data (two in Colombia, one in Chile, and three in the United States).

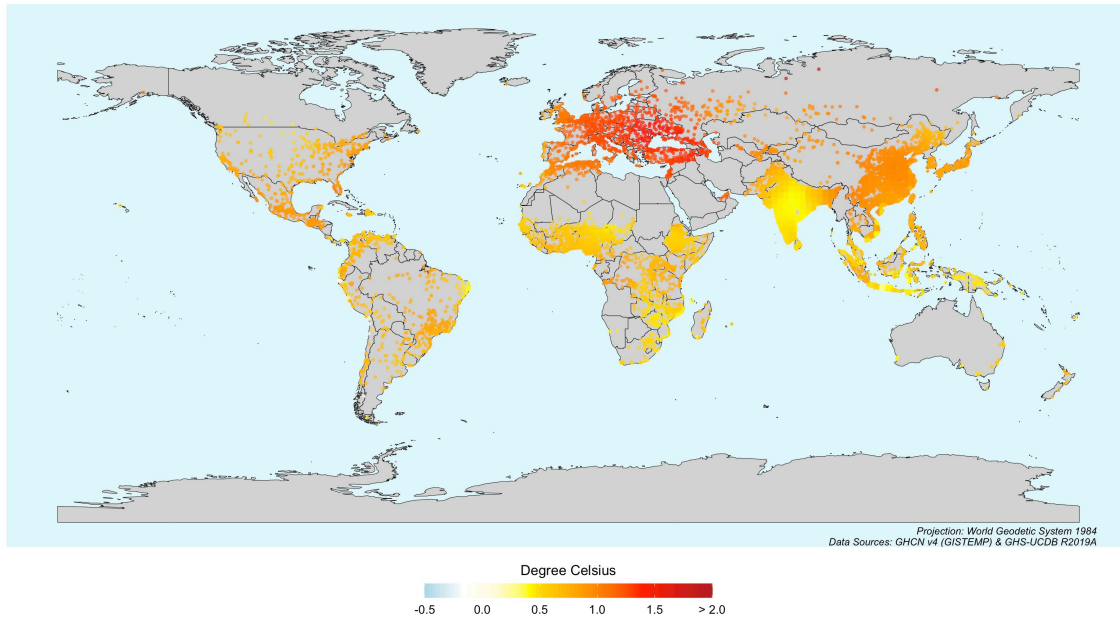


FIGURE 4.4: Average GHCN Surface Air Temperature Anomalies within Sample of GHS Urban Centres – 2015-2023 Relative to the 1981-2010 Baseline Period

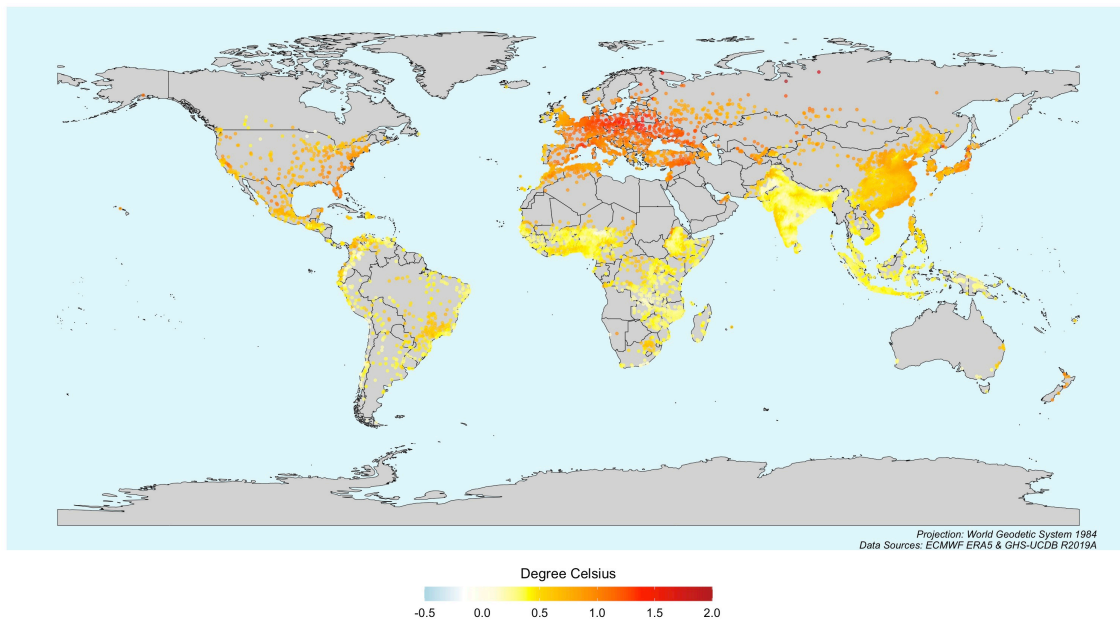


FIGURE 4.5: Average Universal Thermal Comfort Index Anomalies within Sample of GHS Urban Centres – 2015-2023 Relative to 1981-2010 Baseline Period

Both maps display similar spatial trends, showing notable global warming with the most significant deviations observed in the Northern Hemisphere, particularly in the Mediterranean and Central Europe, where most GHCN anomalies reached or even exceeded 1.5°C. Interestingly, when looking at the map in [Figure 4.5](#), which depicts UTCI anomalies, Central Europe displayed higher anomalies (approximately 1.5°C) than the Mediterranean (approximately 1.2°C), clearly distinguishing the two regions. East Asia, including China and Japan, also experienced considerable warming, with many cities having GHCN anomalies exceeding 0.8°C and UTCI anomalies above 0.5°C relative to the baseline. Urban centres in Northern Africa exhibited a similar pattern, with anomalies again being moderately more pronounced considering GHCN data than UTCI values. Northern America, and Mexico further displayed widespread anomalies ranging from approximately 0.6°C to 1 °C in both maps. Moreover, the most affected cities appeared to be located in Northern Russia, especially in Siberia, where average temperatures were 2°C above the baseline in both maps. While warming was also evident in the Southern Hemisphere, it generally remained more moderate compared to the Northern Hemisphere, which is particularly notable in the map considering UTCI anomalies. Temperature anomalies in India, Central Africa, Southeast Asia, mid-to-southern Africa, and urban centres in Latin America, except for a few localized clusters, stayed below 0.5°C based on UTCI data and below 0.8°C considering GHCN data. Urban centres in New Zealand and Australia showed a similar trend. Furthermore, it was noticeable that the map displaying UTCI anomalies has more variability than the one based on GHCN anomalies. This may be attributed to the finer spatial resolution of the UTCI data (0.5°x0.5° grid), which potentially captured more variations than the GHCN data (1°x1° grid). Additionally, anomalies were higher across many regions using GHCN data compared to UTCI data, although the overall spatial patterns remained the same. Nonetheless, both maps indicate significant global warming, with the Northern Hemisphere, particularly Europe, being more affected than the Southern Hemisphere, suggesting that cities in the Global North have the most to gain from joining the GCoM.

After having provided an overview on the spatial patterns of temperature anomalies, the plots in [Figure 4.6](#) depict their temporal trends. Temperature anomalies are displayed using GHCN and UTCI data for the GHS urban centres sample across hot and cold seasons from 2000 to 2024. Anomalies were computed relative to their respective seasonal baseline considering the period from 1981 to 2010. Cold seasonal anomalies are presented on the left, and hot seasonal anomalies are on the right, while the top row illustrates anomalies using GHCN data, and the bottom row presents UTCI anomalies. The black line in each graph denotes the overall average anomaly across all urban centres in the sample, with grey lines depicting individual city-level tracings. The blue dashed line at zero degrees serves as a reference for no deviation from the baseline, whereas the black dashed

line represents the trend. The darker shaded background marks the observation period in the analysis.

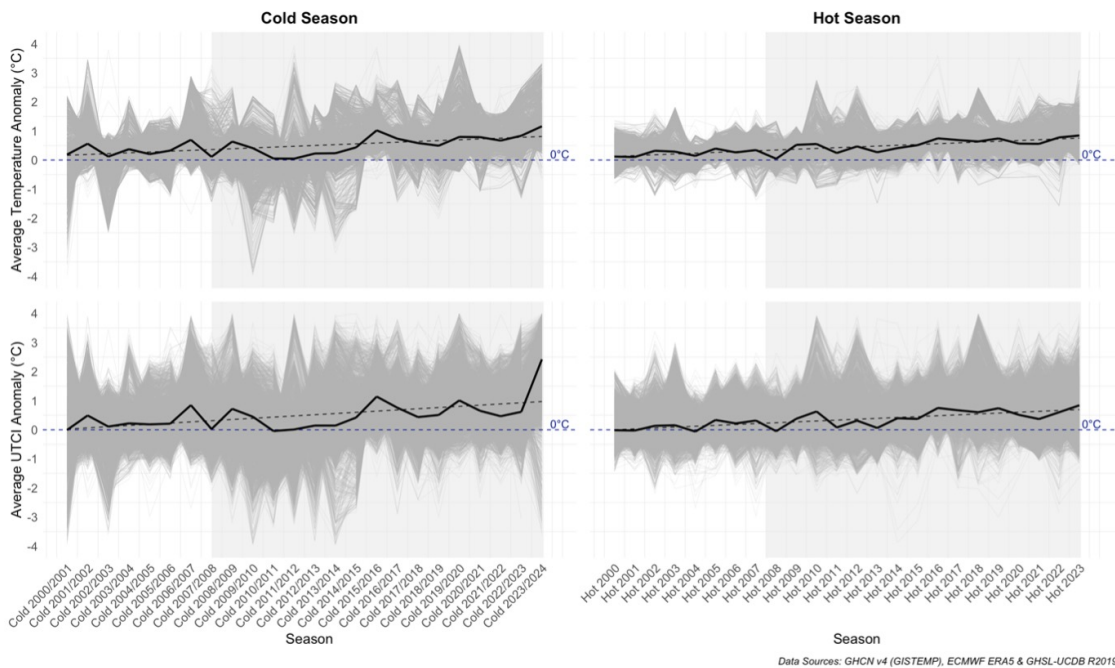


FIGURE 4.6: Temporal Trends of Average GHCN Surface Air Temperature and UTCI Anomalies within Sample of GHS Urban Centres - Hot and Cold Seasons 2000-2024 Relative to the respective 1981 Base Periods

A clear warming trend is evident across all four plots. Although anomalies fluctuated annually, both GHCN and UTCI anomalies rose over time across hot and cold seasons, as indicated by the upward-sloping trendlines, with periods of decline being less significant than those of increase. This reinforces the notion that global warming will continue in the future. Moreover, the fluctuations were more pronounced in cold seasons compared to hot seasons, with a rise in GHCN and UTCI anomalies in recent years, most notably in 2023/2024. In this season, the average GHCN anomaly in the GHS-UCDB sample was 1.3°C, while the UTCI anomaly reached 2.5°C. It is also noteworthy that despite the fluctuations, cold season anomalies remained relatively close to 0°C between 2009/2010 and 2013/2014 before increasing significantly. Similarly, hot season anomalies when considering UTCI returned to the baseline in 2013 before gradually rising again, while GHCN anomalies diverged more from the baseline starting in 2008. Moreover, although less pronounced than in cold seasons, warming trends across hot seasons were also evident, with the trend line reaching 0.7°C in GHCN anomalies and 0.6°C in UTCI anomalies by 2023. Furthermore, as shown in the previous maps illustrating spatial patterns, individual city tracings further emphasized that UTCI anomalies exhibit more variability than GHCN temperature anomalies.

Since the analysis considered both temperature deviations and natural disasters as indicators of climate change exposure, the following will shift focus to the spatial and temporal patterns of weather-related disasters.

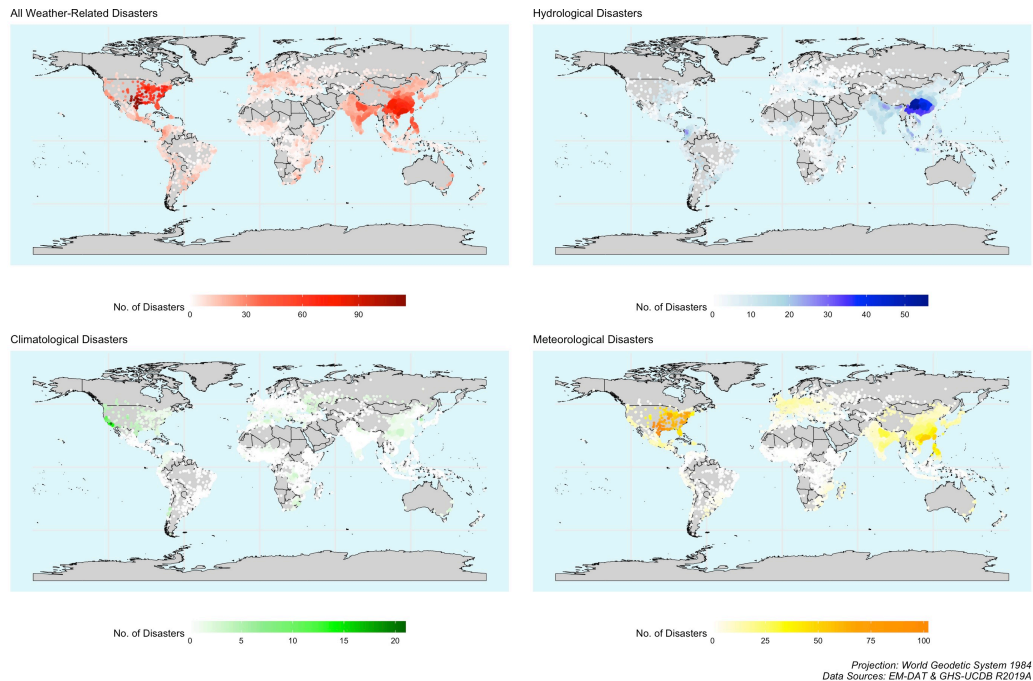


FIGURE 4.7: Weather-Related Disaster Events within Sample of GHS Urban Centres, by Type (April 2000 – March 2024)

To this end, the four maps in [Figure 4.7](#) illustrate the geographical distribution of natural disasters within the sample of GHS urban centres from April 2000 to March 2024, showing both the overall occurrence of weather-related disasters and their individual categories: hydrological, climatological, and meteorological. It is important to note that, due to the aggregation process at higher administrative levels, urban centres may be associated with disasters experienced by neighboring areas or the entire country rather than only those that directly affected them.

The first map in the top left illustrates the total number of weather-related disasters per urban centre, with darker red colors indicating a higher frequency. Clusters of high concentrations are visible in China, Southeast Asia, large parts of India, the eastern United States, and Mexico, where urban centres recorded between 70 and 100 disasters. Moderate disaster frequencies can also be observed across Central America, northern South America, and the Mediterranean region, with disaster counts ranging from 30 to 70. Furthermore, fewer disaster counts, ranging from 10 to 30 records, are noticeable in Europe and sub-Saharan Africa, while urban centres located in Russia, Canada, the Caucasus, and central Africa show little to no occurrences.

Using blue colors, the top right map visualizes hydrological disasters, including all types of floods and wet landslides. A notable concentration is observed in eastern

China, where disaster frequencies exceed 50 per urban centre. Cities surrounding east China, Vietnam, and Bangladesh also display high records, ranging between 30 and 50 occurrences. Moderate disaster frequencies are visible in parts of India, Southeast Asia, and some regions of Central and South America, with recorded occurrences ranging from 10 to 30 events. Regions with low occurrences (fewer than 10 events) are further observed in cities across Europe, Africa, North America, Russia, and Canada.

The geographical distribution of climatological disasters, which include wildfires and droughts, is highlighted in the bottom-left map using a green color gradient. Compared to other disasters, climatological events appeared significantly less frequent, with the highest concentration in parts of North America, particularly the western United States and northern Mexico, showing frequencies between 15 and 20. Moderate representation of disaster counts ranging from 5 to 10 was also found in South American (southern Brazil and Argentina), North African, Middle Eastern, Russian, and Central Asian urban centres, while the rest of the cities in the sample appeared relatively unaffected.

Finally, the last map in the bottom right displays meteorological disasters, including storms and extreme weather events, using a yellow color gradient. Notably, the south-eastern United States appears especially prone to meteorological disasters, with urban centres recording between 75 and over 100 events. Eastern China and the Philippines also show a high occurrence of disasters, with events ranging from 50 to 75. Moderate disaster occurrences, ranging from 25 to 50, are observed in cities in India, Japan, Central Europe, and Mexico. In contrast, urban centres with low to no recorded disasters are noticeable across South America, Russia, Africa, and Southeast Asia.

Consequently, the maps indicate that disasters occurred in spatial clusters, both in general and by specific categories with some areas experiencing multiple types of disasters, while others remained relatively unaffected. For instance, certain regions, such as the United States, South Asia, and Southeast Asia, experienced a high frequency of various categories of natural disasters, with meteorological and climatological events contributing to the frequency of disasters in the eastern United States, while Southeast Asia and India were primarily impacted by meteorological and hydrological disasters. In contrast, others, like Europe, Russia, and parts of Africa, had significantly fewer events, with meteorological disasters appearing as the most prevalent disaster type in Europe. Another observation was that hydrological and meteorological disasters accounted for most weather-related events, whereas climatological disasters appeared relatively rare.

After having explored the spatial patterns of disaster prevalence, the following describes their temporal trends, with the bar plot in [Figure 4.8](#) illustrating the seasonal (hot and cold) occurrence of weather-related disasters in GHS urban centres from 2000 to 2024. Disasters were categorized into climatological (green), hydrological (blue), and meteorological (orange) events, while the lines represent their trends across hot (red) and cold (blue) seasons. It is important to note that, unlike before, this plot represents a total of

5,524 disaster events across all urban centers combined. The number of disasters experienced per city, as depicted in the maps in [Figure 4.7](#), was significantly higher, as multiple cities were often affected by the same disaster simultaneously.

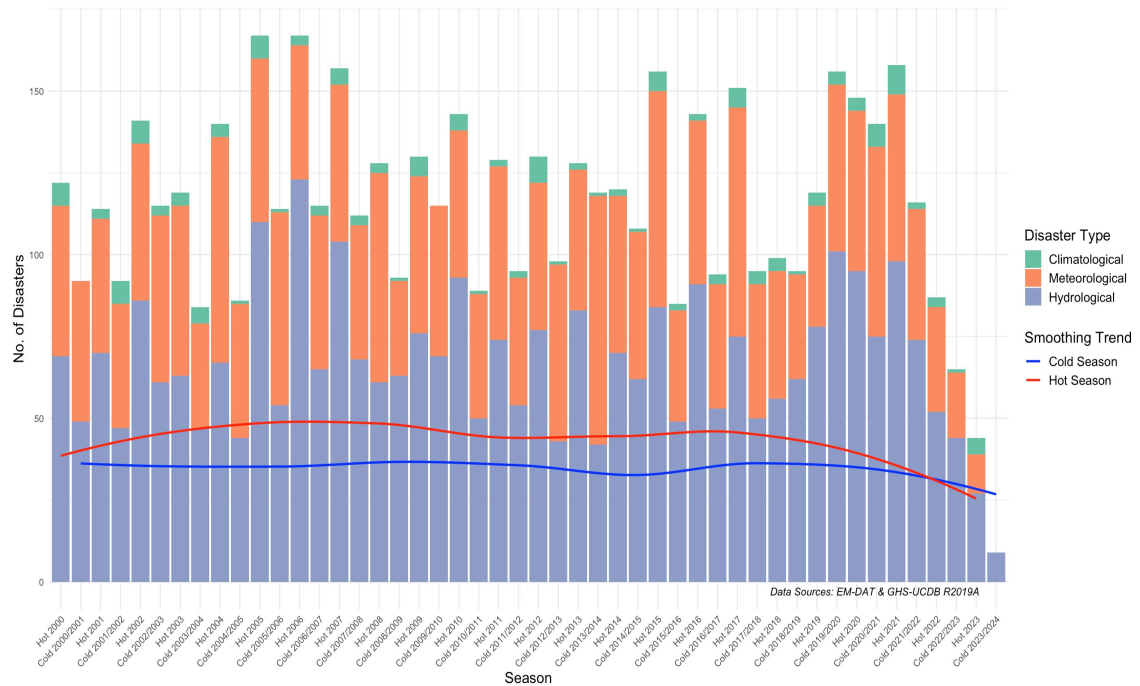


FIGURE 4.8: Weather-Related Disaster Occurrence within Sample of GHS Urban Centres, by Season (Hot/Cold 2000-2024)

Looking at the plot, it becomes apparent that hydrological disasters made up the largest share of weather-related natural disasters, followed by meteorological disasters, while climatological disasters remained relatively rare. The latter was also observed in the spatial visualization. More interestingly, no clear temporal trend emerged from 2000 to 2021, as disaster frequencies seemed to fluctuate rather than follow a consistent trajectory. The most noticeable pattern was the seasonal variation, with disaster frequencies consistently higher in hot seasons than in cold seasons from 2000 to 2022, as indicated by the trend lines. However, this gap has narrowed in recent years, with hot seasons beginning to record lower disaster frequencies than cold seasons as of 2022. Furthermore, it was notable that the more recent seasons showed a general decline in disaster events, with the most significant drop occurring in the cold season of 2023/2024. This last decline may be attributed to EM-DAT's data validation process, which finalizes figures for the current year only at the beginning of the following year and cautions its users ([Centre for Research on the Epidemiology of Disasters, n.d.a](#)). Therefore, to account for this, the last season was excluded from the subsequent analysis when considering disaster estimates.

In summary, the descriptive analysis revealed spatial trends in warming, with temperature anomalies being relatively more pronounced in the Global North than the

Global South, and significant deviations observed in Central Europe, East Asia, and the Mediterranean. Moreover, UTCI anomalies displayed more variation, potentially due to a finer spatial resolution than GHCN temperature anomalies, although both datasets showed the same global warming patterns. Additionally, temporal trends were found to reinforce the warming trend, indicating that both GHCN and UTCI anomalies steadily increased over time. This was particularly pronounced in the recent cold season, while differences in warming across seasons also became evident, with the cold seasons being relatively more affected than the hot season. Weather-related disaster data further highlighted regional patterns, with North America and South and Southeast Asia experiencing the highest occurrences. Regarding the various types of disasters, hydrological disasters dominated the sample, while meteorological disasters were also significantly represented. In contrast, climatological disasters remained rare and were more concentrated in specific regions, such as the West Coast of the United States. Moreover, the seasonal temporal trends confirmed that hot seasons generally experienced more disasters than cold seasons for most of the observation period, although this pattern shifted in recent years. However, no clear temporal trends in disaster occurrence became evident for most of the observed period from 2000 to 2024. These patterns were crucial for the subsequent survival analysis. First, fluctuations in temperature anomalies and disaster exposure were important to determine whether the timing of these climate events coincided with increased network participation. Second, regional disparities in warming and disaster frequency were examined to explore whether these spatial patterns aligned with the geographic distribution of member cities.

4.2 Survival Analysis

4.2.1 Kaplan-Meier Survival Curves

Before estimating the effect of the exposure measures on the hazard of urban centres joining the GCoM, the Kaplan-Meier survival curves in [Figure 4.9](#) provide an overview of their survival probabilities over time. The y-axis represents the survival probability (i.e., the probability that a city has not yet joined the GCoM), while the x-axis denotes the time at risk of failure (i.e., the event that a city becomes a GCoM member). The curves were computed separately for European and non-European cities due to their different eligibility periods, which may have shaped their survival probability. European cities were at risk starting from the cold season of 2007/2008, while non-European cities became eligible in the hot season of 2014. The vertical dashed line at the time at risk point 19 marks the right-censoring for non-European cities, while European cities were censored at time point 33, both corresponding to March 2024.

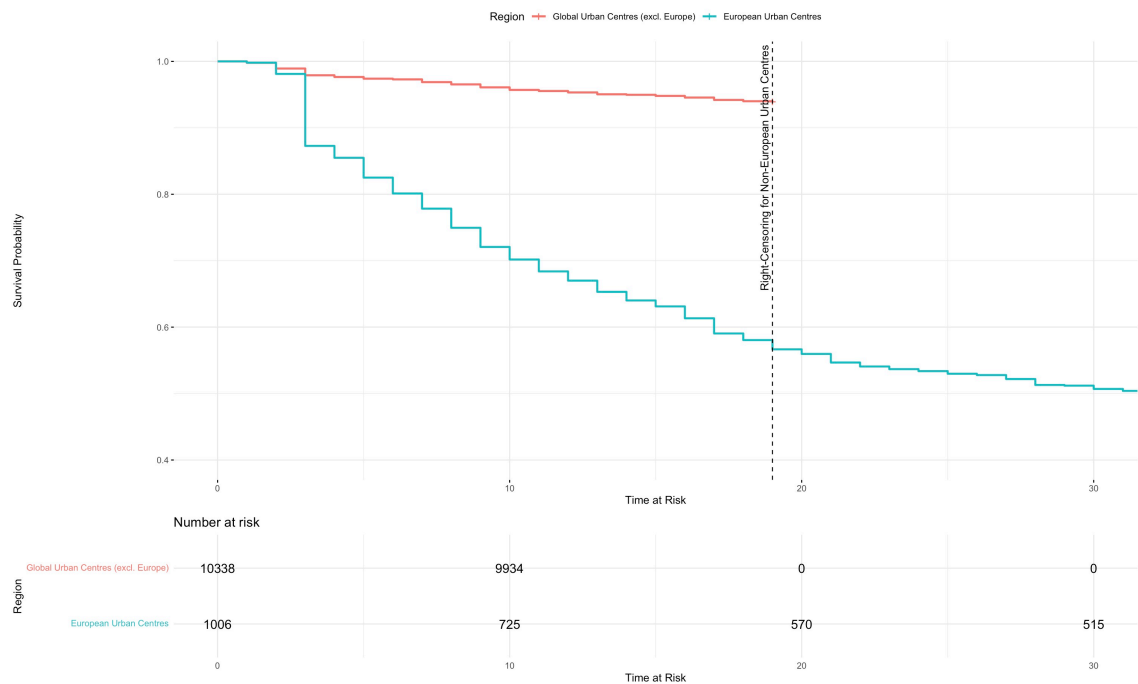


FIGURE 4.9: Kaplan-Meier Survival Curves for European & Global (excl. Europe) Urban Centres in GHS Sample

The Kaplan-Meier survival curves revealed a significantly faster participation rate among European cities (in blue) compared to global urban centres (in red). At the start of the observation period, 1,006 European cities and 10,334 global cities were at risk of joining the GCoM. Over time, participation rates diverged significantly, as indicated by the curves. For instance, by the 10th time at risk point, the survival probability for European cities dropped below 80 percent. At the same time, global cities still had a survival probability close to 95 percent. By the end of their risk periods, 50 percent of European cities had joined (i.e., 501 cities) with the number of at-risk cities declining from 1,006 at the beginning to 505. In contrast, among non-European cities, 9,718 out of 10,334 remained at risk by the end of their risk period (616 cities had joined), resulting in a survival probability of 94 percent. The log-rank test results ($\chi^2 = 1750$, $p < 0.001$) further reinforced European cities' higher overall participation rate, with European cities recording 501 GCoM memberships, significantly higher than the expected 144, while non-European cities had 616 memberships, well below the expected 981.

Since the analysis focused on how climate exposure affects GCoM participation, Kaplan-Meier survival curves were further computed according to the respective GHCN and UTCI anomaly quartiles (0-25%, 25-50%, 50-75%, 75-100%) for European and non-European urban centres, to determine if this showed significant differences in their survival probability (see [Figure 4.10](#)). The quartiles were based on the anomalies derived for the 2015-2023 reference period relative to the 1981-2010 baseline period.

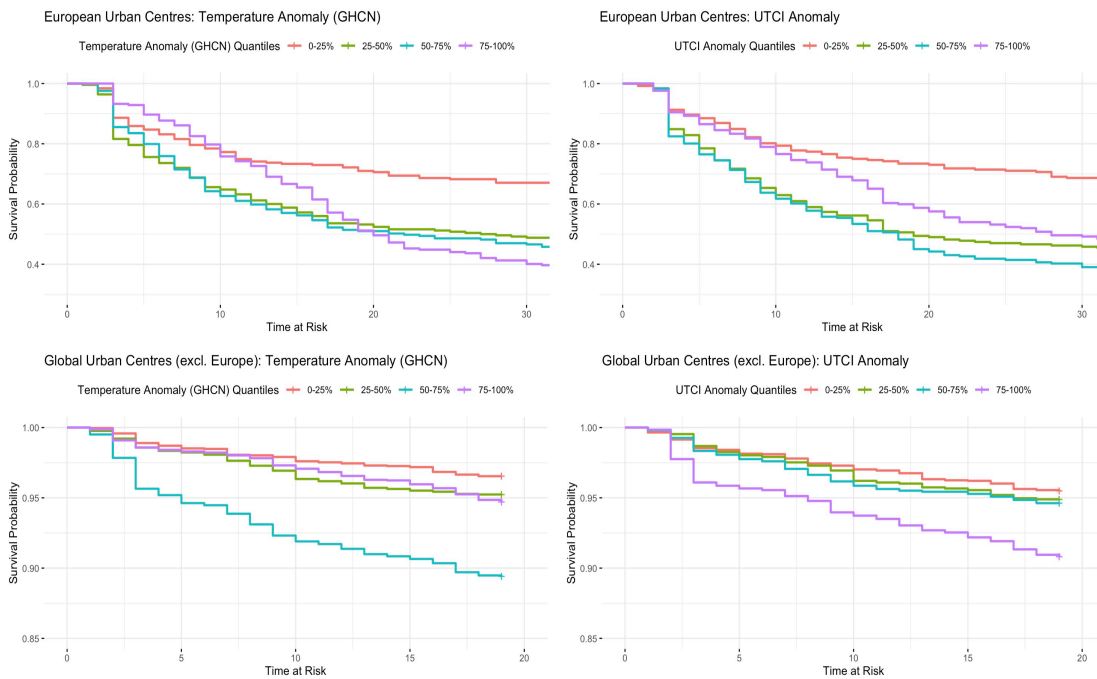


FIGURE 4.10: Kaplan-Meier Survival Curves for European & Global (excl. Europe) Urban Centres in GHS Sample, by Anomaly Quartiles

In the top-left panel, European cities were categorized into quartiles based on temperature anomalies from GHCN data. The pattern observed indicated that cities with higher temperature anomalies (in the 75–100% quartile) had a lower survival probability by the end of the observation period, suggesting they joined the GCoM more quickly. Conversely, cities in the 0–25% quartile displayed the highest survival probability, indicating a slower participation rate. Similar results were found for cities within the lowest UTCI anomalies (0–25%) in the top-right panel, which exhibited the highest survival probability. In contrast to the survival curves plotted using GHCN anomalies, cities in the highest UTCI anomaly quartile (75–100%) no longer had the lowest survival probability, which was instead observed for cities in the 50–75% quartile. Nonetheless, in both plots, the survival rate for the lowest anomaly group remained noticeably higher compared to all other groups.

Turning to non-European cities, the bottom-left panel showed that cities experiencing moderately high temperature anomalies (50–75% quartile) had the sharpest decline in survival probability, indicating a faster rate of GCoM membership. In contrast, cities in the lowest anomaly quartile (0–25%) had the highest survival probability. A similar trend was observed for UTCI anomalies in the bottom-right panel, although the 75–100% quartile now displayed a lower survival probability than the 50–75% quartile.

Thus, across all four panels, both European and non-European cities in the lowest quartile of temperature anomalies consistently showed the highest survival probability,

indicating that minimal climate anomalies were associated with lower GCoM participation. This was corroborated by the log-rank test results.

Among European cities experiencing the lowest GHCN anomalies, there were 84 observed memberships compared to 139 expected ($\chi^2 = 32$, $p < 0.001$), while UTCI anomalies showed 79 observed versus 141 expected ($\chi^2 = 46.8$, $p < 0.001$). Similarly, global cities experiencing the lowest GHCN anomalies recorded 91 observed memberships against 161 expected ($\chi^2 = 139$, $p < 0.001$), and those with low UTCI anomalies had 116 observed compared to 157 expected ($\chi^2 = 62.4$, $p < 0.001$). Hence, cities experiencing the lowest anomalies were slower in joining the GCoM across the global and European subset.

In contrast, among European cities, those in the highest GHCN anomaly quartile (75–100%) recorded 153 observed versus 129 expected memberships, while the middle quartiles (25–50% and 50–75%) exhibited smaller deviations, indicating a more balanced distribution between expected and observed values. Regarding UTCI anomalies, the effect was weaker, with the 75–100% quartile nearly balanced (132 observed vs. 131 expected), whereas the cities in the 50–75% quartile showed stronger participation (153 observed vs. 113 expected). Among global cities, those in the 50–75% quartile (279 observed versus 155 expected) had the strongest association with faster GCoM participation, while those in the 75–100% quartile (133 observed versus 154 expected) showed a weaker link. Regarding UTCI anomalies, global cities in the highest quartile (237 observed versus 153 expected) had earlier membership, whereas those in the 50–75% quartile had fewer memberships than expected (139 observed versus 153 expected). Overall, this suggested differences in participation trends between the 50–75% and 75–100% quartiles depending on whether UTCI or GHCN data were used for both European and global cities. Nonetheless, while it could not be definitively concluded that cities with the highest anomalies had lower survival probabilities, these results consistently indicated that cities experiencing the lowest anomalies were slower in joining the GCoM.

To further examine whether there were significant differences in the survival trajectories of cities affected by weather-related disasters, [Figure 4.11](#) presents Kaplan-Meier survival curves for European (top panel) and non-European (bottom panel) urban centers, divided into quartiles reflecting the number of disasters experienced from 2000 to 2024. The curves show that European urban centers within the 25–50% quartile experienced the steepest decline in survival probability. Conversely, those in the lowest quartile (0–25%) maintained the highest survival probability throughout their time at risk. Cities in the 50–75% and 75–100% quartiles followed similar survival trajectories, positioned between the lowest and the second quartiles. Regarding global urban centers, those within the lowest quartile (0–25%) exhibited the fastest decline in survival probability, while those in the 50–75% and 75–100% quartiles maintained a higher survival probability.

These results indicated that global cities with lower disaster exposure tended to join earlier, whereas in Europe, moderate disaster exposure was more closely associated with early participation. The results of the log-rank test supported this pattern. For global cities ($\chi^2 = 144$, $p < 0.001$), those in the lowest disaster quartile (0–25%) had 254 observed versus 159 expected memberships, suggesting faster participation, while higher quartiles (50–75% and 75–100%) showed a slower rate. In Europe ($\chi^2 = 34.9$, $p < 0.001$), cities within the 25–50% quartile (153 observed versus 106 expected) had the highest participation rate, whereas those in the highest quartile (75–100%) had fewer observed memberships (107 versus 126 expected). Thus, at first glance, this does not suggest associations between higher disaster frequencies and GCoM participation.

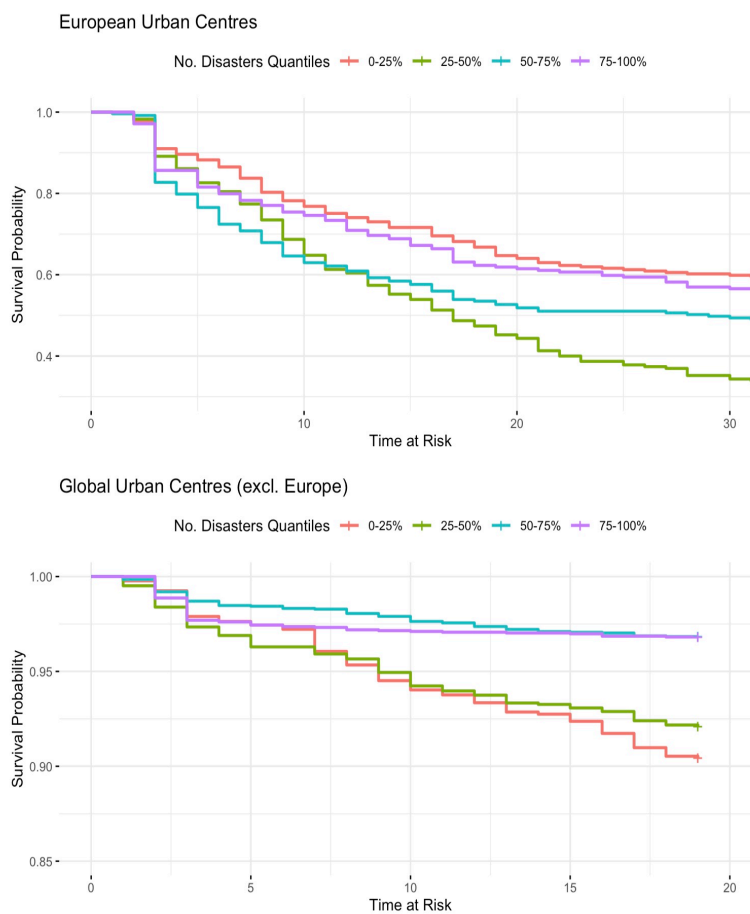


FIGURE 4.11: Kaplan-Meier Survival Curves for European & Global (excl. Europe) Urban Centres in GHS Sample, by Anomaly Quartiles

4.2.2 Baseline Estimation

Before examining the influence of the exposure measures on the hazard of urban centres joining the Global Covenant of Mayors (GCoM), the explanatory power of the factors identified in the literature was explored. This analysis was conducted separately for

European and non-European cities. The results of the discrete time survival models are presented in [Table 4.1](#), with standard errors in parentheses. All models included time at risk as a fixed effect, while Models 3 and 6 incorporated Conley standard errors with a 500 km cutoff to adjust for spatial autocorrelation. Furthermore, Model 1 was estimated without regional fixed effects, whereas Model 4 included fixed effects at the continent level. Country-fixed effects were subsequently added for Models 2, 3, 5, and 6.

TABLE 4.1: Estimation of the Effect of Control Variables on the Logit Hazard of City Participation in the GCoM

	European Urban Centres			Global Urban Centres (excl. Europe)		
	(1)	(2)	(3)	(4)	(5)	(6)
LECZ %	-0.001 (0.002)	-0.005 ** (0.003)	-0.005 *** (0.002)	-0.000 (0.002)	0.000 (0.002)	0.000 (0.002)
No. Endangered Species	0.067 *** (0.007)	0.006 (0.010)	0.006 (0.014)	0.003 *** (0.001)	0.002 ** (0.001)	0.002 * (0.001)
Log Industrial Co2/capita	-0.227 *** (0.059)	-0.143 ** (0.057)	-0.143 ** (0.058)	-0.213 *** (0.041)	-0.052 (0.066)	-0.052 (0.071)
Log PM25 concentration	-0.172 (0.185)	0.382 (0.314)	0.382 (0.400)	-0.482 *** (0.090)	-0.419 *** (0.128)	-0.419 *** (0.134)
Log HDI 2015	0.209 (0.756)	4.591 ** (2.339)	4.591 * (2.578)	1.525 *** (0.387)	1.002 (0.660)	1.002 (0.840)
Log Area (km2)	0.416 *** (0.071)	0.846 *** (0.079)	0.846 *** (0.141)	1.037 *** (0.046)	1.157 *** (0.064)	1.157 *** (0.060)
Log Mins. to Capital	-0.087 *** (0.021)	0.023 (0.026)	0.023 (0.034)	-0.081 *** (0.018)	0.022 (0.024)	0.022 (0.028)
N	21879	21879	21879	189455	189455	189455
No. Cities	1006	1006	1006	10338	10338	10338
No. Periods	33	33	33	19	19	19
Region Fixed Effect	-	Country	Country	Continent	Country	Country
Conley Cut-Off	-	-	500 km	-	-	500 km
McFadden R2	0.117	0.211	0.211	0.245	0.304	0.304
AIC	4215.673	3771.448	3771.448	6329.399	5833.873	5833.873

*** p < 0.01; ** p < 0.05; * p < 0.1.

The results for European urban centres (Models 1 to 3) indicated that the percentage of an area in a low-elevation coastal zone was negatively associated with joining the GCoM when country-fixed effects were included (Models 2 and 3). This aligned with the findings from [Reckien, Flacke, Olazabal and Heidrich \(2015\)](#), although the effect size was small (-0.005). Regarding the number of endangered species, the coefficient initially showed a significant positive association with participation in Model 1 (0.067, p<0.01). However, this significance disappeared once country-fixed effects were introduced. This could have meant that country-level factors drove the effect, or that within-country

variation was too small and absorbed by the fixed effects. Moreover, higher industrial CO₂ emissions per capita appeared to be significantly negatively correlated with GCoM participation across all models (-0.227, $p < 0.01$; -0.143, $p < 0.05$; -0.143, $p < 0.05$). This aligned with previous findings from [Zahran, Brody, Vedlitz, Grover and Miller \(2008a\)](#), which stated that cities with a high reliance on carbon-intensive industries were more averse to climate action. In contrast, regarding PM_{2.5} concentration, no clear link between air pollution levels and GCoM membership was found. More notably, the estimate for HDI demonstrated a significant positive association with GCoM membership once country-fixed effects were included (Models 2 and 3: 4.591, $p < 0.05$), indicating that cities in more developed areas of a country were more likely to join. However, this finding was unexpected, as the estimate did not appear significant in the model without fixed effects, which would have in turn suggested a stronger association with participation when comparing cities across different countries rather than within them. Conversely, city area size showed a consistently strong and significant positive association across all models, with estimates ranging from 0.416 to 0.846 ($p < 0.01$), providing further evidence that larger urban centres were more inclined to take climate action. Finally, the effect of distance to the capital was small and negative in Model 1 (-0.087, $p < 0.1$), implying that being further away from the capital negatively influenced participation. However, this effect became insignificant when country-fixed effects were applied, suggesting that national-level factors better explained variations in participation.

Turning to Models 4 to 6, which present the findings for non-European cities, similarities between the two groups emerged, particularly in the persistent significance of city area size, with larger cities consistently more inclined to join the GCoM across all estimations (1.037, $p < 0.01$; 1.157, $p < 0.01$; 1.157, $p < 0.01$). Furthermore, the initial significance of the estimate for distance to the capital in Model 4 (-0.081, $p < 0.01$) disappeared once country-fixed effects were included, similar to the findings for European cities. However, some patterns diverged, with the percentage of city area within a LECZ showing no association with GCoM participation across all three models. Moreover, while the estimate for PM_{2.5} concentration showed no significant effect for European cities, it appeared significantly negatively associated with GCoM participation for global urban centres in Models 4, 5, and 6 (-0.482, $p < 0.05$; -0.419, $p < 0.01$), suggesting that higher air pollution levels may have discouraged participation. Additionally, industrial CO₂ emissions per capita initially appeared negatively associated in Model 4 (-0.213, $p < 0.05$), but the coefficient became insignificant once country-fixed effects were applied. This suggested that this factor had weaker explanatory power for global network participation compared to its influence on European participation. Another key difference from the European models was that the level of HDI was initially positively associated with membership in Model 4 (1.525, $p < 0.01$) but lost significance in Models 5 and 6 after accounting for country-fixed effects. This did not necessarily imply that HDI had no effect on network participation; rather, it suggested that country-fixed effects may have absorbed the

effect due to high within-country correlation. Finally, a consistent finding across all specifications, which was not observed for European cities, was the number of threatened species. This factor was positively linked to GCoM membership in Models 4 to 6, although the estimate remained close to zero (0.002, $p < 0.01$; 0.003, $p < 0.05$; 0.003, $p < 0.1$).

Regarding model performance, including country-fixed effects significantly improved model fit: McFadden's R^2 increased from 0.117 to 0.211 in the European models and from 0.245 to 0.304 in the global models, while AIC values also decreased substantially. Given that a McFadden R^2 between 0.2 and 0.4 is considered a good fit (McFadden, 1974), the analysis proceeded with the inclusion of country-fixed effects. Additionally, model performance suggested that the control variables had good explanatory power, and variance inflation factors indicated no endogeneity problems due to correlation (see Appendix C). Moreover, the sensitivity of estimates to adjustments using Conley standard errors was moderate (e.g., shifts in the significance level for LECZ and HDI in the European subsets and the number of endangered species in the global subset). Nonetheless, given the spatial correlation in the exposure measures and the dependent variable (see results of Moran's I in Appendix C), their inclusion remained justified. Therefore, all subsequent models retained time at risk as a fixed effect, included all control variables presented here, incorporated country-fixed effects, and addressed potential spatial autocorrelation in the residuals using Conley standard errors with a 500 km cut-off. Finally, Models 3 and 6 were used as baseline comparisons for subsequent models regarding the European and non-European city subsets, respectively.

4.2.3 Considering Temperature Anomalies and Shocks

The specifications presented in this subsection were applied to test for the effect of temperature anomalies and shocks on the logit hazard of European and non-European cities GCoM participation. First, the results are displayed for immediate effects (Table 4.2), then for delayed effects incorporating a one-period lag (Table 4.3), and finally for more persistent effects using the exposure measures' six- and twelve-season moving averages (Table 4.4).

The results presented in Table 4.2 revealed that, considering the European subset (Models 1 to 6), climate anomalies and shocks had little to no significant immediate effect on city-level GCoM participation. This held for crude GHCN and UTCI anomalies, disaggregated positive GHCN anomalies, positive and negative UTCI anomalies, the number of heat and cold shocks, and the number of heat spells. Moreover, Models 1 to 5 yielded a lower AIC than the baseline, suggesting that including the exposure variables did not enhance model fit. The only weak significant effects on participation were observed for negative GHCN anomalies in Model 3 (0.259, $p < 0.10$) and the number of cold UTCI spells (-0.059, $p < 0.10$), with the latter resulting in a slight reduction in AIC. Nonetheless, while these estimates reached significance at the 10 percent level,

TABLE 4.2: Estimation of the Immediate Effect of Temperature Anomalies and Shocks on the Logit Hazard of City Participation in the GCoM

	European Urban Centres						Global Urban Centres (excl. Europe)					
	(1)	(2)	(3)	(4)	(5)	(6)	(7)	(8)	(9)	(10)	(11)	(12)
Anomaly GHCN	-0.171 (0.109)						0.297 *** (0.106)					
Anomaly UTCI		-0.049 (0.083)						0.133 * (0.069)				
Anomaly GHCN (+)			-0.127 (0.192)						0.257 ** (0.110)			
Anomaly GHCN (-)			0.259 * (0.148)						-0.677 (0.476)			
Anomaly UTCI (+)				-0.077 (0.122)						0.090 (0.082)		
Anomaly UTCI (-)				-0.031 (0.164)						-0.372 (0.288)		
No. Heat Shocks UTCI					-0.012 (0.011)						-0.001 (0.004)	
No. Cold Shocks UTCI					0.000 (0.002)						-0.000 (0.001)	
No. Heat Spells UTCI						-0.058 (0.059)						-0.002 (0.025)
No. Cold Spells UTCI						-0.059 * (0.035)						0.023 (0.027)
<i>N</i>	21879	21879	21879	21879	21879	21879	189455	189455	189455	189455	189455	189455
<i>No. Cities</i>	1006	1006	1006	1006	1006	1006	10338	10338	10338	10338	10338	10338
<i>No. Periods</i>	33	33	33	33	33	33	19	19	19	19	19	19
<i>Region Fixed Effect</i>	Country	Country	Country	Country	Country	Country	Country	Country	Country	Country	Country	Country
<i>Conley Cut-Off</i>	500 km	500 km	500 km	500 km	500 km	500 km	500 km	500 km	500 km	500 km	500 km	500 km
<i>McFadden R2</i>	0.211	0.210	0.210	0.210	0.210	0.211	0.305	0.304	0.305	0.304	0.304	0.304
<i>AIC</i>	3770.804	3772.733	3772.619	3774.424	3773.378	3768.427	5824.283	5831.190	5825.532	5832.180	5837.726	5836.911

*** p < 0.01; ** p < 0.05; * p < 0.1.

no consistent pattern emerged across multiple exposure variables, questioning the robustness of the findings. For instance, if there were a meaningful, immediate effect of colder-than-baseline conditions discouraging participation, this would have been reflected at least in the number of cold shocks or negative GHCN and UTCI anomalies. In contrast, the discrete-time survival estimations for the global urban centre subset (excluding Europe) in Models 7 and 8 showed a significant association between higher seasonal GHCN (0.297, $p < 0.01$) and UTCI anomalies (0.113, $p < 0.1$) and an increased hazard of GCoM participation. Moreover, when disaggregating GHCN anomalies into positive and negative deviations (Model 9), positive anomalies remained significant (0.257, $p < 0.01$), which suggested that the effect observed in Model 7 was driven by them. These estimations further showed an improvement in model fit, as indicated by a slightly lower AIC, confirming that exposure variables contributed to the explanatory power. As for the disaggregated positive and negative estimates for UTCI anomalies in Model 10, none were significant, potentially suggesting that the effect in Model 8 was not caused by a specific type of anomaly. Finally, the results for the number of UTCI shocks and spells presented in Models 11 and 12 presented no statistically significant effect on GCoM participation and further resulted in a higher AIC, indicating a weaker fit compared to the baseline. Nonetheless, despite the estimation for disaggregated UTCI anomalies not clarifying which anomalies drove the effect observed in Model 8,

and models considering shocks and spells showing no significant impact, the findings provided some indication that warmer-than-average conditions may directly influence GCoM participation for global cities across three exposure measures. Thus, this result was further tested for robustness by applying inverse probability weights in the analysis in [section 4.1](#).

Furthermore, the bureaucratic process of joining the GCoM, alongside with the time required for a city's decision-making after a shock, could delay GCoM membership. Therefore, the results in [Table 4.3](#) present the estimations on the impact of temperature anomalies and shocks on the hazard of GCoM participation, with a one-period lag.

TABLE 4.3: Estimation of the Delayed Effect (1 Lag) of Temperature Anomalies and Shocks on the Logit Hazard of City Participation in the GCoM

	European Urban Centres						Global Urban Centres (excl. Europe)					
	(1)	(2)	(3)	(4)	(5)	(6)	(7)	(8)	(9)	(10)	(11)	(12)
Anomaly GHCN	-0.090 (0.078)						-0.079 (0.150)					
Anomaly UTCI		-0.085 * (0.045)						-0.132 (0.109)				
Anomaly GHCN (+)			-0.087 (0.124)						0.120 (0.159)			
Anomaly GHCN (-)			0.097 (0.246)						0.730 *** (0.236)			
Anomaly UTCI (+)				-0.115 *** (0.031)						0.033 (0.128)		
Anomaly UTCI (-)				-0.006 (0.216)						0.512 *** (0.142)		
No. Heat Shocks UTCI					-0.010 (0.007)						0.007 (0.005)	
No. Cold Shocks UTCI					0.002 (0.003)						0.004 *** (0.001)	
No. Heat Spells UTCI						-0.052 (0.043)						0.045 * (0.025)
No. Cold Spells UTCI						-0.002 (0.032)						0.070 *** (0.019)
N	21879	21879	21879	21879	21879	21879	189455	189455	189455	189455	189455	189455
No. Cities	1006	1006	1006	1006	1006	1006	10338	10338	10338	10338	10338	10338
No. Periods	33	33	33	33	33	33	19	19	19	19	19	19
Region Fixed Effect	Country	Country	Country	Country	Country	Country	Country	Country	Country	Country	Country	Country
Conley Cut-Off	500 km	500 km	500 km	500 km	500 km	500 km	500 km	500 km	500 km	500 km	500 km	500 km
McFadden R2	0.210	0.210	0.210	0.210	0.210	0.210	0.304	0.304	0.305	0.305	0.305	0.305
AIC	3772.845	3771.722	3774.844	3773.410	3773.267	3774.117	5835.046	5831.438	5828.074	5825.934	5825.175	5826.797

*** p < 0.01; ** p < 0.05; * p < 0.1.

Regarding the models for European cities (Models 1 to 6), the results indicated that higher UTCI anomalies in the previous season decreased the likelihood of GCoM participation (-0.085, p<0.1), which was primarily driven by a negative effect of positive UTCI anomalies (-0.115, p<0.01). However, the higher AICs in both estimations demonstrated a weaker model fit than the baseline model, suggesting that this finding was rather spurious, warranting cautious interpretation. Moreover, this finding was not reinforced by crude or disaggregated GHCN anomalies or heat shocks and spells, which all remained insignificantly associated, suggesting no discernable pattern in lagged

temperature anomalies and shocks on European GCoM participation.

Turning to the results for global urban centres presented in Models 7 to 12, the one-period lag models revealed a shift in dynamics compared to the findings in [Table 4.2](#), where colder-than-average conditions in the previous season appeared to significantly increase the likelihood of GCoM participation, as opposed to warming. Negative GHCN anomalies (0.730, $p < 0.01$) and negative UTCI anomalies (0.512, $p < 0.01$) both showed strong positive effects, while the presence of more cold shocks (0.004, $p < 0.01$) and cold spells (0.070, $p < 0.01$) were linked to higher participation. These estimations also had lower AIC values than the baseline, suggesting that past-season negative climate anomalies and shocks contributed to the explanatory power. To see if these findings hold, it was warranted that they should be tested further for robustness by adjusting for confounding factors. A weak positive association was also found for heat spells (0.045, $p < 0.1$) in Model 12. However, this finding was not reinforced across other specifications, calling into question its robustness.

Recognizing that single climate events may not be sufficient to drive urban climate action since they may be attributed to natural variability rather than climate change, the estimations were also run incorporating the six and twelve-season moving averages of the exposure measures. These results are presented in [Table 4.4](#).

Considering the subsample of European cities, the estimations for the six-period moving averages showed no significant effect, at first indicating no influence of persistent temperature anomalies and shocks on their network participation. However, over a twelve-season horizon, the results shifted. Higher levels of GHCN anomalies now revealed a significant association with GCoM membership (2.611, $p < 0.01$). Moreover, when disaggregated, positive anomalies remained significant (2.495, $p < 0.01$), while negative anomalies appeared with a negative effect (-2.875, $p < 0.05$). These results were partially reinforced when looking at UTCI anomalies, with overall crude anomalies being positively associated with participation (0.798, $p < 0.05$), while negative anomalies significantly reduce the likelihood of joining (-3.058, $p < 0.01$). However, there was no significant effect for positive UTCI anomalies. The models' fit (Model 1 to 4 considering the twelve-period moving averages) also suggested more substantial explanatory power, with lower AIC values compared to both the baseline and the six-period moving average models, and higher McFadden R^2 . That said, the estimations on shocks and spells revealed no significant effects, with weaker model fits compared to the baseline. Nonetheless, the findings suggested across multiple specifications that European cities experiencing prolonged warming are more likely to join the GCoM, whereas those with prolonged cooling are less inclined to participate. However, this is only the case when long-term trends over twelve seasons are considered, with no impact from shorter six-season trends. The robustness of these findings was further evaluated after adjusting for confounding in [section 4.1](#).

TABLE 4.4: Estimation of the Effect of Temperature Anomalies and Shocks (6 & 12 Period Moving Averages) on the Logit Hazard of City Participation in the GCoM

	European Urban Centres						Global Urban Centres (excl. Europe)					
	(1)	(2)	(3)	(4)	(5)	(6)	(7)	(8)	(9)	(10)	(11)	(12)
	6 Period Moving Average											
Anomaly GHCN	0.671 (0.493)						-0.013 (0.338)					
Anomaly UTCI		0.017 (0.330)						-0.431 ** (0.192)				
Anomaly GHCN (+)			0.672 (0.587)						1.241 *** (0.379)			
Anomaly GHCN (-)			-0.669 (0.925)						2.594 *** (0.482)			
Anomaly UTCI (+)				-0.296 (0.331)						0.059 (0.247)		
Anomaly UTCI (-)				-1.110 (0.839)						1.162 *** (0.257)		
No. Heat Shocks UTCI					-0.020 (0.038)						0.004 (0.009)	
No. Cold Shocks UTCI					0.001 (0.007)						0.008 *** (0.002)	
No. Heat Spells UTCI						-0.173 (0.154)						-0.002 (0.058)
No. Cold Spells UTCI						-0.078 (0.083)						0.132 ** (0.056)
<i>McFadden R2</i>	0.211	0.210	0.211	0.211	0.210	0.211	0.304	0.305	0.308	0.306	0.305	0.304
<i>AIC</i>	3768.871	3773.438	3770.871	3769.579	3774.542	3770.922	5835.868	5824.164	5798.276	5816.593	5829.161	5830.399
	12 Period Moving Average											
Anomaly GHCN	2.611 *** (0.782)						0.470 (0.399)					
Anomaly UTCI		0.798 ** (0.396)						-0.459 * (0.248)				
Anomaly GHCN (+)			2.495 *** (0.874)						1.201 ** (0.558)			
Anomaly GHCN (-)			-2.875 ** (1.310)						1.355 (0.855)			
Anomaly UTCI (+)				-0.025 (0.454)						-0.084 (0.370)		
Anomaly UTCI (-)				-3.058 *** (0.916)						1.180 *** (0.433)		
No. Heat Shocks UTCI					0.031 (0.066)						-0.001 (0.012)	
No. Cold Shocks UTCI					0.000 (0.007)						0.007 *** (0.002)	
No. Heat Spells UTCI						-0.070 (0.276)						0.006 (0.080)
No. Cold Spells UTCI						-0.049 (0.107)						0.143 ** (0.061)
<i>McFadden R2</i>	0.215	0.212	0.215	0.215	0.210	0.210	0.304	0.304	0.305	0.305	0.305	0.304
<i>AIC</i>	3747.879	3762.810	3749.789	3750.518	3774.412	3774.703	5834.003	5831.182	5826.691	5828.932	5829.319	5830.007
<i>N</i>	21879	21879	21879	21879	21879	21879	189455	189455	189455	189455	189455	189455
<i>No. Cities</i>	1006	1006	1006	1006	1006	1006	10338	10338	10338	10338	10338	10338
<i>No. Periods</i>	33	33	33	33	33	33	19	19	19	19	19	19
<i>Region Fixed Effect</i>	Country	Country	Country	Country	Country	Country	Country	Country	Country	Country	Country	Country
<i>Conley Cut-Off</i>	500 km	500 km	500 km	500 km	500 km	500 km	500 km	500 km	500 km	500 km	500 km	500 km

*** p < 0.01; ** p < 0.05; * p < 0.1.

As for the subsample considering global urban centres (Models 7 to 12), the trends regarding colder-than-average conditions presented in the one-lagged models in [Table 4.3](#) were reinforced when considering longer timeframes. Higher UTCI anomalies were linked to lower GCoM participation, considering the six-season moving average (-0.431 , $p < 0.05$) and the twelve-season moving average (1.180 , $p < 0.01$). Moreover, this was primarily driven by the significant and positive effect of negative UTCI anomalies in both time horizons. The six-season moving average of negative GHCN anomalies was also positively associated with GCoM participation (2.594 , $p < 0.01$), although the estimate lost significance when considering twelve seasons. Additionally, experiencing more cold shocks (six seasons: 0.008 , $p < 0.01$; twelve seasons: 0.007 , $p < 0.01$) and cold spells (six seasons: 0.132 , $p < 0.05$; twelve seasons: 0.143 , $p < 0.05$) was positively correlated with joining the GCoM. All in all, this suggested that prolonged cold conditions are consistently positively linked to GCoM participation outside of Europe. Moreover, the model fit improved to the baseline across Models 8 to 12, with the strongest enhancement seen in Model 9, which accounted for disaggregated temperature anomalies. Another finding was that sustained warmer-than-baseline temperatures also showed correlation, at least when considering GHCN anomalies. While overall temperature anomalies remained insignificant, disaggregated anomalies showed a significant effect for positive anomalies (1.241 , $p < 0.01$), considering the six-season moving average. Similarly, considering twelve seasons, positive anomalies retained a significant association with participation (1.201 , $p < 0.01$), whereas negative anomalies lost significance compared to the six-season models. Despite other exposure measures not confirming this finding, its persistence across both timeframes, along with the twelve-season model considering disaggregated GHCN anomalies (Model 9) having the best model fit, suggested it cannot be easily dismissed. Thus, this finding was tested for robustness while accounting for potential confounders alongside the result of the strong positive influence of colder-than-average conditions.

4.2.4 Considering Weather-Related Natural Disasters

Having examined the impacts of temperature anomalies and shocks, this subsection presents the results from the discrete-time survival models estimating the effects of weather-related disaster occurrences and fatalities on the logit hazard of urban centres' GCoM participation. The analysis follows the same structure as before, first displaying the findings for immediate effects ([Table 4.5](#)), then delayed effects ([Table 4.6](#)), and finally longer-term exposure using six- and twelve-season moving averages ([Table 4.7](#)).

The results regarding European cities, presented in Models 1 to 4 in [Table 4.5](#) indicated, on one hand, no significant influence of crude weather-related disasters or their associated fatalities on GCoM participation. On the other hand, the occurrence of hydrological disasters (-0.619 , $p < 0.05$) and deaths (-0.422 , $p < 0.01$) appeared to hinder participation in

the same season. This could suggest that flood events are not directly perceived as stemming from climate change or are disruptive, which may delay participation decisions. Hence, due to the persistence across both measures, this finding was further considered in the subsequent analysis. Additionally, climatological disaster-related deaths had a strong negative impact, with a large estimate (-10.280, $p < 0.01$). However, the effect size called into question the robustness of the finding, as this would translate to an increase in the logarithm of fatalities from climatological disasters of 1, decreasing the odds of participation by 99.997% (Odds ratio: $3.431027e-05$). As this meant GCoM participation becoming nearly impossible when experiencing deaths from a climatological disaster, which lacks practicality, and given that odds ratios this high are unlikely and often explained by underlying issues in the estimation, the interpretation of this result should be cautioned. Since climatological disasters are rare and spatially clustered events, it is more likely that this resulted in overfitting or near-perfect separation in the estimation process.

TABLE 4.5: Estimation of the Immediate Effect of Weather-Related Disaster Occurrence and Deaths on the Logit Hazard of City Participation in the GCoM

	European Urban Centres				Global Urban Centres (excl. Europe)			
	(1)	(2)	(3)	(4)	(5)	(6)	(7)	(8)
No. Disasters	-0.057 (0.099)				-0.153 * (0.078)			
No. Climatological Disasters		-0.638 (0.755)				0.365 (0.314)		
No. Meteorological Disasters		0.126 (0.120)				-0.227 ** (0.115)		
No. Hydrological Disasters		-0.619 ** (0.282)				-0.029 (0.142)		
Log Mean Disaster Deaths			0.003 (0.052)				-0.033 (0.056)	
Log Mean Climatological Deaths				-10.280 *** (0.366)				0.442 ** (0.185)
Log Mean Meteorological Deaths				0.065 (0.042)				0.018 (0.075)
Log Mean Hydrological Deaths				-0.422 *** (0.111)				-0.112 ** (0.057)
<i>N</i>	21373	21373	19663	19663	179737	179737	167305	167305
<i>No. Cities</i>	1006	1006	930	930	10338	10338	9601	9601
<i>No. Periods</i>	32	32	32	32	18	18	18	18
<i>Region Fixed Effect</i>	Country	Country	Country	Country	Country	Country	Country	Country
<i>Conley Cut-Off</i>	500 km	500 km	500 km	500 km	500 km	500 km	500 km	500 km
<i>McFadden R2</i>	0.208	0.209	0.205	0.207	0.302	0.302	0.301	0.302
<i>AIC</i>	3757.175	3755.069	3517.424	3510.488	5770.308	5769.905	5243.852	5239.418

*** $p < 0.01$; ** $p < 0.05$; * $p < 0.1$.

As for the results considering the global subset (Models 5 to 8), a weak significant negative effect (-0.153, $p < 0.1$) was found for disaster occurrence on participation, which was primarily driven by the number of meteorological disasters (-0.227, $p < 0.05$).

Furthermore, hydrological deaths had a significant negative effect (-0.112, $p < 0.05$), while the logarithm of climatological deaths appeared positively associated to GCoM participation. Although this initially implied that cities experiencing more fatalities from droughts or wildfires were more likely to join the GCoM in the same season, while floods acted as a barrier, it is important to consider that climatological disasters are rare events. As demonstrated in the European subset, findings related to this measure should be interpreted with caution. Moreover, the findings on disaster occurrences did not align with those on disaster-related fatalities and vice versa, making it difficult to identify clear patterns. While the overall number of disasters was significantly associated with GCoM participation, the number of fatalities was not. Similarly, meteorological disasters were shown to be significant predictors, but their associated death tolls were not. In contrast, hydrological disasters showed a significant effect when considering fatalities but not when looking at their overall frequency. The same was observed for climatological disasters, where related deaths appeared significant, but the total number of events did not. Given these inconsistencies and sensitivities in the estimates, no further testing was conducted, although this doesn't mean that the results are invalid.

Furthermore, to account for potential delays when experiencing disasters that may influence the timing of GCoM participation, the results for the one-period lag effects are presented in [Table 4.6](#).

Considering European cities, as with the estimations testing for immediate effects, overall disasters from the previous season showed no statistically significant effect on GCoM participation. However, when disaggregated by disaster type, only lagged climatological disasters exhibited a weakly significant positive association (0.490, $p < 0.1$). However, as seen in the estimates regarding immediate effects, all conclusions about climatological disasters should be cautioned. Concerning fatalities from natural disasters, only the overall measure showed a significant negative effect (-0.033, $p < 0.01$). Conversely, fatalities by disaster type revealed no significant influence, suggesting that no specific category of disasters influenced this result. Nonetheless, the low AIC in comparison to Models 1, 2, and 4 suggested that much explanatory power was added, thus this result was considered in further testing.

Turning toward the results for the global sample, across Models 5 to 8, none of the estimates were statistically significant, and all models exhibited higher AIC values compared to those considering immediate effects, indicating a poorer model fit. Therefore, weather-related disasters in the previous season did not appear to drive GCoM participation for global cities.

TABLE 4.6: Estimation of the Delayed Effect (1 Lag) of Weather-Related Disaster Occurrence and Deaths on the Logit Hazard of City Participation in the GCoM

	European Urban Centres				Global Urban Centres (excl. Europe)			
	(1)	(2)	(3)	(4)	(5)	(6)	(7)	(8)
No. Disasters	0.020 (0.046)				-0.107 (0.073)			
No. Climatological Disasters		0.490 * (0.251)				0.339 (0.450)		
No. Meteorological Disasters		0.036 (0.098)				-0.174 (0.108)		
No. Hydrological Disasters		-0.195 (0.246)				0.026 (0.129)		
Log Mean Disaster Deaths			-0.033 *** (0.010)				-0.014 (0.041)	
Log Mean Climatological Deaths				-0.054 (0.736)				0.216 (0.213)
Log Mean Meteorological Deaths				-0.016 (0.023)				-0.066 (0.045)
Log Mean Hydrological Deaths				-0.145 (0.092)				0.034 (0.053)
<i>N</i>	21373	21373	19663	19663	179737	179737	167305	167305
<i>No. Cities</i>	1006	1006	930	930	10338	10338	9601	9601
<i>No. Periods</i>	32	32	32	32	18	18	18	18
<i>Region Fixed Effect</i>	Country	Country	Country	Country	Country	Country	Country	Country
<i>Conley Cut-Off</i>	500 km	500 km	500 km	500 km	500 km	500 km	500 km	500 km
<i>McFadden R2</i>	0.208	0.208	0.205	0.205	0.302	0.302	0.301	0.301
<i>AIC</i>	3757.380	3759.553	3517.073	3520.435	5773.221	5773.973	5244.255	5245.973

*** $p < 0.01$; ** $p < 0.05$; * $p < 0.1$.

To further evaluate the more persistent effects over longer time horizons, [Table 4.7](#) presents the impacts of weather-related disaster exposure on the hazard of GCoM participation, incorporating six- and twelve-season moving averages for all disaster measures. Turning to European urban centres, the models incorporating six-season moving averages revealed some notable patterns. Both the total number of disasters (0.804, $p < 0.05$) and the logarithm of average disaster-related fatalities (0.124, $p < 0.05$) were significantly associated with an increased likelihood of GCoM participation. Models 2 and 4 further revealed that this effect primarily stemmed from meteorological disasters, as evidenced by the strong positive associations with the number of disasters experienced (1.504, $p < 0.01$) and the logarithm of associated deaths (0.157, $p < 0.01$). This implied that cities experiencing more meteorological disasters (i.e., extreme temperature events and storms) over a longer time horizon were more likely to join the GCoM. Conversely, hydrological and climatological disasters showed no significant influence, while fatalities from hydrological disasters was observed to negatively affect participation (-0.348, $p < 0.05$). These findings were reinforced when turning to the estimates for twelve-season moving averages, with the occurrence of disasters (1.032, $p < 0.10$) and disaster-related fatalities

(0.078, $p < 0.10$) continuing to show a positive association with GCoM participation. This effect was again primarily caused by meteorological disasters (2.640, $p < 0.01$) and related fatalities (0.096, $p < 0.05$). Moreover, hydrological disasters exhibited a significant negative effect (-2.427, $p < 0.01$), and hydrological deaths also showed a negative association (-0.396, $p < 0.10$), reinforcing the previous findings that exposure to floods may present a barrier for European cities to participate in the GCoM. In addition, the lower AIC scores in all eight models suggested a better model fit, when considering longer time horizons, than those considering immediate and lagged effects. Thus, these results indicated that while cities impacted by recurring storms and extreme weather seek out network membership, those experiencing repeated flooding may be less inclined. The robustness of these findings was further examined while considering selection bias in the **subsequent analysis**.

Moreover, considering global urban centres, the results presented in Models 5 to 8 for the estimates averaged over six periods differed significantly from the European findings. Neither the occurrence nor fatalities from overall, meteorological, or hydrological disasters showed a significant association with GCoM participation. Conversely, climatological disasters appeared with a strong negative estimate (-2.892, $p < 0.05$). This remained consistent when using twelve-season moving averages, with climatological disasters (-5.575, $p < 0.01$). However, as was the case for the European subset when estimating immediate effects (Table 4.5), the large estimate (-5.575) translated into a 99.6% decrease in the odds of cities adhering to the GCoM (Odds ratio = 0.003789703) with an increase of 1, which was a highly unlikely effect size. This reinforced the notion that any interpretation of the estimations concerning climatological disasters should be cautious, hence why this finding was dismissed in the subsequent analysis. Finally, no significant associations were found for other disaster types or total disaster occurrences, implying that other persistent disasters did not influence GCoM participation in non-European cities.

TABLE 4.7: Estimation of the Weather-Related Disaster Occurrence and Deaths (6 & 12 Period Moving Averages) on the Logit Hazard of City Participation in the GCoM

	European Urban Centres				Global Urban Centres (excl. Europe)			
	(1)	(2)	(3)	(4)	(5)	(6)	(7)	(8)
	6 Period Moving Average							
No. Disasters	0.804 ** (0.316)				-0.058 (0.166)			
No. Climatological Disasters		-0.681 (1.114)				-2.892 ** (1.385)		
No. Meteorological Disasters		1.504 *** (0.498)				-0.136 (0.185)		
No. Hydrological Disasters		-0.406 (0.550)				0.087 (0.320)		
Log Mean Disaster Deaths			0.124 ** (0.052)				-0.025 (0.052)	
Log Mean Climatological Deaths				-0.010 (0.349)				0.070 (0.384)
Log Mean Meteorological Deaths				0.157 *** (0.050)				-0.056 (0.082)
Log Mean Hydrological Deaths				-0.348 ** (0.150)				0.019 (0.044)
<i>McFadden R2</i>	0.210	0.211	0.207	0.208	0.302	0.302	0.301	0.301
<i>AIC</i>	3750.336	3745.495	3509.210	3503.651	5775.866	5771.797	5244.053	5247.163
	12 Period Moving Average							
No. Disasters	1.032 * (0.599)				-0.283 (0.186)			
No. Climatological Disasters		2.372 (2.652)				-5.575 *** (1.782)		
No. Meteorological Disasters		2.640 *** (0.798)				-0.303 (0.207)		
No. Hydrological Disasters		-2.427 *** (0.940)				-0.479 (0.535)		
Log Mean Disaster Deaths			0.078 * (0.043)				-0.061 (0.066)	
Log Mean Climatological Deaths				0.269 (0.466)				-0.071 (0.392)
Log Mean Meteorological Deaths				0.096 ** (0.041)				0.046 (0.101)
Log Mean Hydrological Deaths				-0.396 * (0.211)				-0.070 (0.054)
<i>McFadden R2</i>	0.210	0.214	0.206	0.207	0.302	0.304	0.301	0.301
<i>AIC</i>	3751.389	3728.426	3513.881	3510.768	5769.391	5759.131	5243.008	5245.990
<i>N</i>	21373	21373	19663	19663	179737	179737	167305	167305
<i>No. Cities</i>	1006	1006	930	930	10338	10338	9601	9601
<i>No. Periods</i>	32	32	32	32	18	18	18	18
<i>Region Fixed Effect</i>	Country	Country	Country	Country	Country	Country	Country	Country
<i>Conley Cut-Off</i>	500 km	500 km	500 km	500 km	500 km	500 km	500 km	500 km

*** $p < 0.01$; ** $p < 0.05$; * $p < 0.1$.

4.2.5 Adjusting for Confounding

The descriptive analysis in [Chapter 4.1](#) revealed regional differences in exposure, with cities in the Global North experiencing higher temperature anomalies than those in the Global South. Furthermore, it was shown that disaster occurrence was spatially clustered, with some regions being more affected than others. This raised concerns about selection bias, as regions in the Global North, where anomalies were more pronounced, tend to be more affluent than those in the Global South ([Thomas-Slayter, 2003](#)). Thus, those may have also been more likely to join the GCoM, as findings from [Nohrstedt, Hileman, Mazzoleni et al. \(2022\)](#) and [Zahran, Grover, Brody and Vedlitz \(2008b\)](#) suggested. In addition, if cities in disaster-prone regions were systematically different (either more resilient or less reactive), unadjusted estimates in the previous analysis may have presented distorted effects on GCoM participation. In other words, they may have reflected pre-existing regional differences rather than their true exposure impact. To account for this, Inverse Probability Weighting (IPW) was applied to the findings from the two previous subsections to correct for selection bias and isolate the independent effect of the exposure measures on GCoM participation. By adjusting, among others, for potential socio-economic and regional confounding, comparability between cities with varying climate exposure was enhanced, which improved the estimates' reliability.

The results of the estimations after implementing IPW are presented through Average Dose-Response Functions (ADRFs). ADRFs display how the expected probability of city-level GCoM participation varied at different binned averages of the exposure level. Presenting the results via ADRFs for continuous treatment levels is the recommended approach by [Greifer \(2025b\)](#), as the conditional estimates are biased after weighting. In the following plots depicting ADRFs, the black line indicates the predicted probability at various levels of binned exposure averages (blue dots). The gray area further represents the confidence band, and the red dashed line serves as a reference for zero predicted probability. It is important to note that unlike the conditional estimates, which isolated the effects of the exposure measures while holding other variables constant, as presented in the previous findings, the ADRFs provide estimates across all included covariates. Hence, given that all cities, especially non-European ones, had a low baseline probability of joining the GCoM, even a significant effect of the exposure variable may result in only a small increase in the overall expected probability of participation.

That said, before presenting the results, it should be noted that not all weighted estimations achieved covariate balance and that some were discarded due to methodological constraints. As this analysis focused on inverse probability weighting methods for continuous treatments, estimations including count variables, such as those concerning immediate and lagged disaster occurrences and temperature shocks and spells, were excluded. Furthermore, some estimations exhibited effective sample sizes (ESS) values of 100 percent, which was due to the weights not reducing the effective number of observations since they were nearly uniform across observation. This may pose no issues

as it may indicate that confounding was minimal, hence, the covariates were already balanced, and there may have been little need for adjustment in the first place. However, this may also point toward an issue on the specifications of the GPS model, in which case the adjusted results should not be used to confirm robustness and causal relationships (Chesnaye et al., 2021). In contrast, a small ESS suggested poor model fit, indicating differences between high- and low-exposure cities that the model struggled to balance (Maia Polo and Vicente, 2023). Moreover, a third issue was that covariates remained imbalanced in some cases despite weighting (i.e., the SMDs were above the absolute 0.1 threshold). Nonetheless, despite these limitations, the implementation of weights was successful for most estimations, with the evaluation of the covariate balance achieved through the weighting process provided in the love plots in Appendix D, which display the Pearson correlation between the covariates and exposure measures before and after weighting and provide the covariate with the highest SMD.

One of the findings in section 4.3 was that global cities exhibited an immediate association between warmer-than-average conditions and a greater likelihood of GCoM participation when considering UTCI, GHCN, and positive GHCN anomalies. The IPW-adjusted results for this finding are illustrated via ADRFs in Figure 4.12, with the predicted probabilities across all binned averages of the exposure levels in the computation of the ADRF significant at the one percent level. The weighting process improved covariate balance and comparability among global cities, as indicated by the shift of the correlations toward zero in the love plots, and all standardized mean differences remaining significantly below the 0.1 threshold (see Figure D.1 in Appendix D).

The adjusted results indicate an upward trend in all ADRFs, suggesting that higher anomalies corresponded to a higher probability of joining. However, confidence intervals widen as the anomalies increased, also reflecting greater uncertainty. Yet, they diverge from the zero-probability line toward a higher predicted probability across all three plots. For crude GHCN anomalies (Plot 1), cities at the lowest binned average anomaly of -0.31°C had a 0.0123% predicted probability of joining, which increased to 0.0230% at the highest anomaly of 1.44°C , reflecting a 0.0107 percentage point rise. Similarly, the expected probability of GCoM participation regarding UTCI anomalies increased from 0.0129% at -0.78°C to 0.0194% at 2.17°C , equivalent to an increase of 0.0065 percentage points (Plot 2). Considering positive GHCN anomalies, cities with no anomaly had a predicted probability of adherence of 0.0134%, which increased to 0.0227% at 1.44°C , i.e., a rise of 0.0093 percentage points (Plot 3). Therefore, even though the absolute increase in predicted probability was small (as anticipated given the very low seasonal probability of joining the GCoM, especially in non-European cities), the IPW-adjusted results supported the previous findings and provided additional evidence for a direct effect of warmer-than-baseline conditions on GCoM participation among

non-European cities. However, it should be kept in mind that the wide confidence intervals indicated substantial uncertainty. Additionally, the lack of significant effects for heat spells, heat shocks, and positive UTCI anomalies suggested that, although a valid finding, this may not be one of the main drivers of participation.

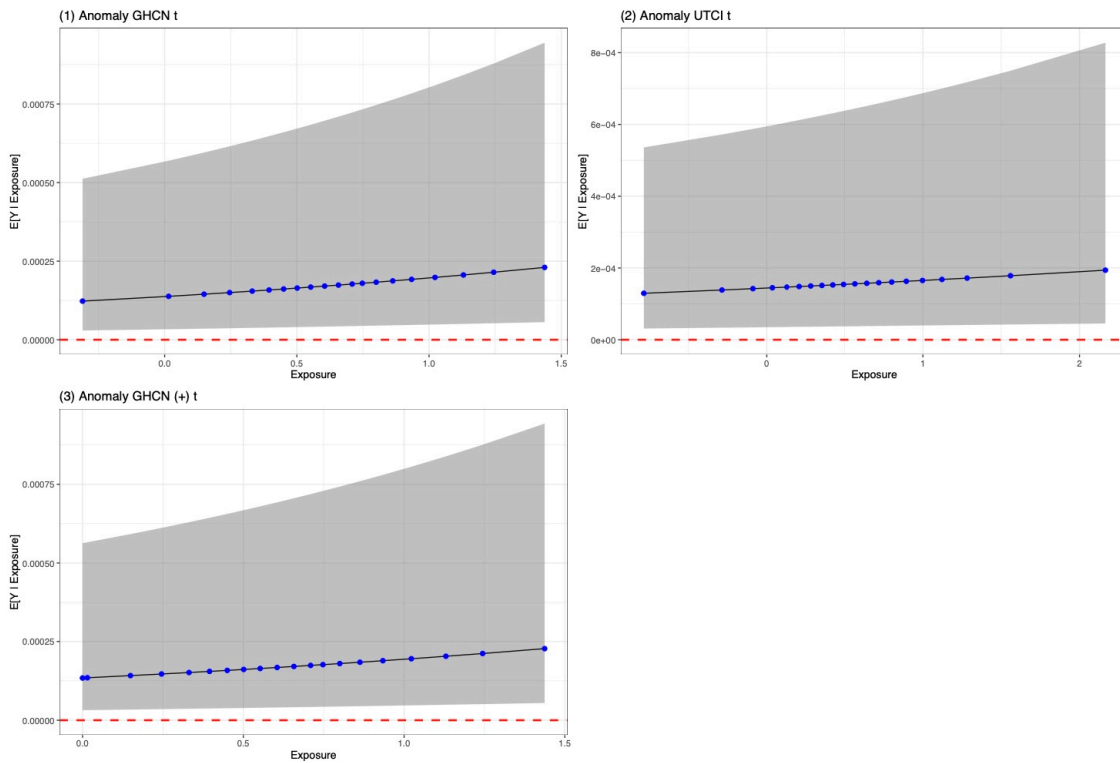


FIGURE 4.12: Average Dose Response Functions for IPW-Adjusted Estimates of Immediate Temperature Anomalies and Shocks in Global (excl. Europe) Urban Centres

While immediate positive temperature deviations initially were found to encourage GCoM participation in global cities, the impact of cold-related anomalies became more pronounced when considering lagged effects. This finding was supported by the positive significant effects of past season negative UTCI, GHCN anomalies, and the number of cold shocks and spells. However, in this case, adjusting for confounding proved difficult. First, the lagged effects of cold shocks and spells could not be tested due to them being count variables. Moreover, while weighting for negative UTCI and GHCN anomalies, the unusually high effective sample sizes of nearly 100 percent further raised concerns (see love plots in [Figure D.1 in Appendix D](#)). The most probable reason was that seasonal negative anomalies were less systematically related to covariates because they were more uncommon than positive ones, appearing as external shocks. In this case, the GPS Model had low explanatory power, even raising a negative McFadden R^2 (-0.02 in both cases), indicating that the covariates did not explain the exposure well. This made the inverse probability weights unreliable, and the results were discarded. Thus, while the

analysis in Table 4.3 initially suggested that past season colder-than-average temperatures influence GCoM participation, these findings could not be reliably reinforced by implementing weights, which is an acknowledged limitation of this analysis.

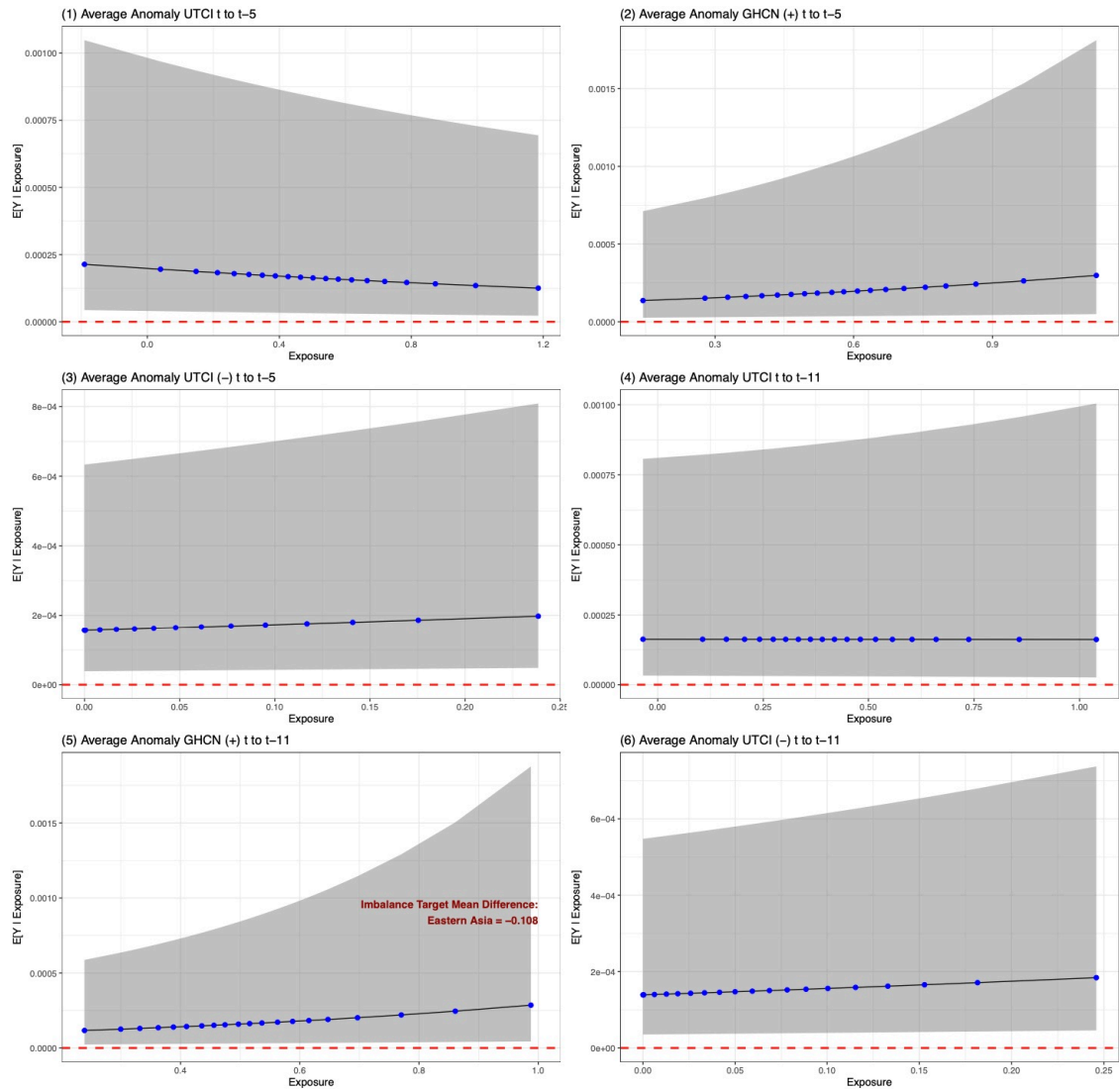


FIGURE 4.13: Average Dose Response Functions for IPW-Adjusted Estimates of Temperature Anomalies and Shocks in Global (excl. Europe) Urban Centres (6 & 12 Period Moving Averages)

The previous findings further suggested that prolonged cold conditions increased the hazard of GCoM participation for global cities. However, sustained warming was also found to shape participation in the long run. These findings were supported by the significant effects of six- and twelve-season moving averages of crude and negative UTCI anomalies, positive GHCN anomalies, the number of cold shocks and spells, and the six-season moving average of negative GHCN anomalies. The IPW-adjusted results from these findings are presented in Figure 4.13. It should be noted that the estimation

for the effects of the six-period negative GHCN anomalies failed, as all weights returned zero values, further indicating model specification issues when considering colder-than-average conditions. Moreover, the estimations for longer-term averages of cold shocks and spells were discarded because the estimation process failed to achieve covariate balance, as seen in [Appendix D](#). Despite these limitations, IPW-adjusted models for the remaining exposure measures offered valuable insights, with all estimated probabilities highly significant at the one percent level and all effective sample sizes exceeding 78 percent (see [Figure D.1 and D.2 in Appendix D](#)). Covariance balance was further achieved in all cases except for the estimation of the twelve-season moving average for positive GHCN anomalies, with the Eastern Asia covariate slightly exceeding the standardized mean difference threshold at -0.108, as indicated in Plot 5. However, since this remained close to the absolute 0.1 threshold and the literature suggested that an absolute 0.2 standard mean difference is in the acceptable range ([Kang et al., 2022](#)), the result was still considered.

Regarding UTCI anomalies averaged over six seasons, the ADRF (Plot 1) showed a downward trend, with the predicted probability of participation decreasing from 0.0214% at the lowest anomaly of -0.19°C to 0.0125% at the highest anomaly of 1.18°C , reflecting a 0.0089 percentage point decline. Furthermore, the ADRF in Plot 3 indicated that cities that experienced negative UTCI anomalies showed a slight increase in probability, from 0.0157% at 0°C to 0.0198% at 0.24°C , corresponding to a 0.0041 percentage point rise. Regarding positive GHCN anomalies (Plot 2), the probability of participation increased from 0.0137% in cities with no anomaly to 0.0298% in those with the highest anomaly of 1.12°C , which reflected a 0.0161 percentage point increase. At first glance, these findings appeared contradictory, as higher UTCI anomalies seemed to reduce participation while an increase in positive GHCN anomalies exhibited the strongest positive effect.

Considering the twelve-season time horizon, the IPW-adjusted results are shown in Plots 4 to 6. For cities experiencing UTCI anomalies, the predicted probability remained nearly unchanged, with those at the lower anomaly of -0.03°C having a probability of 0.0162%, compared to 0.0161% for those at the higher binned anomaly of 1.04°C . Thus, it no longer indicated a meaningful relationship between overall UTCI anomalies and GCoM participation, emphasizing that the results from the previous survival estimations were influenced by confounding factors. Additionally, it proved that the results from the six-season estimations in Plot 1 are at best short-lived. In contrast, negative UTCI anomalies showed a slight upward trend, with the probability increasing from 0.0139% for cities experiencing no anomaly to 0.0184% for those at 0.25°C , reflecting a 0.0045 percentage point increase. Positive GHCN anomalies, however, exhibited a much stronger effect, as participation probability increased from 0.0117% at an anomaly of 0.24°C to 0.0286% at 0.99°C , corresponding to a 0.0169 percentage point rise.

Overall, at first glance, the results presented inconsistencies. The downward trend

for UTCI anomalies over six seasons disappeared when extended to twelve seasons, suggesting that any discouraging effect of higher UTCI anomalies on participation was temporary or sensitive. However, the positive effect of negative UTCI anomalies persisted, indicating that cities experiencing cooler-than-expected conditions may have slightly increased participation. Nonetheless, compared to positive GHCN anomalies, the percentage point increase in predicted probability from the lowest to the highest bin was very small, suggesting that if negative UTCI anomalies positively influenced participation, the effect was weak and not the primary driver. Moreover, the highest binned average represented 0.25°C, which relatively to the positive anomalies does not represent a stark deviation. The lack of a clear pattern for negative GHCN anomalies over twelve seasons further undermined confidence in this finding. That said, the inability to test cold spells and shocks leaves the possibility for a different results. In contrast, positive GHCN anomalies consistently showed a much stronger effect on participation across both six and twelve seasons, with a relatively high percentage point increase from the lowest to the highest binned average. Even so, this finding should be interpreted with caution. If positive temperature anomalies were the primary driver of participation, a similar effect would likely be seen for positive UTCI anomalies. Moreover, while predicted probabilities increased at higher positive GHCN anomalies, they did so with growing uncertainty, making the interpretation of these effects more difficult. Additionally, other explanations for the conflicting results could be that both long-term positive and negative temperature anomalies act as drivers that cancel each other out in crude anomalies or that the effects are highly context-dependent. However, these possibilities were not explored further within this analysis.

Shifting focus to the European subset, the findings suggested across multiple specifications that European cities experiencing prolonged warming over twelve seasons were more likely to join the GCoM. In contrast, those with prolonged cooling over the same time horizon were less inclined to participate. This was shown through the significant effects for crude, positive, and negative GHCN anomalies and crude and negative UTCI anomalies. The IPW-adjusted estimations concerning these findings are illustrated via ADRFs in [Figure 4.14](#). The weighting process significantly improved covariate balance and comparability for European cities, as evident from the shifts of correlation toward zero in the love plots (see [Figure D.3 in Appendix D](#)). The effective sample size remained high, exceeding 89 percent across estimations, indicating minimal data loss. Standardized mean differences were low, with the highest at 0.061 for Southern Europe in the positive GHCN anomaly estimation, well below the 0.1 threshold. Additionally, the predicted probabilities across all binned averages were statistically significant at the one percent level.

The IPW-adjusted ADRF in [Figure 4.14](#) confirmed previous findings, showing an upward trend for both crude UTCI and GHCN anomalies, with a more substantial effect

for GHCN anomalies (Plot 1 and 2). For GHCN anomalies, the predicted probability of city participation increased from 0.0573% at -0.07°C to 1.59% at 1.31°C , reflecting a 1.53 percentage point rise. Similarly, regarding UTCI anomalies, the probability rose from 0.16% at experiencing -0.03°C to 0.71% at 1.72°C , i.e., a 0.56 percentage point increase. The ADRF for positive GHCN anomalies (Plot 3) reinforced this trend, with the probability for cities to participate in the GCoM growing from 0.12% at 0.32°C to 1.12% at 1.31°C , equivalent to a 1.01 percentage point increase. However, as anomaly values increased, confidence intervals widened, indicating greater variability in predicted probabilities at higher exposure levels. In contrast, long-term cooling trends were observed to reduce the likelihood of participation, further aligning with previous findings. For negative GHCN anomalies (Plot 4), the predicted probability dropped from 0.61% at 0°C to 0.21% at -0.31°C , reflecting a 0.40 percentage point decrease. A similar pattern appeared for negative UTCI anomalies (Plot 5), where participation probability declined from 0.64% at 0°C to 0.20% at -0.37°C , corresponding to a drop of 0.44 percentage points.

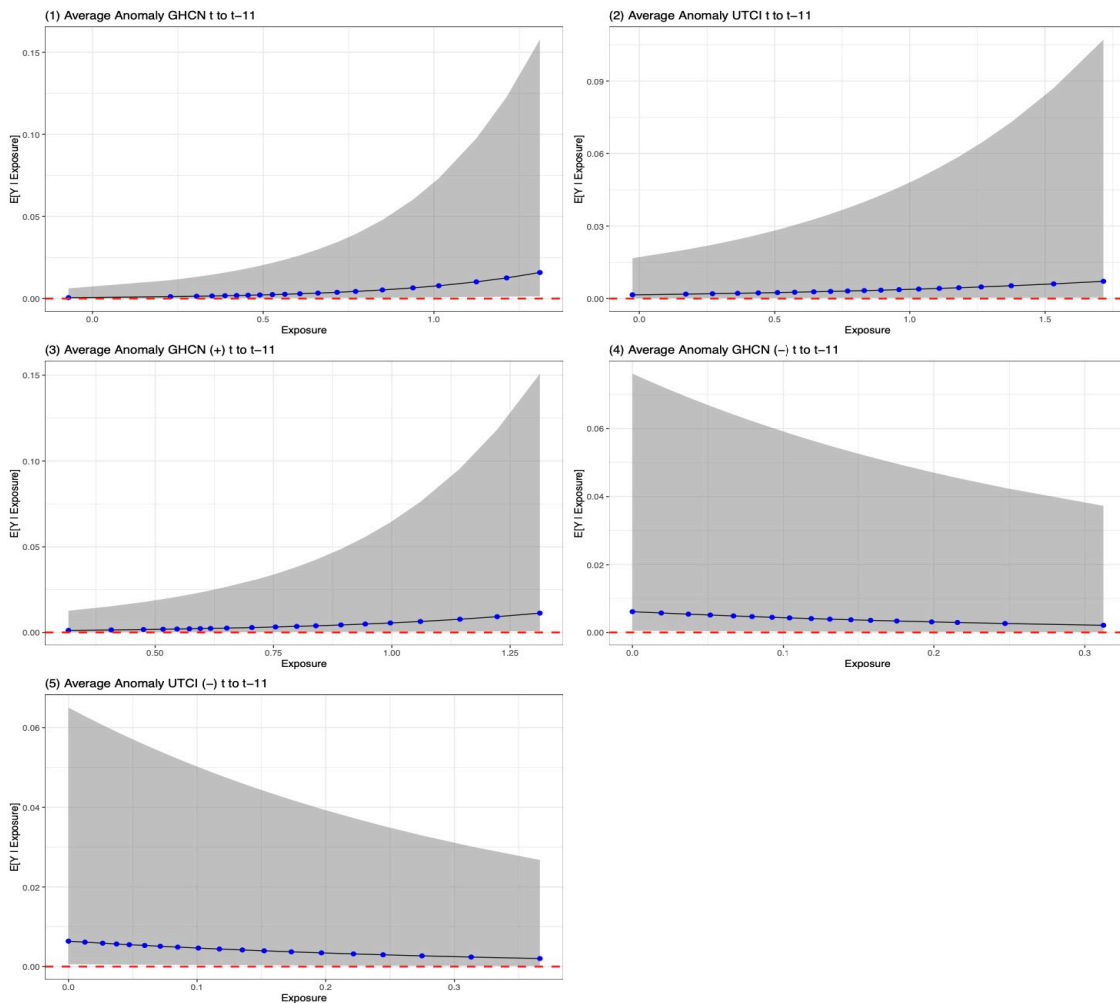


FIGURE 4.14: Average Dose Response Functions for IPW-Adjusted Estimates of Temperature Anomalies and Shocks in European Urban Centres (6 & 12 Period Moving Averages)

Thus, the previous findings indicating that European cities experiencing long-term warming trends were more likely to join the GCoM, while sustained cooling trends were associated with lower participation probabilities, were reinforced after adjusting for confounding. The consistency of these trends across multiple exposure measures, including both UTCI and GHCN anomalies, further supported this conclusion. That said, the finding only held when considering longer time horizons, spanning at least twelve seasons or six years, and only when considering anomalies, as opposed to weather shocks and spells, highlighting the importance of perceptible long-term changes. Moreover, it should be kept in mind that the confidence intervals remained wide.

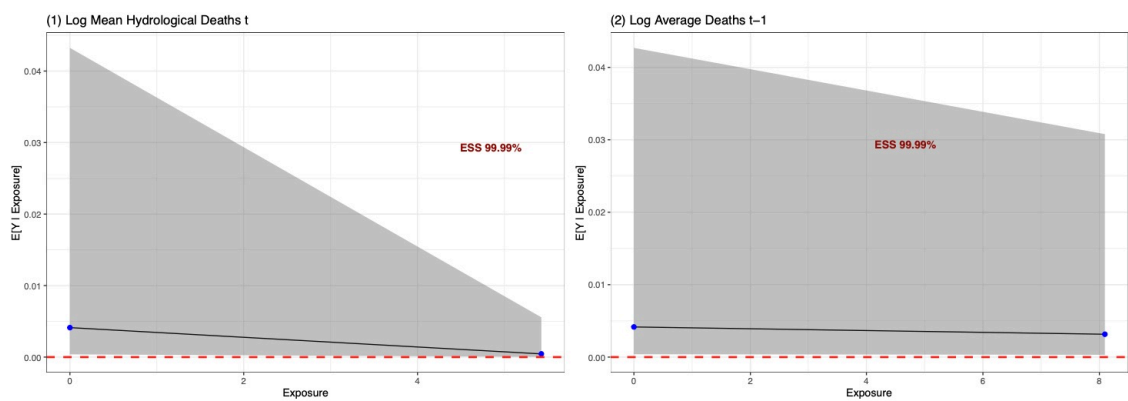


FIGURE 4.15: Average Dose Response Functions for IPW-Adjusted Estimates of Immediate and Delayed (one-lag) Weather-Related Disasters in European Urban Centres

Regarding the findings on weather-related disasters, previous results indicated that for European cities, the number of hydrological disasters and crude and hydrological fatalities discouraged GCoM participation. This was also observed for crude fatalities experienced in the past season. However, adjusting these results for confounding proved challenging. Similar to cold shocks and spells, estimations for the immediate effects of the number of hydrological disasters could not be tested due to the count-based nature of the variable. Additionally, weighting for both the immediate and lagged effects of hydrological and crude fatalities did not adjust for confounding. As shown in the love plots in [Figure D.4 in Appendix D](#), the effective sample size for both estimations was nearly 100 percent. This was due to the covariates' failure to explain variation in the exposure measures, with the GPS model again returning a McFadden R^2 of approximately 0 in both cases. Furthermore, due to limited variation in the variables, the ADRF computations resulted in predicted probabilities being generated for only two bins, as seen in Plots 1 and 2 in [Figure 4.15](#) making the estimates unreliable for detecting a consistent trend. Given these limitations, the persistence of the findings from the previous estimations on immediate and lagged effects of weather-related disasters on

European GCoM participation could not be reliably confirmed.

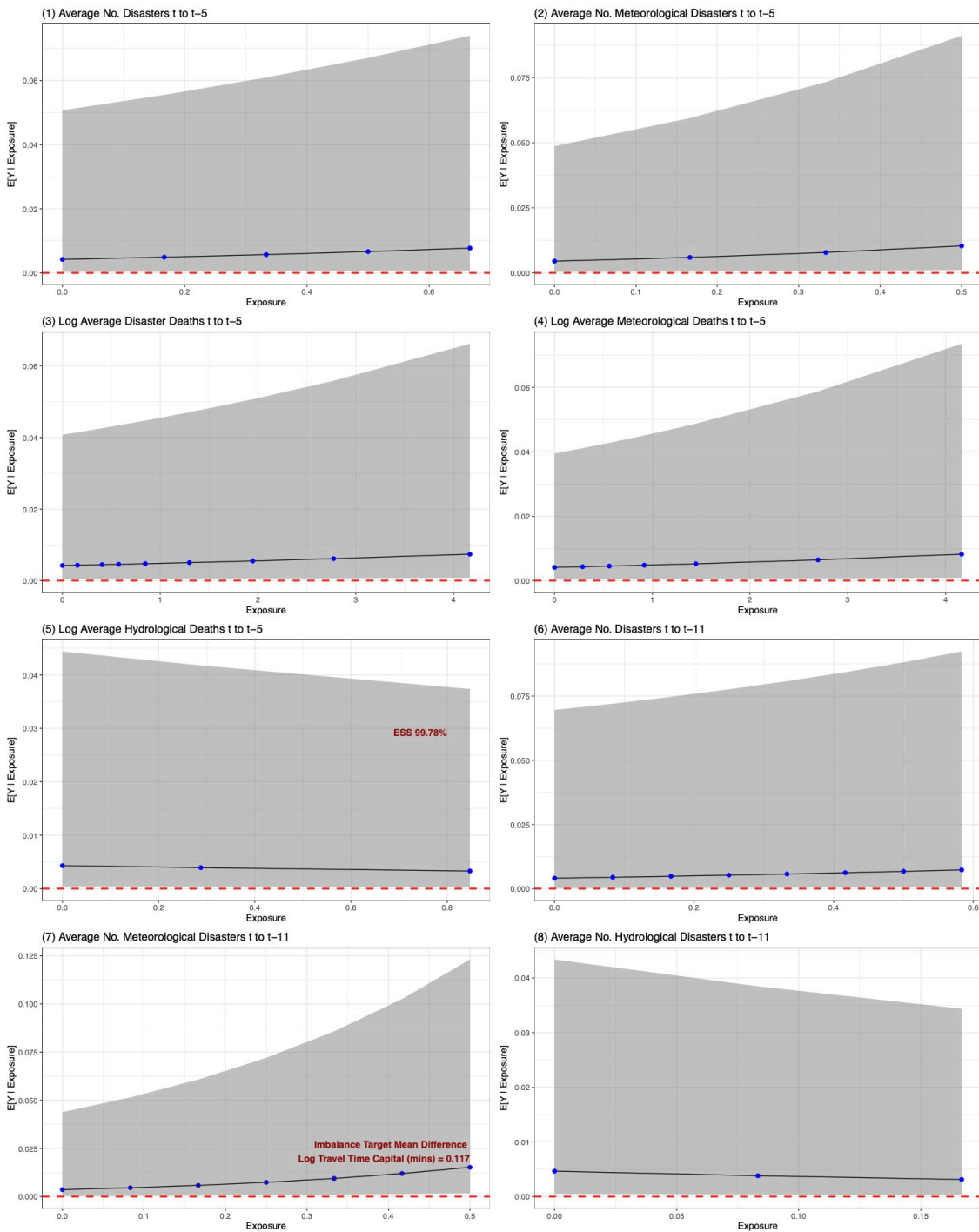


FIGURE 4.16: Average Dose Response Functions for IPW-Adjusted Estimates of Weather-Related Disasters in European Urban Centres (6 & 12 Period Moving Averages) (1)

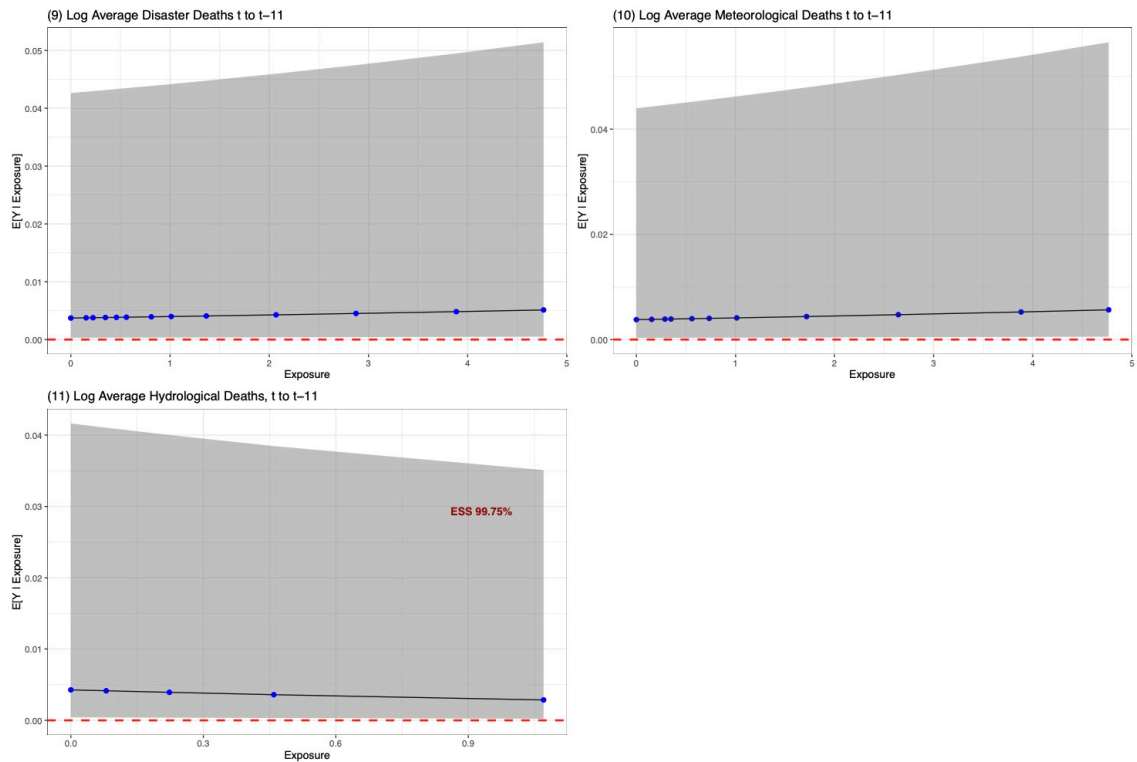


FIGURE 4.17: Average Dose Response Functions for IPW-Adjusted Estimates of Weather-Related Disasters in European Urban Centres (6 & 12 Period Moving Averages) (2)

Turning to the findings considering more persistent effects over longer time horizons, the previous results suggested that the number of disasters and associated fatalities significantly influenced GCoM participation in Europe, likely driven by the strong effect of meteorological disasters and related fatalities. Additionally, hydrological disasters and associated deaths were found to discourage participation. The IPW-adjusted results for these findings are presented in Figures 4.16 and 4.17. Overall, most weighting estimations were successful, with covariates achieving balance and a good effective sample size (see Figure D.4 and D.5 in Appendix D). That said, the adjustment issue for hydrological deaths persisted, resulting in high effective sample sizes. Consequently, the previously observed adverse effects of hydrological deaths averaged over the six-, and twelve-season periods require caution (Plot 5 in Figure 4.16 and Plot 11 in Figure 4.17). Nonetheless, the estimation for the number of hydrological disasters (Plot 9 in Figure 4.17) over a twelve-season horizon achieved balance, providing some insights into the effect of this type of disaster. It should further be noted that in the weighted estimation concerning the twelve-season average for meteorological disasters (Plot 11 in Figure 4.16), IPW weights did not fully account for confounding related to the travel time to the capital. However, the results remained interpretable with a standard mean differential imbalance of 0.11, which was only slightly above the 0.1 threshold and still below an acceptable absolute 0.2 threshold.

Despite these limitations, the remaining results provided valuable insights, with all predicted probabilities returned at the one percent significance level.

The IPW-adjusted results on the estimations considering the six-season moving averages of weather-related exposure (Plots 1 to 5 in [Figure 4.16](#)), confirmed the findings from the survival estimations. The average number of disasters over six seasons was associated with an increase in predicted probability from 0.42% at zero disasters to 0.77% at 0.67 disasters, corresponding to a 0.35 percentage point increase. A similar but stronger effect was observed for meteorological disasters, where participation probability rose from 0.45% at zero events to 1.04% at 0.50 events, reflecting a 0.59 percentage point increase. Regarding disaster-related fatalities, cities with the highest number of deaths saw participation probability increase from 0.42% at zero fatalities to 0.74% at 4.17 log average fatalities, which translated to a 0.32 percentage point rise. The effect was even stronger for fatalities from meteorological disaster, where probability increased from 0.41% at zero fatalities to 0.82% at 4.16 log fatalities, reflecting a 0.41 percentage point increase. However, in all cases, confidence intervals widened as the exposure measure increased, pointing toward a higher level of uncertainty at the upper end.

Further considering twelve-season moving averages, the IPW-adjusted ADRFs reinforced the observed trends. The average number of disasters over twelve seasons remained associated with an increase in predicted probability from 0.41% at zero disasters to 0.73% at 0.58 disasters, i.e., a 0.32 percentage point increase. Similarly, the log of average fatalities from natural disasters showed an increase in participation probability from 0.37% at zero fatalities to 0.51% at 4.77 log fatalities, i.e., a 0.14 percentage point rise. Meteorological disasters again displayed the strongest association with GCoM participation, with predicted probability rising from 0.36% at zero experienced meteorological disasters to 1.52% at 0.50 disasters, corresponding to a 1.16 percentage point increase. The effect of meteorological disaster fatalities followed the same pattern, with probability increasing from 0.38% at zero fatalities to 0.57% at 4.77 log fatalities, a 0.19 percentage point increase. Hence, these results suggested that cities experiencing sustained meteorological disasters showed were more inclined to join the GCoM. While some uncertainty remained, as evidenced by the wide confidence bands, this pattern was evident in the number of disasters and related fatalities and remained consistent across the six- and twelve-season time horizons.

That said, hydrological disasters exhibited an opposite trend. Cities experiencing more hydrological disasters saw a decrease in participation probability, from 0.47% at zero disasters to 0.31% at 0.17 disasters, reflecting a 0.15 percentage point decline over a twelve-season horizon (Plot 8 in [Figures 4.16](#)). While the confidence interval remained wide, it narrowed as the occurrence of disasters increased. These findings suggested that hydrological disasters may have discouraged participation in European cities. However, it should be kept in mind that this result was based on an ADRF of only three binned averages, due to the lack of variability in the variable. Nonetheless, the consistency of

this finding across both immediate and longer time horizons, as well as across the occurrence and death measures in the survival estimations, indicated that this result cannot be discarded and should be further tested.

Chapter 5

Discussion

Following this chapter, the results from the empirical analysis are discussed in relation to the hypotheses outlined in [Chapter 3.1](#), distinguishing between the European and non-European contexts. The limitations of the analysis are also addressed, along with potential avenues for future research.

First, hypothesis H1-A proposed that cities are more likely to join the GCoM when confronted with a temperature shock. This was quantitatively assessed by evaluating both the immediate and lagged effects of temperature anomalies and shocks, measured through crude, positive, and negative anomalies, as well as heat and cold shocks and spells, on the logit hazard of European and non-European cities joining the GCoM.

On one hand, the survival analysis results revealed no consistent pattern among European cities. On the other hand, for non-European cities, the results suggested that warmer-than-average conditions triggered same-season participation, with significant effects observed across three exposure measures. This finding remained consistent even after adjusting for confounding factors. However, the wide confidence intervals indicated some uncertainty, and the absence of significant effects for at least positive UTCI anomalies implied that while positive temperature deviations might influence same-season participation outside of Europe, they are not the primary driver of participation. Adding to this finding was that past-season negative temperature anomalies and shocks across four exposure measures were also significantly linked to increased participation in global cities. However, IPW constraints limited further testing, leaving the robustness of this result unverified, which is a known limitation of this analysis. Nevertheless, the persistence of these effects in the lagged models warrants further investigation to understand the relationship better.

Thus, while the hypothesis can be rejected concerning European cities, findings at the global level provide support, albeit with considerable uncertainty. These suggest that positive temperature deviations positively affect same-season GCoM participations outside of Europe.

Second, hypothesis H1-B formulated whether cities experiencing a weather-related disaster were more likely to join the GCoM. To assess this, the analysis tested the

immediate and lagged effects of crude and different types of disasters, including their occurrences and related fatalities on GCoM participation.

On one hand, considering European cities, the survival analysis revealed mixed results. Climatological disasters appeared to hinder same-season participation, but the extreme effect size indicated this was due to estimation errors. Furthermore, hydrological disasters and fatalities were shown to negatively impact participation, implying that floods may not be viewed as a significant climate action driver. The estimations with one lag further revealed a significant positive effect for climatological disasters and a significant negative effect for crude fatalities. However, the impact of climatological disasters was not reassessed due to previous estimation issues concerning the variable, and the IPW adjustments did not clarify the robustness of the other significant findings. Regarding global cities, disaster exposure showed no consistent impact on same-season participation and highlighted stark sensitivities across various disaster types, along with related occurrences and death tolls. Additionally, lagged effects showed no significant estimates, and higher AIC values weakened the argument for delayed disaster-driven GCoM participation. Despite the sensitivities and uncertainties, the hypothesis can be definitely rejected in European and non-European contexts for all disaster types, when excluding climatological ones. Although the negative effects of same-season hydrological disasters and past-season crude fatalities in Europe could not be confirmed through IPW, they remained negative, offering no support for a positive impact on GCoM participation. This finding contrasts with that of [Baccini and Leemann \(2021\)](#), who observed a short-term increase in support for pro-climate policies following floods in Switzerland, suggesting that disasters might trigger temporary shifts in public sentiment in Europe. In the global context, all significant estimates were also negative, except for climatological deaths, providing little support for a positive disaster impact on same-season GCoM participation. These results align with [Rowan \(2022\)](#), who found no influence of temperature shocks or natural disasters on climate mitigation policies, even considering political regime type or wealth. Nonetheless, it should be noted that on the contrary, [Nohrstedt, Hileman, Mazzoleni et al. \(2022\)](#) observed that wealthier and politically stable cities were more likely to implement adaptation measures after disasters. Thus, while the hypothesis is rejected, future research should explore whether these findings are context-dependent and subject to moderation effects. Moreover, the estimation issues encountered with climatological disasters leave open the possibility of their influence, as they demonstrated a positive impact on participation in the lagged model for Europe and an immediate positive effect considering all other cities. Future research should, therefore, investigate their impact using alternative methods, which adjust for rare events.

Third, Hypothesis (H2-A) proposed that cities experiencing prolonged changing temperature patterns are more likely to join the GCoM. This hypothesis was examined by

considering six- and twelve-season moving averages of the crude, positive, negative UTCI and GHCN anomaly measures, as well as the averaged heat and cold shocks and spells experienced.

Early in the analysis, a pattern already emerged when examining the survival trajectories of cities based on their temperature anomaly quartile (using the 2015-2023 reference period and 1981-2010 base period) in the Kaplan-Meier curves. Cities with the lowest temperature anomalies were slower to join the GCoM, while those with anomalies above the 50th percentile had a faster participation rate, both within and outside of Europe. That said, the survival estimations revealed no significant effect from medium-term temperature trends (considering six-season moving averages) on GCoM participation in Europe. However, longer-term trends (considering twelve-season moving averages) consistently showed that European cities with prolonged warming were more likely to join the GCoM. In contrast, those with prolonged cooling had lower participation rates, which was further confirmed after adjusting for confounding, although the confidence intervals remained wide. Nonetheless, despite the uncertainty, since the findings were consistent across multiple exposure measures and in the weighted estimations, the hypothesis can be accepted in the European context, with long-term positive temperature deviations increasing GCoM involvement and sustained negative deviations discouraging participation. This aligns with [Hoffmann, Muttarak, Peisker et al. \(2022\)](#), who found that temperature anomalies led to higher Green Party votes in European Parliament elections, but contrasts with [Reckien, Flacke, Olazabal and Heidrich \(2015\)](#), who observed that warmer summers hindered climate action plans in Europe, and [Rowan \(2022\)](#), who challenged the assumption that temperature anomalies consistently drive climate policy shifts.

In the global context, rejecting or accepting the hypothesis proved more challenging. Survival estimations initially showed that prolonged cold conditions were consistently linked to GCoM participation across both six- and twelve-season measures. In contrast, positive GHCN anomalies were also significantly associated with participation. However, the IPW-adjusted results revealed that the negative significant effect of the twelve-season moving average of crude UTCI anomalies was initially confounded. That said, the positive effect of negative UTCI anomalies remained after applying IPW adjustments, but the results were uncertain due to wide confidence intervals and only appeared in one exposure measure. Similarly, the positive association with GHCN anomalies persisted after weighting but was also accompanied by high uncertainty and was not confirmed by other exposure measures. These results likely reflect opposing effects of long-term positive and negative temperature deviations or the influence of contextual factors, which warrants further investigation into how economic and governance structures mediate their relationship with GCoM participation. Nonetheless, because of the high degree of uncertainty, the hypothesis cannot be conclusively accepted or rejected in the global context.

Finally, hypothesis H2-B examined whether cities experiencing repeated weather-related natural disasters were more likely to join the GCoM. This was tested using the six- and twelve-season averages of the overall number of weather-related disasters and related deaths, disaggregated for meteorological, hydrological, and climatological disasters.

At first glance, the Kaplan-Meier curves revealed no direct relationship between higher disaster frequencies and faster GCoM participation for European and non-European cities. However, in the survival estimations and IPW-adjusted results for European cities, meteorological disasters were linked to increased GCoM participation, with a strong association for both the number of disasters and fatalities across six- and twelve-season moving averages. Despite some uncertainty due to wide confidence intervals, the robustness of the pattern suggests that repeated exposure to storms and extreme weather drives cities in Europe to take climate action. In contrast, survival results showed that cities with repeated flooding were less likely to participate. Adjusting for confounding in hydrological disasters was more challenging, but the consistency of this pattern across occurrences and fatalities and immediate and long-term estimations gives credit to the findings. One possible explanation may be that floods are not as directly linked to climate change as meteorological events, although this requires further investigation. Thus, while the hypothesis can be confidently accepted for meteorological disasters in Europe, it can be rejected for hydrological disasters, though with some degree of uncertainty. These findings align with [Ji and Darnall \(2022\)](#), who found that only winter storms and geological hazards influenced sustainability planning, while water-related hazards had no impact, further providing evidence on the varying effects of different disaster types on climate action. As for non-European cities, only climatological disasters showed a consistent negative effect over twelve seasons. However, the extreme magnitude of this estimate suggested potential estimation issues since it implied an almost complete reduction in the odds of joining the GCoM. Other disaster types and overall disaster exposure had no significant effects, indicating that persistent disasters did not strongly influence GCoM participation in non-European cities. Therefore, this hypothesis can be rejected for cities outside Europe, which is consistent with [Rowan \(2022\)](#).

Overall, these findings highlighted significant differences in how European and non-European cities respond to climate-related exposure, particularly regarding their participation in trans-municipal climate networks like the GCoM. This became evident in the Kaplan-Meier survival curves, which showed that European cities joined the GCoM more quickly than non-European cities, likely due to the GCoM initially being open only to European cities. Furthermore, in response to the research question (how exposure to climate shocks and disasters influences a city's decision to join climate networks), several interesting patterns emerged. The results showed that temperature shocks had no significant immediate effect on participation in Europe. However, positive temperature

deviations influenced same-season participation outside of Europe, while the delayed effects of negative anomalies were less clear. Regarding weather-related disasters, when excluding climatological disasters, no immediate effects were observed in either context that would increase the likelihood of GCoM participation. More consistent findings were observed when considering long-term trends, with the influence of meteorological disasters and prolonged warming on participation in Europe. This suggested that European cities are more likely to respond to sustained climatic changes than isolated extreme events. On the other hand, hydrological disasters, particularly floods, appeared to hinder participation, although this finding could not be conclusively confirmed. In the global context, however, repeated natural disasters did not have a clear impact on GCoM participation, suggesting that they are not an influential driver. At the same time, considerable uncertainty surrounded the findings on long-term temperature changes in international cities. Thus, depending on the regional context and the time-horizons considered, exposure to climate threats can act as a driver for participation in TMNs.

Despite these insights, it was noticeable that many findings were accompanied by a considerable level of uncertainty and sensitivity, indicating the need for further investigation. This uncertainty suggests that context-dependent factors may influence the effects, as highlighted in the literature (Hoffmann et al., 2022; Nohrstedt et al., 2022) and underscore that climate exposure may not be the primary driver of climate action. Instead, decisions about participation may be moderated by a combination of governance capacity, and economic resources with climate exposure serving as a secondary trigger rather than a primary determinant, as was suggested by Zahran, Brody, Vedlitz, Grover and Miller (2008a). The results further highlighted the importance of city size in shaping GCoM participation, with larger cities consistently demonstrating a higher likelihood of engagement in both the European and global subsets, potentially also being a factor that moderates the observed effects.

On a methodological level, the analysis underscored the importance of using multiple temperature datasets, as findings diverged depending on whether UTCI or GHCN anomalies were used. Adjusting for confounding factors also proved essential, as failure to do so would have led to false conclusions in at least one case. Additionally, regional disparities in exposure and affluence, especially between the Global North and South, further emphasized the importance of accounting for selection bias.

That said, several limitations of the analysis should be considered. First, disaster events were often linked to multiple administrative levels, introducing a measurement error and making it difficult to assign their impact accurately to the precise urban boundary. Second, biases resulting from missing data in the disaster fatality measure could only be partially addressed. Third, the analysis focused only on GCoM participation as a proxy for network participation, excluding alternative networks like smaller, lesser-known

TMNs. This left the possibility that a city may have joined another TMN after a climate event, which was not accounted for. Fourth, while using country-fixed effects was necessary to control for broader national influences and underlying economic and governance conditions, it may have absorbed much of the variation in the exposure effects. This could have led to an underestimation of their actual impact on participation. Fifth, while inverse probability weighting was applied to adjust for confounding, it did not account for all potential biases. This method is not a one-size-fits-all approach, as different exposure measures may require distinct modeling specifications, and as it was not applied to count-based variables. Moreover, while IPW adjusts for observable confounders and strengthens causal implications, other characteristics contributing to confounding may still have influenced the results, as not all factors could be included in the GPS model. Finally, the analysis did not adjust for rare events, which was reflected in the difficulty of isolating the true impact of climatological disasters.

The findings of this analysis open multiple avenues for future research. Given the uncertainty in the results, future studies should investigate sensitivities in the exposure measures and test for moderation effects across varying levels of city affluence and city size. Moreover, future studies should explore alternative modeling approaches to address the issues that arose due to introducing country-fixed effects. Additionally, refining the application of IPW, such as adjusting for count-based variables and adapting the specifications to each exposure measure separately, would improve reliability. At the same time, the persistent effect of prolonged colder-than-average conditions outside of Europe remains intriguing. Given its consistency across multiple specifications, future research should explore this relationship further. Similarly, the negative effect of hydrological events in Europe was not fully confirmed, and future studies should also aim to isolate the true impact of climatological disasters on network participation. Moreover, the sensitivities in the immediate effects of weather-related disasters on in the global context of GCoM participation warrant deeper investigation. Finally, the divergence in results between UTCI and GHCN anomalies highlights the importance of incorporating both re-analysis and weather station data in future research, as relying on a single measure may lead to biased conclusions.

Despite its limitations, this analysis contributed to the literature on urban climate action. It provided one of the most comprehensive empirical assessments of how climate exposure influences city participation in TMNs, both in scope and geographical reach, while highlighting key regional differences between Europe and the global context. By distinguishing between immediate and long-term climate exposures, the analysis also enhanced the understanding of how cities make decisions while considering different time horizons.

Chapter 6

Conclusion

The increasing intensity of climate change presents major challenges for cities, as rising temperatures, extreme weather, and natural disasters amplify their existing vulnerabilities. In response, many cities have decided to take action to mitigate and adapt to these changes, with one strategy being the participation in trans-municipal climate networks (TMNs). This thesis empirically examined how seasonal temperature anomalies, shocks, and weather-related disasters influence urban participation in these networks by modeling the decision-making process of 11,344 cities to join the Global Covenant of Mayors for Climate and Energy (GCoM). The analysis employed geographic information system techniques and integrated multiple data sources, including the Joint Research Centre's Global Human Settlement - Urban Centre Database (Florczyk et al., 2019), GHCNv4 temperature anomalies (GISTEMP Team, 2024), the Universal Thermal Climate Index (Di Napoli et al., 2021), and the Emergency Events Database (Centre for Research on the Epidemiology of Disasters, 2024). Moreover, the analysis employed discrete-time survival analysis and strengthened the robustness of the findings by adjusting for selection bias through inverse probability weighting (IPW).

The findings revealed regional differences in TMN participation. European cities joined the GCoM faster than their non-European counterparts, likely due to its initial exclusivity. Long-term climate patterns played a significant role in Europe, with persistent positive temperature deviations and repeated meteorological disasters, such as extreme temperatures and storms, positively influencing participation rates. In contrast, outside Europe, long-term temperature patterns showed no consistent impact that could be conclusively confirmed, and repeated natural disasters did not drive participation. Instead, positive temperature deviations were found to have an immediate effect, influencing same-season membership decisions. These results suggested that exposure to climate threats can influence TMN participation depending on the regional context and time horizons considered.

That said, many findings were accompanied by a high degree of uncertainty, indicating that other factors, such as governance capacity, economic resources, and city size, might moderate the effects of climate exposures. Thus, while climate exposure was

shown to act as a trigger, it is unlikely to be the primary determinant of participation. However, these considerations were not explored, an aspect that this analysis lacked. Additionally, methodological limitations must be considered, including measurement errors in disaster data, potential underestimation of exposure effects due to the inclusion of country-fixed effects, and challenges in accounting for rare climatological disasters. Furthermore, not all weighted estimations successfully adjusted for confounders, and the application was not adjusted for count-based variables, which limited the effectiveness of IPW.

Given these uncertainties and limitations, several avenues for future research emerge. Further investigation is needed into context-dependent effects, particularly the role of city-level affluence, governance capacity, and city size in moderating climate exposure's influence on network participation. Refining the IPW method used and exploring alternative modeling approaches to address the challenges of including country-fixed effects would enhance the robustness of results. Additionally, unresolved considerations, such as the persistence of prolonged colder-than-average conditions outside Europe, the unconfirmed impact of hydrological disasters in Europe, and the role of climatological disasters in network participation, warrant further exploration. Finally, expanding the analysis beyond the GCoM to include smaller TMNs would provide a more comprehensive understanding of urban network participation, as many cities may engage in alternative networks not captured in this analysis.

Despite its limitations, this analysis contributed to the understanding of the role of exposure to climate threats in trans-municipal network participation. It offered one of the most comprehensive empirical assessments in terms of scope and highlighted regional disparities and the varying impacts of short- and long-term climate shifts. Future research can build on these findings to further refine the understanding of the factors driving cities to engage in climate action.

Chapter 7

Bibliography

- Allison, P. D. (1982) “Discrete-Time Methods for the Analysis of Event Histories,” *Sociological Methodology*, 13, 61–98, [10.2307/270718](https://doi.org/10.2307/270718). 20
- Baccini, L. and L. Leemann (2021) “Do natural disasters help the environment? How voters respond and what that means,” *Political Science Research and Methods*, 9 (3), 468–484, [10.1017/psrm.2020.25](https://doi.org/10.1017/psrm.2020.25). 8, 10, 13, 68
- Bansard, J.S., P.H. Pattberg, and O. Widerberg (2017) “Cities to the rescue? Assessing the performance of transnational municipal networks in global climate governance,” *International Environmental Agreements*, 17, 229–246, [10.1007/s10784-016-9318-9](https://doi.org/10.1007/s10784-016-9318-9). 2
- Brennan, M. M., S. Whitmee, C. V. Braneon, N. Meinsma, and R. Green (2022) “Sea Level Rise and City-Level Climate Action,” *European Journal of Environment and Public Health*, 6 (2), em0111, [10.21601/ejeph/12046](https://doi.org/10.21601/ejeph/12046). 3, 10
- Castán Broto, Vanesa (2017) “Urban Governance and the Politics of Climate change,” *World Development*, 93, 1–15, <https://doi.org/10.1016/j.worlddev.2016.12.031>. 2
- Centre for Research on the Epidemiology of Disasters (2024) “Emergency Events Database (EMDAT),” Université Catholique de Louvain, Dataset: <https://www.emdat.be/>. 4, 17, 73
- (n.d.a) “EM-DAT: The International Disaster Database,” <https://public.emdat.be/data>, Accessed: 6 March 2025. 35
- (n.d.b) “Entry Criteria Protocols,” <https://doc.emdat.be/docs/protocols/entry-criteria/>, Accessed: 6 March 2025. 17
- (n.d.c) “Spatial Information and Geocoding,” EM-DAT Documentation, Retrieved from <https://doc.emdat.be/docs/data-structure-and-content/spatial-information/>. 17
- Chesnaye, Nathalie C., Vianda S. Stel, Giovanni Tripepi, Friedo W. Dekker, Edward L. Fu, Carmine Zoccali, and Kitty J. Jager (2021) “An introduction to inverse probability of treatment weighting in observational research,” *Clinical Kidney Journal*, 15 (1), 14–20, [10.1093/ckj/sfab158](https://doi.org/10.1093/ckj/sfab158). 55

- CIESIN, Columbia University (2013) “Low Elevation Coastal Zone (LECZ) Global Dataset,” NASA Socioeconomic Data and Applications Center (SEDAC), [10.7927/H4MW2F2J](https://doi.org/10.7927/H4MW2F2J). 18
- Cliff, Andrew David and J Keith Ord (1981) *Spatial processes: models & applications*: Taylor & Francis. 21
- Coalition for Urban Transitions (2019) “Climate Emergency, Urban Opportunity: How National Governments Can Secure Economic Prosperity and Avert Climate Catastrophe by Transforming Cities,” <https://urbantransitions.global/wp-content/uploads/2019/09/Climate-Emergency-Urban-Opportunity-report.pdf>, Accessed: 5 March 2025. 1
- Collins, M., M. Sutherland, L. Bouwer et al. (2019) “Extremes, Abrupt Changes and Managing Risk,” in Pörtner, H.-O., D.C. Roberts, V. Masson-Delmotte et al. eds. *IPCC Special Report on the Ocean and Cryosphere in a Changing Climate*, 589–655, Cambridge, UK and New York, NY, USA: Cambridge University Press, [10.1017/9781009157964.008](https://doi.org/10.1017/9781009157964.008). 1
- Conley, T.G. (1999) “GMM estimation with cross sectional dependence,” *Journal of Econometrics*, 92 (1), 1–45, [https://doi.org/10.1016/S0304-4076\(98\)00084-0](https://doi.org/10.1016/S0304-4076(98)00084-0). 22
- Copernicus Climate Change Service (2024) “Global Climate Highlights 2023,” <https://climate.copernicus.eu/global-climate-highlights-2023>, Accessed: 5 March 2025. 1
- Crippa, M., D. Guizzardi, M. Muntean et al. (2018) “Gridded emissions of air pollutants for the period 1970–2012 within EDGAR v4.3.2,” *Earth System Science Data*, 10 (4), 1987–2013, [10.5194/essd-10-1987-2018](https://doi.org/10.5194/essd-10-1987-2018). 19
- Dawson, A. (2017) *Extreme Cities: The Peril and Promise of Urban Life in the Age of Climate Change*: Verso Books. 1, 13
- Dell, Melissa, Benjamin F. Jones, and Benjamin A. Olken (2014) “What Do We Learn from the Weather? The New Climate-Economy Literature,” *Journal of Economic Literature*, 52 (3), 740–798, [10.1257/jel.52.3.740](https://doi.org/10.1257/jel.52.3.740). 16, 22
- Di Napoli, C., C. Barnard, C. Prudhomme, H. L. Cloke, and F. Pappenberger (2021) “ERA5-HEAT: A global gridded historical dataset of human thermal comfort indices from climate reanalysis,” *Geoscience Data Journal*, 8 (1), 2–10, [10.1002/gdj3.102](https://doi.org/10.1002/gdj3.102). 3, 16, 73
- Eisenack, K. (2024) “Why local governments set climate targets: Effects of city size and political costs,” *Environmental & Resource Economics*, 87 (11), 2935–2965, [10.1007/s10640-024-00919-1](https://doi.org/10.1007/s10640-024-00919-1). 19

- European Commission (2016) “The Covenant of Mayors: Cities and regions stepping up climate and energy action,” Accessed: 6 March 2025, February 4, https://ec.europa.eu/commission/presscorner/detail/it/ip_16_2247, European Commission Press Corner. 11, 20, 28
- Fiala, D., G. Havenith, P. Bröde, B. Kampmann, and G. Jendritzky (2012) “UTCI-Fiala multi-node model of human heat transfer and temperature regulation,” *International Journal of Biometeorology*, 56, 429–441, [10.1007/s00484-011-0424-7](https://doi.org/10.1007/s00484-011-0424-7). 16
- Field, C.B., V. Barros, T.F. Stocker et al. (2012) *Managing the Risks of Extreme Events and Disasters to Advance Climate Change Adaptation*, Cambridge, UK and New York, NY, USA: Cambridge University Press, 582, A Special Report of Working Groups I and II of the Intergovernmental Panel on Climate Change. 1, 13
- Florczyk, Aneta, Christina Corbane, Marcello Schiavina et al. (2019) “GHS-UCDB R2019A - GHS Urban Centre Database 2015, multitemporal and multidimensional attributes,” <http://data.europa.eu/89h/53473144-b88c-44bc-b4a3-4583ed1f547e>, [10.2905/53473144-b88c-44bc-b4a3-4583ed1f547e](https://doi.org/10.2905/53473144-b88c-44bc-b4a3-4583ed1f547e). 3, 14, 73
- Food and Agriculture Organization of the United Nations (2018) “Global Administrative Unit Layers (GAUL),” <http://www.fao.org/geonetwork/srv/en/main.home>. 17
- Gabbe, C. J., G. Pierce, E. Petermann, and A. Marecek (2024) “Why and How Do Cities Plan for Extreme Heat?” *Journal of Planning Education and Research*, 44 (3), 1316–1330, [10.1177/0739456X211053654](https://doi.org/10.1177/0739456X211053654). 2, 9, 10, 13, 18
- Gesing, F. (2018) “Transnational Municipal Climate Networks and the Politics of Standardisation: The Contested Role of Climate Data in the New Global Covenant of Mayors for Climate and Energy,” *Politics and Governance*, 6 (3), 126–135, [10.17645/pag.v6i3.1111](https://doi.org/10.17645/pag.v6i3.1111). 12
- Giordono, Leanne, Hilary Boudet, Anna Karmazina, Casey Taylor, and Brent Steel (2018) “Opposition “overblown”? Community response to wind energy siting in the Western United States,” *Energy Research Social Science*, 43, [10.1016/j.erss.2018.05.016](https://doi.org/10.1016/j.erss.2018.05.016). 8
- GISTEMP Team (2024) “GISS Surface Temperature Analysis (GISTEMP), version 4,” *J. Geophys. Res. Atmos.*, 124 (12), 6307–6326, [10.1029/2018JD029522](https://doi.org/10.1029/2018JD029522), NASA Goddard Institute for Space Studies. Dataset: data.giss.nasa.gov/gistemp/. 3, 15, 73
- Global Burden of Disease Collaborative Network (2017) “Global Burden of Disease Study 2017 (GBD 2017) Air Pollution Exposure Estimates,” Dataset, <https://www.healthdata.org/research-analysis/gbd>. 20

- Global Covenant of Mayors for Climate & Energy (2021) “Impact Report 2021,” <https://www.globalcovenantofmayors.org/impact2021/>, Accessed: 6 March 2025. 12
- (n.d.a) “Our cities,” <https://www.globalcovenantofmayors.org/our-cities/>, Accessed: 6 March 2025. 15
- (n.d.b) “Who we are,” <https://www.globalcovenantofmayors.org/who-we-are/>, Accessed: 5 March 2025. 2, 11
- Greifer, N. (2025b) “Estimating Effects After Weighting,” <https://cran.r-project.org/web/packages/WeightIt/vignettes/estimating-effects.html>, Accessed: 6 March 2025. 25, 26, 54
- Greifer, Noah (2025a) “Assessing Balance in Matching,” R package vignette, <https://cran.r-project.org/web/packages/MatchIt/vignettes/assessing-balance.html>. 25
- Gurney, R. M., S. Meng, S. Rumschlag, and A. F. Hamlet (2022) “The Influences of Political Affiliation and Weather-Related Impacts on Climate Change Adaptation in U.S. Cities,” *Weather, Climate, and Society*, 14, 919–931, 10.1175/WCAS-D-21-0030.1. 10
- Hazlett, C. and M. Mildenerger (2020) “Wildfire exposure increases pro-environment voting within Democratic but not Republican areas,” *American Political Science Review*, 114 (4), 1359–1365, 10.1017/S0003055420000441. 2, 8, 10, 13
- Heidrich, O., D. Reckien, M. Olazabal et al. (2016) “National climate policies across Europe and their impacts on cities strategies,” *Journal of Environmental Management*, 168, 36–45, 10.1016/j.jenvman.2015.11.043. 2
- Hirano, K. and G.W. Imbens (2004) “The Propensity Score with Continuous Treatments,” in Shewhart, W.A., S.S. Wilks, A. Gelman, and X.-L. Meng eds. *Applied Bayesian Modeling and Causal Inference from Incomplete-Data Perspectives*, Chap. 7: Wiley, 10.1002/0470090456.ch7. 24, 25
- Hoffmann, R., R. Mutarak, J. Peisker et al. (2022) “Climate change experiences raise environmental concerns and promote Green voting,” *Nature Climate Change*, 12, 148–155, 10.1038/s41558-021-01263-8. 2, 8, 10, 13, 16, 17, 69, 71
- Hsu, A., J. Tan, Y.M. Ng et al. (2020) “Performance determinants show European cities are delivering on climate mitigation,” *Nature Climate Change*, 10, 1015–1022, 10.1038/s41558-020-0879-9. 12
- International Union for Conservation of Nature (2023) “The IUCN Red List of Threatened Species,” <https://www.iucnredlist.org/>. 18

- Ji, H. and N. Darnall (2022) "How do external conditions affect the design of local governments' sustainability strategies?" *Regulation & Governance*, 16, 910–929, [10.1111/rego.12334](https://doi.org/10.1111/rego.12334). 2, 9, 10, 13, 18, 70
- Jones, Rebecca Louise, Aditi Kharb, and Sandy Tubeuf (2023) "The untold story of missing data in disaster research: a systematic review of the empirical literature utilising the Emergency Events Database (EM-DAT)," *Environmental Research Letters*, 18 (10), 103006, [10.1088/1748-9326/acfd42](https://doi.org/10.1088/1748-9326/acfd42). 18
- Jurgilevich, Alexandra, Aleksi Räsänen, Fanny Groundstroem, and Sirkku Juhola (2017) "A systematic review of dynamics in climate risk and vulnerability assessments," *Environmental Research Letters*, 12 (1), [10.1088/1748-9326/aa5508](https://doi.org/10.1088/1748-9326/aa5508). 7
- Kalbfleisch, John D. and Ross L. Prentice (2002) *The Statistical Analysis of Failure Time Data*, Wiley Series in Probability and Statistics: John Wiley & Sons, Inc. [10.1002/9781118032985](https://doi.org/10.1002/9781118032985). 23
- Kang, J., E. Ji, J. Kim, and et al. (2022) "Evaluation of Patients' Adverse Events During Contact Isolation for Vancomycin-Resistant Enterococci Using a Matched Cohort Study With Propensity Score," *JAMA Network Open*, 5 (3), e221865, [10.1001/jamanetworkopen.2022.1865](https://doi.org/10.1001/jamanetworkopen.2022.1865). 58
- Kern, K. and H. Bulkeley (2009) "Cities, Europeanization and Multi-level Governance: Governing Climate Change through Transnational Municipal Networks," *JCMS: Journal of Common Market Studies*, 47, 309–332, [10.1111/j.1468-5965.2009.00806.x](https://doi.org/10.1111/j.1468-5965.2009.00806.x). 11
- Kona, A., F. Monforti-Ferrario, P. Bertoldi et al. (2021) "Global Covenant of Mayors, a dataset of greenhouse gas emissions for 6200 cities in Europe and the Southern Mediterranean countries," *Earth System Science Data*, 13 (7), 3551–3564, [10.5194/essd-13-3551-2021](https://doi.org/10.5194/essd-13-3551-2021). 12
- Kummu, M., M. Taka, and J. H. A. Guillaume (2018) "Gridded global datasets for Gross Domestic Product and Human Development Index over 1990–2015," *Scientific Data*, 5, 180004, [10.1038/sdata.2018.4](https://doi.org/10.1038/sdata.2018.4). 19
- Lee, B.K., J. Lessler, and E.A. Stuart (2011) "Weight trimming and propensity score weighting," *PLOS ONE*, 6 (3), e18174, [10.1371/journal.pone.0018174](https://doi.org/10.1371/journal.pone.0018174). 25
- Lenssen, N., G.A. Schmidt, M. Hendrickson, P. Jacobs, M. Menne, and R. Ruedy (2024) "A GISTEMPv4 observational uncertainty ensemble," *J. Geophys. Res. Atmos.*, 129 (17), e2023JD040179, [10.1029/2023JD040179](https://doi.org/10.1029/2023JD040179). 15
- Lichstein, J.W., T.R. Simons, S.A. Shriver, and K.E. Franzreb (2002) "Spatial autocorrelation and autoregressive models in ecology," *Ecological Monographs*, 72, 445–463, [10.1890/0012-9615\(2002\)072\[0445:SAAAMI\]2.0.CO;2](https://doi.org/10.1890/0012-9615(2002)072[0445:SAAAMI]2.0.CO;2). 21

- Maia Polo, F. and R. Vicente (2023) "Effective sample size, dimensionality, and generalization in covariate shift adaptation," *Neural Computing and Applications*, 35, 18187–18199, [10.1007/s00521-021-06615-1](https://doi.org/10.1007/s00521-021-06615-1). 55
- McCarthy, J.J., O.F. Canziani, N.A. Leary, D.J. Dokken, and K.S. White eds. (2001) *Climate Change 2001: Impacts, Adaptation, and Vulnerability. Contribution of Working Group II to the Third Assessment Report of the Intergovernmental Panel on Climate Change*, Cambridge: Cambridge University Press. 2, 7
- McFadden, D. (1974) "Conditional Logit Analysis of Quantitative Choice Behaviour," in Zarembka, P. ed. *Frontiers in Econometrics*, New York: Academic Press. 43
- Melica, G., A. Treville, C. Franco De Los Rios et al. (2022) "Covenant of Mayors: 2022 assessment," Technical Report EUR 31291 EN, Publications Office of the European Union, Luxembourg, [10.2760/930988](https://doi.org/10.2760/930988), JRC130957. 11, 12
- Miller, H.J. (2004) "Tobler's First Law and Spatial Analysis," *Annals of the Association of American Geographers*, 94 (2), 284–289, [10.1111/j.1467-8306.2004.09402005.x](https://doi.org/10.1111/j.1467-8306.2004.09402005.x). 21
- MIT Climate Portal (2021) "Urban Heat Islands," <https://climate.mit.edu/explainers/urban-heat-islands>, Accessed: 5 March 2025. 1
- Naimi, Ashley I., Erica E. M. Moodie, Nathalie Auger, and Jay S. Kaufman (2014) "Constructing Inverse Probability Weights for Continuous Exposures; a Comparison of Methods," *Epidemiology*, 25 (2), 292–299, [10.1097/EDE.000000000000053](https://doi.org/10.1097/EDE.000000000000053). 24, 25
- National Aeronautics and Space Administration (NASA) (n.d.) "The Carbon Cycle," Retrieved from <https://earthobservatory.nasa.gov/features/CarbonCycle>, <https://earthobservatory.nasa.gov/features/CarbonCycle>, NASA Earth Observatory. 19
- Nguyen Long, L.A. and R.M. Krause (2021) "Managing policy-making in the local climate governance landscape: The role of network administrative organizations and member cities," *Public Administration*, 99, 23–39, [10.1111/padm.12684](https://doi.org/10.1111/padm.12684). 2, 11
- Nohrstedt, D., J. Hileman, M. Mazzoleni et al. (2022) "Exploring disaster impacts on adaptation actions in 549 cities worldwide," *Nature Communications*, 13, 3360, [10.1038/s41467-022-31059-z](https://doi.org/10.1038/s41467-022-31059-z). 3, 9, 10, 17, 18, 54, 68, 71
- Organisation for Economic Co-operation and Development (2020) "Monitoring exposure to climate-related hazards," https://www.oecd.org/en/publications/monitoring-exposure-to-climate-related-hazards_da074cb6-en.html, [Accessed: 6 March 2025]. 7
- Orttung, Robert (2019) *Capital cities as innovators in sustainability policy and practice*, 3–24, [10.4324/9780429426049-1](https://doi.org/10.4324/9780429426049-1). 19

- Osofsky, H. M. (2015) "Rethinking the Geography of Local Climate Action: Multi-Level Network Participation in Metropolitan Regions," *Utah Law Review*, 2015, 173, https://scholarship.law.umn.edu/faculty_articles/359. 12
- Pablo Romero, Maria, Rafael Pozo-Barajas, and Antonio Sánchez-Braza (2015) "Understanding local CO2 emissions reduction targets," *Renewable and Sustainable Energy Reviews*, 48, 10.1016/j.rser.2015.04.014. 11
- Picavet, M. E. B., L. S. V. de Macedo, R. A. Bellezoni, and J. A. Puppim de Oliveira (2023) "How can Transnational Municipal Networks foster local collaborative governance regimes for environmental management?" *Environmental Management*, 71 (3), 505–522, 10.1007/s00267-022-01685-w. 11, 13
- Poelman, H. and L. Dijkstra (2014) "A harmonised definition of cities and rural areas: the new degree of urbanisation," Technical Report WP 01/2014, European Commission Directorate-General for Regional and Urban Policy, <https://gkhub.earthobservations.org>. 14
- Pörtner, H.-O., D.C. Roberts, M. Tignor et al. (2022) *Climate Change 2022: Impacts, Adaptation and Vulnerability*, Cambridge, UK and New York, NY, USA: Cambridge University Press, 3056, 10.1017/9781009325844, Contribution of Working Group II to the Sixth Assessment Report of the Intergovernmental Panel on Climate Change. 1, 7, 13
- Reckien, D., J. Flacke, M. Olazabal, and O. Heidrich (2015) "The Influence of Drivers and Barriers on Urban Adaptation and Mitigation Plans—An Empirical Analysis of European Cities," *PLOS ONE*, 10 (8), e0135597, 10.1371/journal.pone.0135597. 2, 9, 10, 12, 18, 19, 41, 69
- Reckien, Diana, Monica Salvia, Oliver Heidrich et al. (2018) "How are cities planning to respond to climate change? Assessment of local climate plans from 885 cities in the EU-28," *Journal of Cleaner Production*, 191, 207–219, 10.1016/j.jclepro.2018.03.220. 2, 11, 12, 13, 20, 28
- Rosenzweig, C., W. Solecki, P. Romero-Lankao, S. Mehrotra, S. Dhakal, and S. Ali Ibrahim (2018) *Climate Change and Cities: Second Assessment Report of the Urban Climate Change Research Network*: Cambridge University Press. 1
- Rowan, S. (2022) "Extreme weather and climate policy," *Environmental Politics*, 32 (4), 684–707, 10.1080/09644016.2022.2127478. 3, 8, 10, 17, 22, 68, 69, 70
- Ruiz-Campillo, X., O. Gil, and C. García Fernández (2022) "Ready for Climate Change? An Assessment of Measures Adopted by 45 Mediterranean Coastal Cities to Face Climate Change," in Leal Filho, W. and E. Manolas eds. *Climate Change in the Mediterranean and Middle Eastern Region*, 269–291, Cham: Springer, 10.1007/978-3-030-78566-6_13. 1, 9, 10, 11

- Salvia, Monica, Marta Olazabal, Paris A. Fokaides et al. (2021a) "Climate mitigation in the Mediterranean Europe: An assessment of regional and city-level plans," *Journal of Environmental Management*, 295, 113146, <https://doi.org/10.1016/j.jenvman.2021.113146>. 9, 10, 19
- Salvia, Monica, Diana Reckien, Filomena Pietrapertosa et al. (2021b) "Will climate mitigation ambitions lead to carbon neutrality? An analysis of the local-level plans of 327 cities in the EU," *Renewable and Sustainable Energy Reviews*, 135, 110253, <https://doi.org/10.1016/j.rser.2020.110253>. 12
- Stryzhak, O., M. Tupa, and J. Rodzik (2022) "Relationship between the level of human development and institutional quality," *Economics & Sociology*, 15 (2), 274–295, [10.14254/2071-789X.2022/15-2/17](https://doi.org/10.14254/2071-789X.2022/15-2/17). 19
- Suresh, K., C. Severn, and D. Ghosh (2022) "Survival prediction models: an introduction to discrete-time modeling," *BMC Medical Research Methodology*, 22, 207, [10.1186/s12874-022-01679-6](https://doi.org/10.1186/s12874-022-01679-6). 20
- Thomas-Slayter, Barbara P. (2003) *Southern Exposure: International Development and the Global South in the Twenty-First Century*, United States: Kumarian Press, 11. 54
- Tutz, Gerhard and Matthias Schmid (2016) "Modeling Discrete Time-to-Event Data," [10.1007/978-3-319-28158-2](https://doi.org/10.1007/978-3-319-28158-2). 20, 22, 23
- UN-Habitat (2016) *World Cities Report 2016: Urbanization and Development – Emerging Futures*: United Nations Human Settlements Programme (UN-Habitat), <https://unhabitat.org/sites/default/files/download-manager-files/WCR-2016-WEB.pdf>, Accessed: 6 March 2025. 1
- United Nations Development Programme (n.d.) "Human Development Index (HDI)," Accessed: March 8, 2025, from <https://hdr.undp.org/data-center/human-development-index#/indicies/HDI>. 19
- United Nations Framework Convention on Climate Change (2025) "Global Climate Action Portal," <https://climateaction.unfccc.int/>, [Accessed: 5 March 2025]. 3, 11
- Wei, Yiheng, Dunxian She, Jun Xia, Gangsheng Wang, Qin Zhang, Shengzhi Huang, Yu Zhang, and Tianyue Wang (2024) "Climate change dominates the increasing exposure of global population to compound heatwave and humidity extremes in the future," 02, [10.21203/rs.3.rs-3378606/v1](https://doi.org/10.21203/rs.3.rs-3378606/v1). 7
- Weiss, D. J., A. Nelson, H. S. Gibson, W. Temperley, S. Peedell, A. Lieber, B. Hanchard, and A. J. Tatem (2018) "A global map of travel time to cities to assess inequalities in accessibility in 2015," *Nature*, 553 (7688), 333–336, [10.1038/nature25181](https://doi.org/10.1038/nature25181). 19

- Westreich, Daniel and Sander Greenland (2013) “The table 2 fallacy: presenting and interpreting confounder and modifier coefficients,” *American Journal of Epidemiology*, 177 (4), 292–298, [10.1093/aje/kws412](https://doi.org/10.1093/aje/kws412). 26
- World Bank (2010) *World Development Report 2010: Development and Climate Change*, Washington, DC: World Bank, <https://openknowledge.worldbank.org/entities/publication/e917b047-3a48-5688-9804-0466417304fd>, Accessed: 5 March 2025. 1
- World Meteorological Organization (2024) “WMO confirms that 2023 smashes global temperature record,” <https://wmo.int/news/media-centre/wmo-confirms-2023-smashes-global-temperature-record>, Accessed: 5 March 2025. 1
- Xing, Y.F., Y.H. Xu, M.H. Shi, and Y.X. Lian (2016) “The impact of PM2.5 on the human respiratory system,” *Journal of Thoracic Disease*, 8 (1), E69–74, [10.3978/j.issn.2072-1439.2016.01.19](https://doi.org/10.3978/j.issn.2072-1439.2016.01.19). 19
- Zahran, S., S. D. Brody, A. Vedlitz, H. Grover, and C. Miller (2008a) “Vulnerability and Capacity: Explaining Local Commitment to Climate-Change Policy,” *Environment and Planning C: Government and Policy*, 26 (3), 544–562, [10.1068/c2g. 2, 3, 8, 10, 18, 19, 42, 71](https://doi.org/10.1068/c2g.2.3.8.10.18.19.42.71)
- Zahran, S., H. Grover, S.D. Brody, and A. Vedlitz (2008b) “Risk, stress, and capacity: Explaining metropolitan commitment to climate protection,” *Urban Affairs Review*, 43 (4), 447–474, [10.1177/1078087407304688](https://doi.org/10.1177/1078087407304688). 3, 9, 10, 18, 19, 54
- Zhu, Y., D.L. Coffman, and D. Ghosh (2015) “A Boosting Algorithm for Estimating Generalized Propensity Scores with Continuous Treatments,” *Journal of Causal Inference*, 3 (1), 25–40, [10.1515/jci-2014-0022](https://doi.org/10.1515/jci-2014-0022). 25

Appendix A

The link to the repository containing the do-files for the computation of the empirical models can be found here:

<https://tinyurl.com/repositorygcom>.

Appendix B

	Min	Median	Mean	Max	SD
GCoM Member	0.000	0.000	0.099	1.000	0.299
LECZ (%)	0.000	0.000	7.681	100.004	24.334
No. Endangered Species	1.000	21.000	28.549	340.000	42.097
Industrial Co2/capita	0.000	0.118	0.654	165.610	3.500
PM 2.5 concentration	1.550	34.608	38.015	118.834	23.652
HDI 2015	0.317	0.683	0.660	1.000	0.146
Area (km2)	1.000	18.000	51.858	6622.000	198.119
Mins. to Capital	0.010	448.033	615.434	16717.419	711.801
Temperature Anomaly 2015-2023	-0.162	0.652	0.713	2.160	0.245
UTCI Anomaly 2015-2023	-0.521	0.434	0.510	1.979	0.243
No. Disasters 2000-2024	0.000	14.000	20.124	115.000	19.897
No. Climatological Disasters 2000-2024	0.000	0.000	0.328	21.000	0.927
No. Meteorological Disasters 2000-2024	0.000	7.000	10.401	102.000	12.693
No. Hydrological Disasters 2000-2024	0.000	7.000	9.394	56.000	9.752

FIGURE B.1: Summary Statistics of Time-Invariant Variables in Sample of GHS Urban Centres

	Min	Median	Mean	Max	SD
GCoM Join Event	0.000	0.000	0.005	1.000	0.073
Anomaly UTCI	-4.417	0.569	0.686	8.793	0.838
Anomaly UTCI (+)	0.000	0.569	0.740	8.793	0.764
Anomaly UTCI (-)	0.000	0.000	0.054	4.417	0.196
No. Heat Shocks UTCI	0.000	12.000	15.091	133.000	12.404
No. Cold Shocks UTCI	0.000	0.000	20.044	183.000	46.268
No. Heat Spells UTCI	0.000	1.000	1.688	17.000	1.874
No. Cold Spells UTCI	0.000	0.000	1.119	18.000	2.441
No. Disasters	0.000	0.000	0.469	12.000	1.203
No. Climatological Disasters	0.000	0.000	0.008	3.000	0.091
No. Meteorological Disasters	0.000	0.000	0.224	7.000	0.675
No. Hydrological Disasters	0.000	0.000	0.236	9.000	0.760
Mean Disaster Deaths	0.000	0.000	36.612	3275.000	200.727
Mean Climatological Deaths	0.000	0.000	0.092	234.000	3.219
Mean Meteorological Deaths	0.000	0.000	11.448	3275.000	86.870
Mean Hydrological Deaths	0.000	0.000	30.576	2830.000	195.164

FIGURE B.2: Summary Statistics of Time-Varying Variables in Sample of GHS Urban Centres

Appendix C

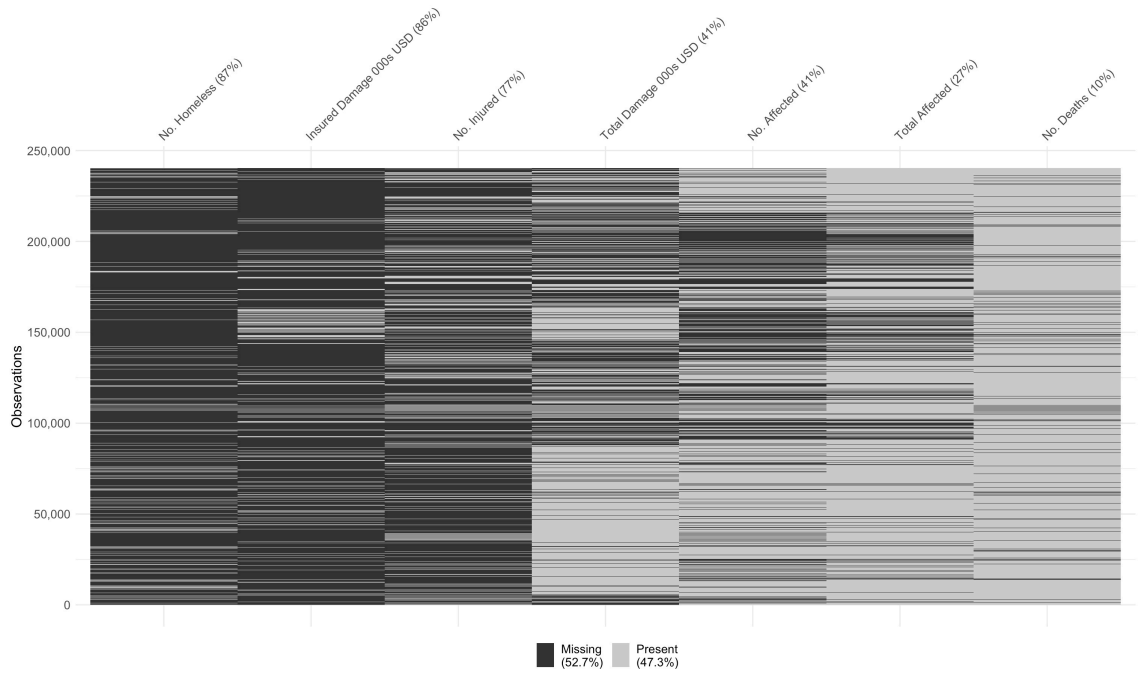


FIGURE C.1: Missingness in Human-Impact Variables in Weather-related Disaster Observations within Sample of GHS Urban Centres (April 2000 - March 2024)

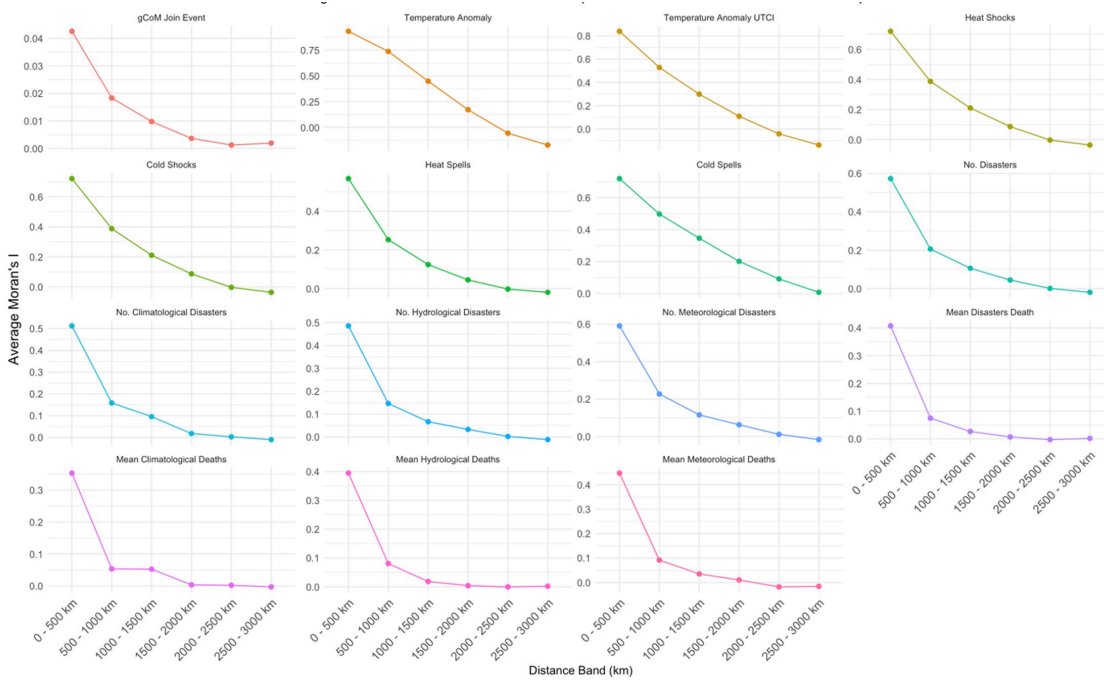


FIGURE C.2: Average Moran's I Across Distance Bands for Exposure Variables in Sample of GHS Urban Centres

Distance Band	(1)	(2)	(3)	(4)	(5)	(6)	(7)	(8)
Models for European Urban Centres								
0 - 500 km	0.1688 (time = 4)	0.1684 (time = 4)	0.1689 (time = 4)	0.1700 (time = 4)	0.1684 (time = 4)	0.1688 (time = 4)	0.1684 (time = 4)	0.1688 (time = 4)
500 - 1000 km	0.1047 (time = 11)	0.1018 (time = 11)	0.1014 (time = 11)	0.0969 (time = 11)	0.1011 (time = 11)	0.1038 (time = 11)	0.1011 (time = 11)	0.1038 (time = 11)
1000 - 1500 km	0.0740 (time = 18)	0.0741 (time = 18)	0.0760 (time = 18)	0.0742 (time = 18)	0.0737 (time = 18)			
1500 - 2000 km	0.0622 (time = 30)	0.0624 (time = 30)	0.0606 (time = 30)	0.0617 (time = 30)	0.0627 (time = 30)	0.0628 (time = 30)	0.0627 (time = 30)	0.0628 (time = 30)
2000 - 2500 km	0.0545 (time = 3)	-	0.0568 (time = 3)	0.0544 (time = 19)	0.0565 (time = 3)	0.0561 (time = 3)	0.0565 (time = 3)	0.0561 (time = 3)
2500 - 3000 km	-	-	0.0520 (time = 19)	-	-	-	-	-
Models for Global Urban Centres (excl. Europe)								
0 - 500 km	0.0723 (time = 12)	0.0725 (time = 12)	0.0729 (time = 12)	0.0732 (time = 12)	0.0726 (time = 12)	0.0724 (time = 12)	0.0726 (time = 12)	0.0724 (time = 12)
500 - 1000 km	0.0644 (time = 11)	0.0644 (time = 11)	0.0640 (time = 11)	0.0639 (time = 11)	0.0635 (time = 11)	0.0637 (time = 11)	0.0635 (time = 11)	0.0637 (time = 11)
1000 - 1500 km	0.0611 (time = 5)	0.0586 (time = 5)	0.0580 (time = 5)	0.0588 (time = 5)	0.0602 (time = 5)	0.0592 (time = 5)	0.0602 (time = 5)	0.0592 (time = 5)
1500 - 2000 km	0.0549 (time = 17)	0.0560 (time = 17)	0.0562 (time = 17)	0.0563 (time = 17)	0.0556 (time = 17)	0.0553 (time = 17)	0.0556 (time = 17)	0.0553 (time = 17)
2000 - 2500 km	-	0.0540 (time = 4)	0.0547 (time = 4)	0.0542 (time = 4)	0.0541 (time = 4)	0.0543 (time = 4)	-	0.0543 (time = 4)

Note: (1) Anomaly GHCN. (2) Anomaly UTCI. (3). Heat & Cold Shocks - UTCI. (4) Heat & Cold Spells - UTCI. (5) No. Disasters. (6) No. Disasters by Type. (7) Log Disaster Deaths. (8) Log Disaster Deaths by Type.

FIGURE C.3: Significant Moran's I ($|\hat{I}| \geq 0.05, p < 0.1$) in Model Residuals, using various Exposure Variables Across Distance Bands

Term	European Urban Centres			Global Urban Centres (excl. Europe)		
	VIF	VIF 95% CI	Increased SE	VIF	VIF 95% CI	Increased SE
No. Endangered Species	1.79	[1.76, 1.83]	1.34	1.31	[1.31, 1.32]	1.15
Log PM 2.5 concentration	1.17	[1.16, 1.19]	1.08	1.14	[1.14, 1.15]	1.07
Log Industrial Co2/capita	1.86	[1.82, 1.89]	1.36	1.31	[1.30, 1.32]	1.14
Log HDI 2015	1.59	[1.57, 1.62]	1.26	1.16	[1.15, 1.16]	1.08
Log Area (km²)	3.28	[3.21, 3.35]	1.81	1.64	[1.63, 1.65]	1.28
Log Mins. to Capital	3.84	[3.75, 3.93]	1.96	1.25	[1.24, 1.25]	1.12

FIGURE C.4: Variation Inflation Factors for the Estimation of the Effect of Control Variables on the Logit Hazard of City Participation in the GCoM

Appendix D



FIGURE D.1: Love Plots: Covariate Balance Before & After IPW for Global (excl. Europe) Urban Centres Temperature Anomalies & Shock Estimations (1)

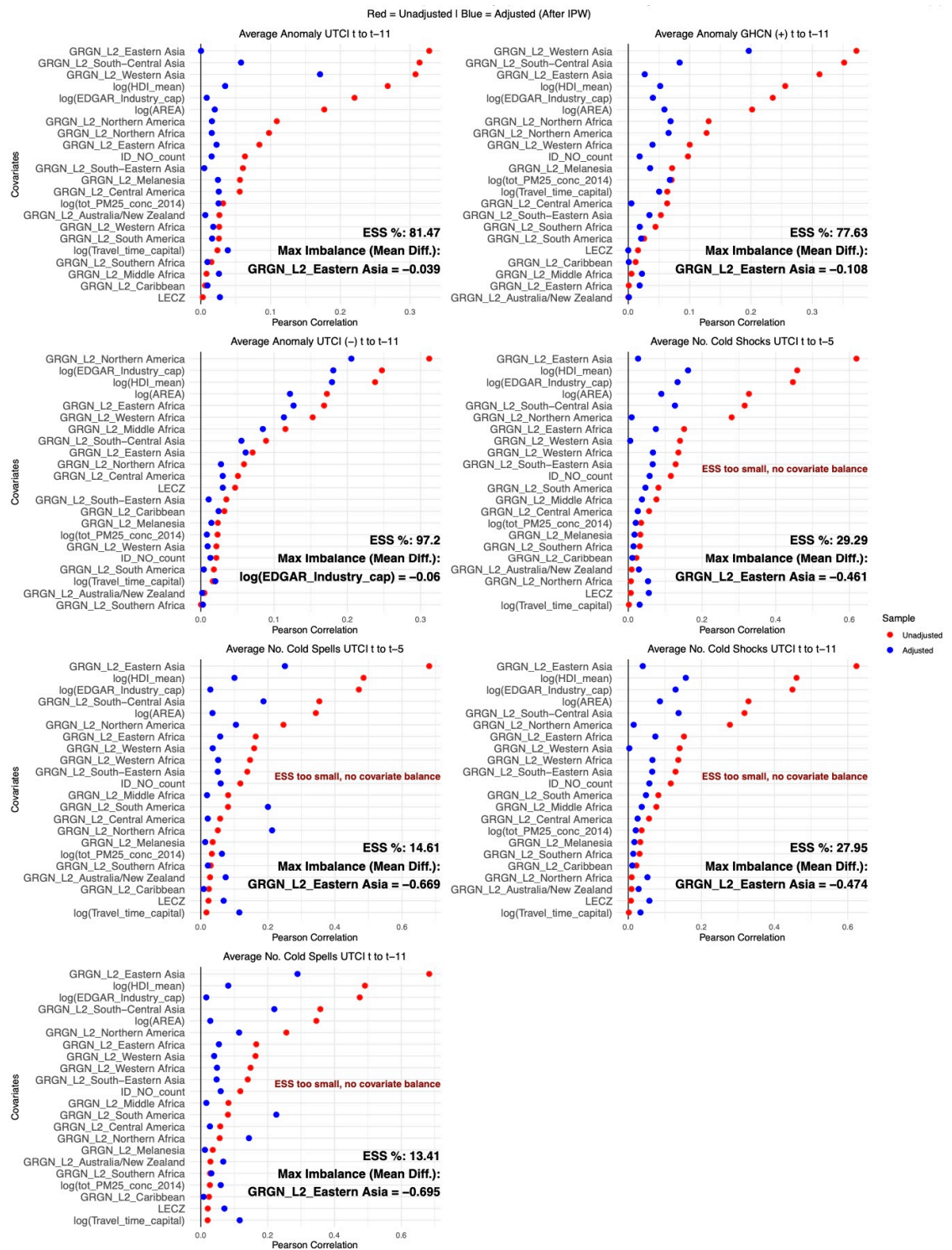


FIGURE D.2: Love Plots: Covariate Balance Before & After IPW for Global (excl. Europe) Urban Centres Temperature Anomalies & Shock Estimations (2)

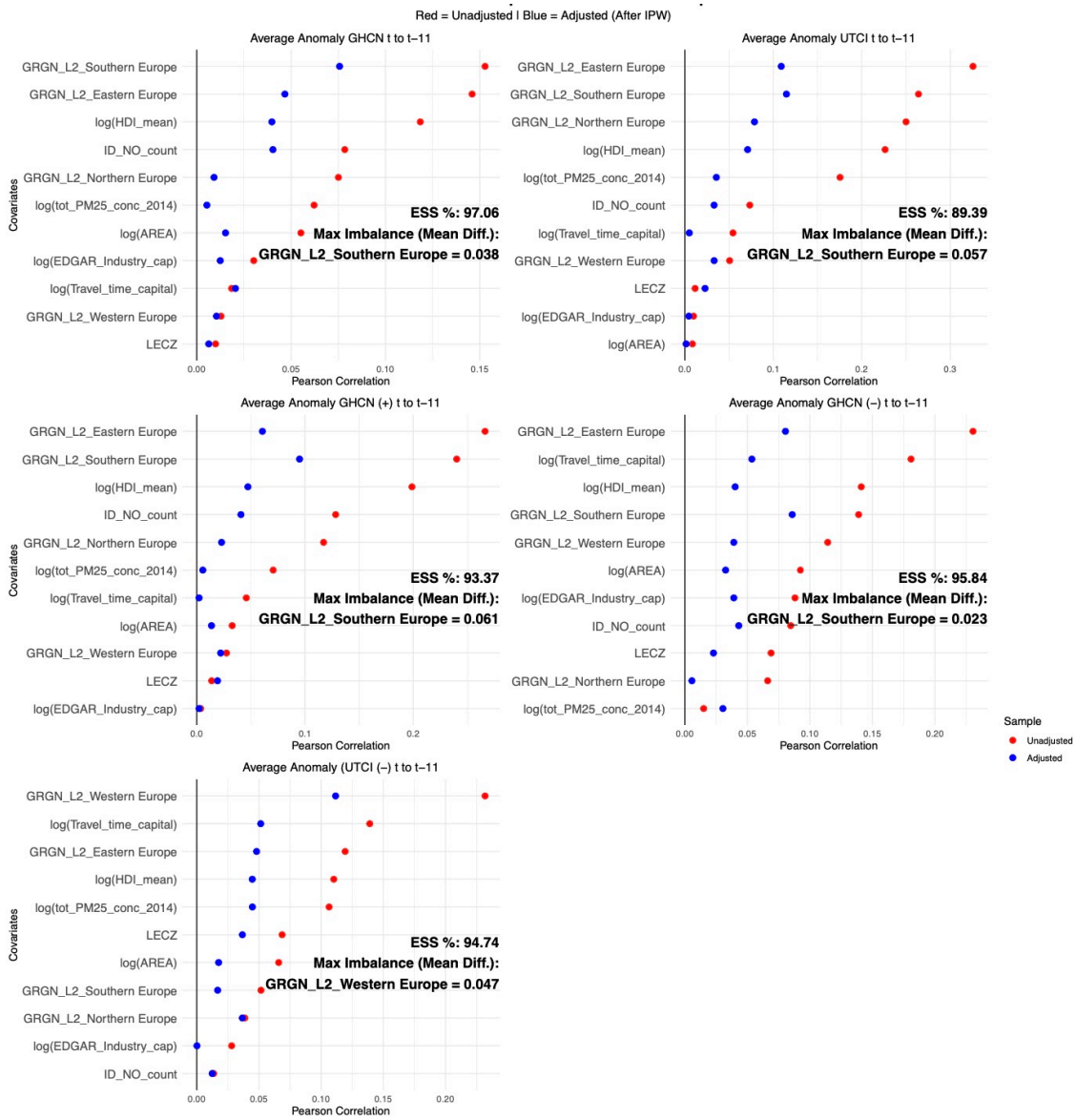


FIGURE D.3: Love Plots: Covariate Balance Before & After IPW for European Urban Centres Temperature Anomalies & Shocks Estimations

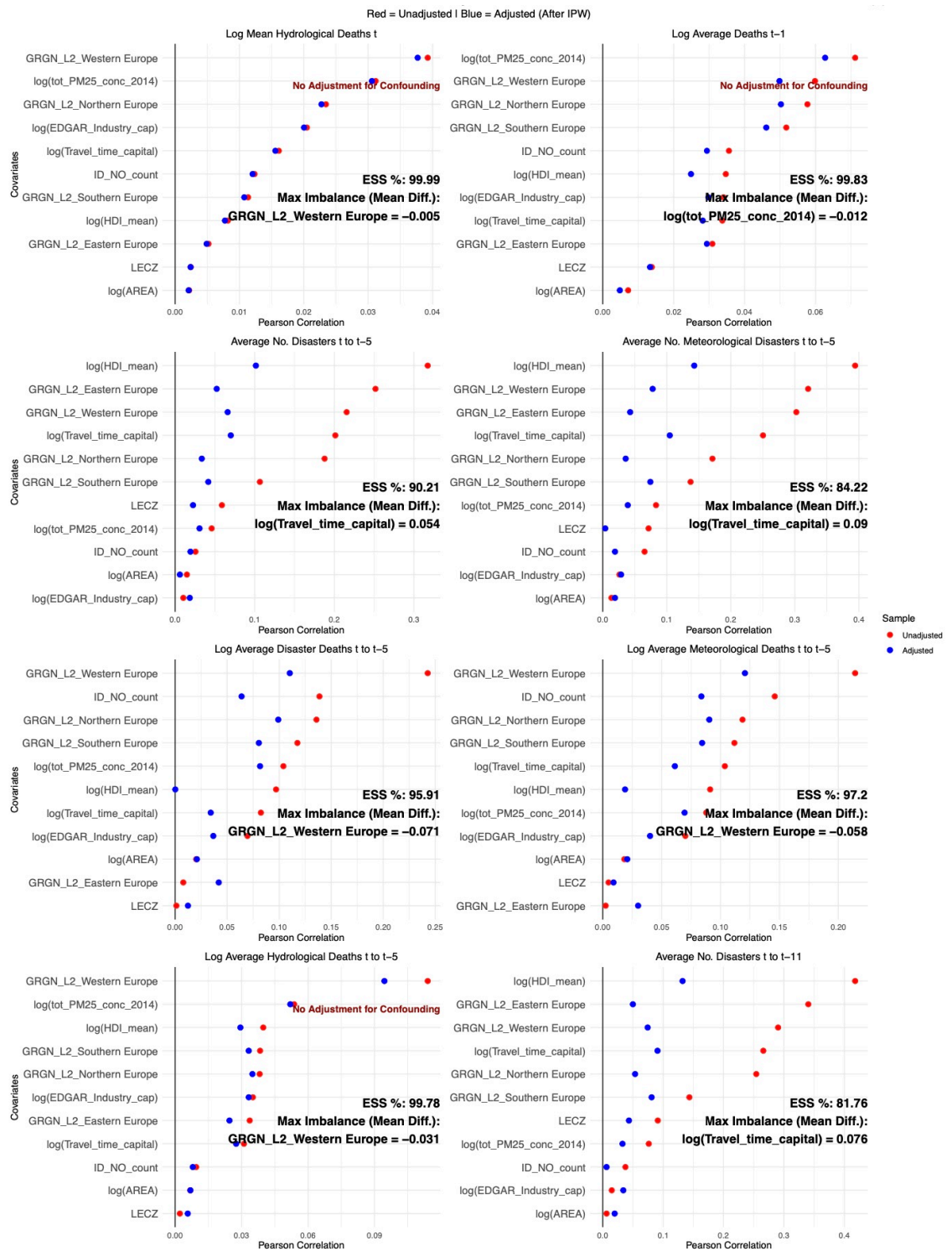


FIGURE D.4: Love Plots: Covariate Balance Before & After IPW for European Urban Centres Weather-Related Disasters Estimations (1)

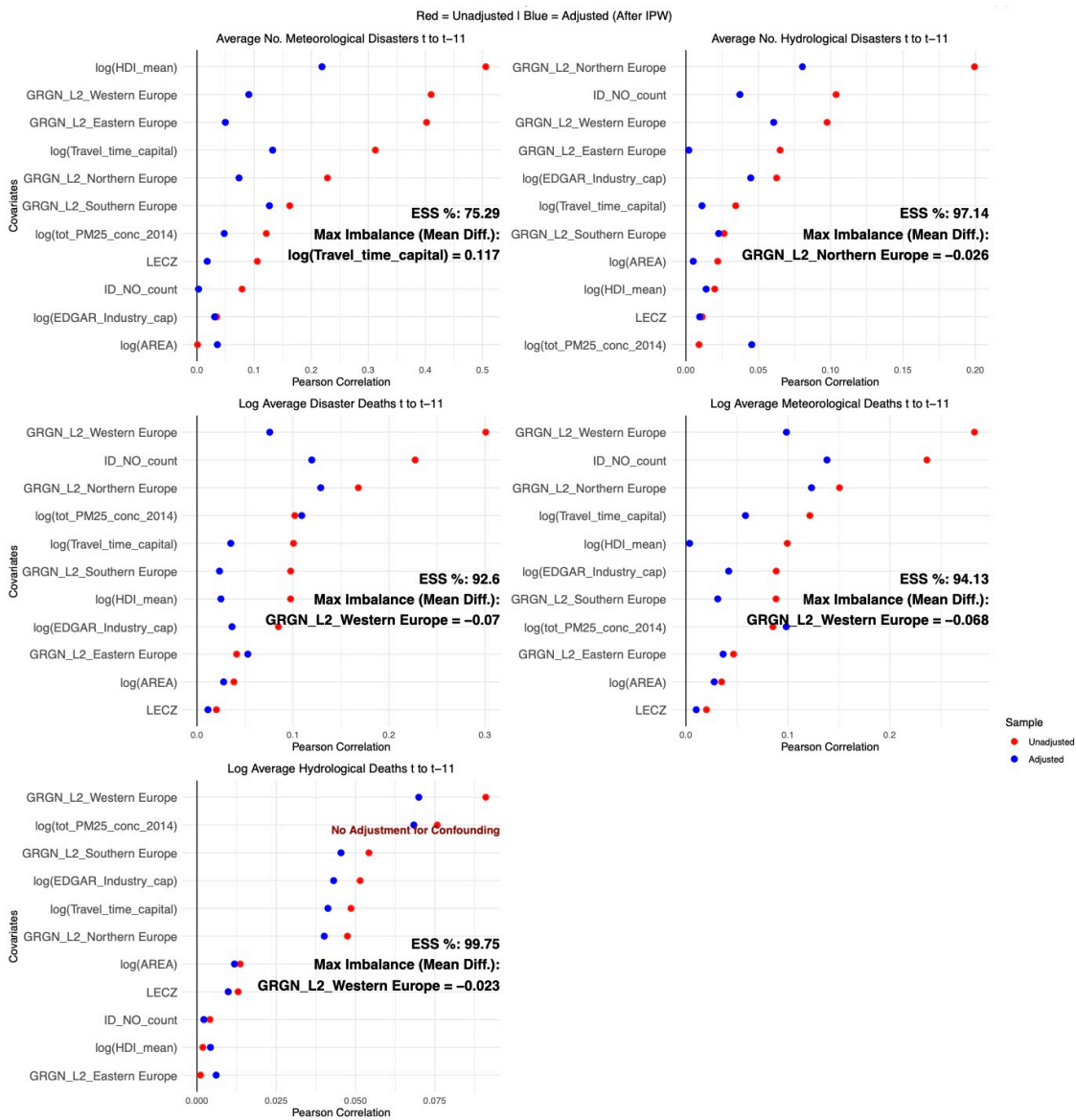


FIGURE D.5: Love Plots: Covariate Balance Before & After IPW for European Urban Centres Weather-Related Disasters Estimations (2)

Appendix E - Data Documentation

Column Name	Type & Description	Original Dataset
ID_HDC_G0	Character – Unique identifier for each Urban Centre as provided in the GHS Urban Centre Database.	Global Human Settlement - Urban Centre Database (GHS-UCDB).
Season_Join_Range	Character – Indicates the corresponding hot or cold season for the observation.	
stamp	Numeric – Unique identifier for each Season_Join_Range in the dataset.	
AREA	Numeric – total land area (in square kilometers) of Urban Centres delineated in 2000, within the boundaries of the 2015 Urban Centre.	GHS-UCDB. Derived from: Global Human Settlement Population (GHS-POP); Global Human Settlement Built-Up (GHS-BUILT) datasets.
latitude	Numeric – Latitude coordinate of the geometric centroid of the Urban Centre.	GHS-UCDB.
longitude	Numeric – Longitude coordinate of the geometric centroid of the Urban Centre.	GHS-UCDB.
CTR_MN_ISO	Character – ISO 3 country code representing the main country of the Urban Centre.	GHS-UCDB.
GRGN_L1	Character – Major geographical region classification based on the main country.	GHS-UCDB. Derived from: United Nations, Department of Economic and Social Affairs (UNDESA).
GRGN_L2	Character – Detailed geographical region classification based on the main country.	GHS-UCDB. Derived from: UNDESA.
UC_NM_MN	Character – Primary name of the Urban Centre.	GHS-UCDB. Derived from: The Global Rural-Urban Mapping Project (GRUMP), v1; Natural Earth Populated Places, v4.1.0; GeoNames.
UC_NM_LST	Character – List of assigned names for the Urban Centre.	GHS-UCDB. Derived from: The Global Rural-Urban Mapping Project (GRUMP), v1; Natural Earth Populated Places, v4.1.0; GeoNames.
pop_2015	Numeric – Total population in 2015 within the polygon of the Urban Centre.	GHS-UCDB. Derived from: Global Human Settlement Population (GHS-POP).
Travel_time_capital	Numeric – Estimated travel time to the country's capital, expressed in minutes.	Global Friction Surface 2015.
tot_emmis_indus_2015_non_s h	Numeric – Total CO ₂ emissions per tonnes, from the industrial sector in 2012, using non-short-cycle organic fuels, calculated within the polygon Urban Centre.	GHS UCDB. Derived from: GHS UCDB, EDGAR v4.3.2.
tot_PM25_conc_2014	Numeric – Total concentration of PM _{2.5} for the reference year 2014, calculated within the polygon of the Urban Centre. Expressed in µg/m ³ .	GHS-UCDB. Derived from: Global Burden of Disease (GBD) 2017.
HDI_mean	Numeric – Mean Human Development Index (HDI) value averaged over the Urban Centre polygon.	Gridded global datasets for Gross Domestic Product and Human Development Index over 1990–2015.
GDP_per_cap_PPP_mean	Numeric – Numeric – Mean GDP per capita, measured in constant 2011 international dollars (USD, PPP-adjusted) averaged over the Urban Centre polygon.	Gridded global datasets for Gross Domestic Product and Human Development Index over 1990–2015.

ID_NO_count	Numeric – Number of species threatened by climate change (by IUCN Red List classification) in the Urban Centre area.	IUCN Red List of Threatened Species.
LECZ	Numeric – Percentage of the Urban Centre's area that lies in the Low Elevation Coastal Zone (LECZ, <10m above sea level).	Low Elevation Coastal Zone (LECZ) Global Dataset.
Europe	Binary (0/1) – Identifier indicating whether the Urban Centre lies within European boundaries as defined by GRGN L1.	Derived from: GHS-UCDB.
EDGAR_Industry_cap	Numeric – Total per capita CO ₂ emissions from the industrial sector in 2012, using non-short-cycle organic fuels.	Derived from: GHS-UCDB; GHS-POP.
Anomaly_2015_2023_GHCN	Numeric – Mean temperature anomaly averaged over the polygon of the Urban Centre, for the period 2015-2023, using the 1981-2010 baseline.	GISS Surface Temperature Analysis (GISTEMP), v4.
gcom_id	Character – If the Urban Centre is a Global Covenant of Mayors (gCoM) member, this is the Organization ID it is linked to in the gCoM database; otherwise, NA.	GCoM Member Data.
joinDate	Date – If the Urban Centre is a gCoM member, this is the date it officially joined; otherwise, NA.	GCoM Member Data.
member	Binary (0/1) – Indicator of whether the Urban Centre is a gCoM member (1) or not (0).	GCoM Member Data.
anomaly_UTCI_2015_2023	Numeric – Mean Universal Thermal Climate Index (UTCI) anomaly averaged over the polygon of the Urban Centre, for the period 2015-2023, using the 1981-2010 baseline.	Thermal comfort indices derived from ERA5 reanalysis.
sum_n_dis	Numeric – Total number of weather-related disasters (Climatological, Hydrological & Meteorological) from April 2000 to March 2024 linked to the Urban Centre polygon.	Emergency Events Database (EM-DAT).
sum_n_dis_Climatological	Numeric – Total number of climatological disasters from April 2000 to March 2024 linked to the Urban Centre polygon.	EM-DAT.
sum_n_dis_Hydrological	Numeric – Total number of hydrological disasters from April 2000 to March 2024 linked to the Urban Centre polygon.	EM-DAT.
sum_n_dis_Meteorological	Numeric – Total number of meteorological disasters from April 2000 to March 2024 linked to the Urban Centre polygon.	EM-DAT.
event	Binary (0/1) – 1 if the Urban Centre joined GCoM within the corresponding Season_Join_Range; otherwise 0.	Derived from: GHS-UCDB; GCoM Member Data.
Event_cumulative	Binary (0/1) – 1 if the Urban Centre has already joined GCoM, all subsequent Season_Join_Range values are coded 1 once a city joins; otherwise 0.	Derived from: GHS-UCDB; GCoM Member Data.
UTCI_anomaly	Numeric – Mean Universal Thermal Climate Index (UTCI) anomaly averaged over the polygon of the Urban Centre, for the given period, using the 1981-2010 respective baseline.	Thermal comfort indices derived from ERA5 reanalysis.

Sum_Positive_Spells_UTCI_perc	Numeric – Total count of heat spells experienced by the Urban Centre (three or more consecutive days exceeding the 95th percentile of UTCI, based on the 1981–2010 reference window) within the given period.	Thermal comfort indices derived from ERA5 reanalysis.
Sum_Negative_Spells_UTCI_perc	Numeric – Total count of cold spells experienced by the Urban Centre (three or more consecutive days below the 5th percentile of UTCI, based on the 1981–2010 reference window) within the given period.	Thermal comfort indices derived from ERA5 reanalysis.
Sum_Positive_Shocks_UTCI_perc	Numeric – Total count of heat shocks experienced by the Urban Centre (single days exceeding the 95th percentile of UTCI, based on the 1981–2010 reference window) within the given period.	Thermal comfort indices derived from ERA5 reanalysis.
Sum_Negative_Shocks_UTCI_perc	Numeric – Total count of cold shocks experienced by the Urban Centre (single days below the 5th percentile of UTCI, based on the 1981–2010 reference window) within the given period.	Thermal comfort indices derived from ERA5 reanalysis.
temperature_anomaly	Numeric – Mean temperature anomaly averaged over the polygon of the Urban Centre, for the given period, using the respective 1981-2010 baseline.	GISS Surface Temperature Analysis (GISTEMP), v4.
n_dis_season	Numeric – Total count of weather-related (Climatological, Hydrological & Meteorological) disasters linked to the Urban Centre within the given period.	EM-DAT.
deaths_mean_season	Numeric – Average of deaths from weather-related (Climatological, Hydrological & Meteorological) disasters linked to the Urban Centre for the given period.	EM-DAT.
n_dis_Climatological	Numeric – Total count of Climatological disasters linked to the Urban Centre within the given period.	EM-DAT.
n_dis_Hydrological	Numeric – Total count of Hydrological disasters linked to the Urban Centre within the given period.	EM-DAT.
n_dis_Meteorological	Numeric – Total count of Meteorological disasters linked to the Urban Centre within the given period.	EM-DAT.
deaths_mean_Climatological	Numeric – Average of deaths from weather-related Climatological disasters linked to the Urban Centre for the given period.	EM-DAT.
deaths_mean_Hydrological	Numeric – Average of deaths from weather-related Hydrological disasters linked to the Urban Centre for the given period.	EM-DAT.
deaths_mean_Meteorological	Numeric – Average of deaths from weather-related Meteorological disasters linked to the Urban Centre for the given period.	EM-DAT.
pos_a_temp_UTCI	Numeric – Anomaly from UTCI, retaining only positive values (values ≥ 0), while setting negative values to 0.	Thermal comfort indices derived from ERA5 reanalysis.

neg_a_temp_UTCI	Numeric – Anomaly from UTCI, retaining only negative values (values ≤ 0), while setting positive values to 0.	Thermal comfort indices derived from ERA5 reanalysis.
pos_a_temp_GHCN	Numeric – Temperature anomaly from GHCN, retaining only positive values (values ≥ 0), while setting negative values to 0.	GISS Surface Temperature Analysis (GISTEMP), v4.
neg_a_temp_GHCN	Numeric – Temperature anomaly from GHCN, retaining only negative values (values ≤ 0), while setting positive values to 0.	GISS Surface Temperature Analysis (GISTEMP), v4.
Year	Numeric – The respective year of the observation. For cold seasons, the start year of the season is recorded.	
Europe_2015	Binary (0/1) – Identifies whether the Urban Centre lies within Europe (as defined by GRGN_L1) and whether the Season_Join_Range is before the hot season 2014.	
lag_[variable]_1	Numeric – The respective variable lagged by one observation period.	
mean_[variable]_6	Numeric – The mean of the respective variable, computed over the current and last five observation periods.	
mean_[variable]_12	Numeric – The mean of the respective variable, computed over the current and last eleven observation periods.	
geom	Geometric data – Geometric representation of the Urban Centre polygon, defining its spatial extent.	GHS-UCDB.

Data Sources:

Balk, Deborah, Francesca Pozzi, Gregory Yetman, Uwe Deichmann, and Andrew Nelson. (2006) “The Global Rural-Urban Mapping Project (GRUMP): A new mapping approach to urban extent [Data report],” Center for International Earth Science Information Network (CIESIN), Columbia University, <https://sedac.ciesin.columbia.edu/data/set/grump-v1-urban-extents>.

CIESIN, Columbia University (2013) “Low Elevation Coastal Zone (LECZ) Global Dataset,” NASA Socioeconomic Data and Applications Center (SEDAC), 10.7927/H4MW2F2J.

Centre for Research on the Epidemiology of Disasters (CRED). (2024) “EM-DAT: The International Disaster Database,” <https://public.emdat.be/data>.

Di Napoli, C., C. Barnard, C. Prudhomme, H. L. Cloke, and F. Pappenberger (2021) “ERA5-HEAT: A global gridded historical dataset of human thermal comfort indices from climate reanalysis,” *Geoscience Data Journal*, 8 (1), 2–10, 10.1002/gdj3.102.

Florczyk, Aneta, Christina Corbane, Marcello Schiavina et al. (2019) “GHS-UCDB R2019A -GHS Urban Centre Database 2015, multitemporal and multidimensional attributes,” <http://data.europa.eu/89h/53473144-b88c-44bc-b4a3-4583ed1f547e>, 10.2905/53473144-b88c-44bc-b4a3-4583ed1f547e.

GeoNames. (2018) “GeoNames Geographical Database [Dataset],” GeoNames, <https://www.geonames.org/>.

GISTEMP Team (2024) “GISS Surface Temperature Analysis (GISTEMP), version 4,” *J. Geophys. Res. Atmos.*, 124 (12), 6307–6326, 10.1029/2018JD029522, NASA Goddard Institute for Space Studies. Dataset: data.giss.nasa.gov/gistemp/.

Global Burden of Disease Collaborative Network (2017) “Global Burden of Disease Study 2017 (GBD 2017) Air Pollution Exposure Estimates,” Dataset, <https://www.healthdata.org/research-analysis/gbd>.

Global Covenant of Mayors for Climate & Energy (n.d.a) “Our cities”, <https://www.globalcovenantofmayors.org/our-cities/>.

International Union for Conservation of Nature (IUCN) (2023) “The IUCN Red List of Threatened Species,” <https://www.iucnredlist.org/>.

Kummu, M., M. Taka, and J. H. A. Guillaume (2018) “Gridded global datasets for Gross Domestic Product and Human Development Index over 1990–2015,” *Scientific Data*, 5, 180004, 10.1038/sdata.2018.4.

Patterson, Tom, and Nathaniel Kelso. (2018) “Natural Earth Populated Places, Version 4.1.0 [Dataset],” Natural Earth, <https://www.naturalearthdata.com/>.

Schiavina, Marcello, Sergio Freire, and Kytt MacManus. (2019) “GHS population grid multitemporal (1975, 1990, 2000, 2015) R2019A,” European Commission, Joint Research Centre (JRC), <http://data.europa.eu/89h/0c6b9751-a71f-4062-830b-43c9f432370f>, 10.2905/42E8BE89-54FF-464E-BE7B-BF9E64DA5218.

United Nations, Department of Economic and Social Affairs (UNDESA). (2018) “World Population Prospects: The 2018 Revision,” United Nations, <https://population.un.org/wup/>.

Weiss, D. J., A. Nelson, H. S. Gibson, W. Temperley, S. Peedell, A. Lieber, B. Hanchard, and A. J. Tatem (2018) “A global map of travel time to cities to assess inequalities in accessibility in 2015,” *Nature*, 553 (7688), 333–336, 10.1038/nature25181.